DEVELOPMENT AND APPLICATION OF LARGE-SCALE OPTOGENETIC MAPPING IN THE MOUSE CORTEX

by

Diana Heather Lim
B.Sc. (Hons), The University of Lethbridge, 2009

A THESIS SUBMITTED IN PARTIAL FULFILLMENT OF
THE REQUIREMENTS FOR THE DEGREE OF

DOCTOR OF PHILOSOPHY

in

The Faculty of Graduate and Postdoctoral Studies
(Neuroscience)

THE UNIVERSITY OF BRITISH COLUMBIA
(Vancouver)

March 2015

Abstract

One of the major goals in neuroscience is to understand and map the connectivity of the brain. While this is no small undertaking, recent technological advances have allowed brain mapping to reach unprecedented levels. Optogenetic tools have been developed that permit selective manipulation and investigation of neural systems. Here, we have mapped *in vivo* intracortical activity in the mouse by combining arbitrary point optogenetic stimulation and regional voltage-sensitive dye (VSD) imaging.

We first show that optogenetic photostimulation using channelrhodopsin-2 (ChR2) led to cortical maps that were similar to the maps generated with sensory stimulation. ChR2-evoked maps confirmed known intrahemispheric relationships (such as between barrel cortex and motor cortex) and known interhemispheric relationships (such as between homotopic areas). We used ChR2 point stimulation to map a number of cortical areas and used network analysis to examine relationships between cortical areas. We found asymmetrical connections between primary and secondary sensory cortex and defined the parietal association cortex as a hub node.

We then applied this mapping method to map altered cortical connectivity in the early and late stages after a targeted cortical stroke (1 week post-stroke and 8 weeks post-stroke, respectively). Network analysis based on ChR2-evoked responses revealed a symmetrical bilateral sham network that was disrupted after stroke. At 1 week post-stroke, we observed wide-spread depression of ChR2-evoked activity that extended to the contralesional hemisphere. By 8 weeks post-stroke significant recovery was observed. When we considered the network as a whole, we found that scaling the ChR2-evoked activity from the stroke groups to match the sham group mean resulted in a relative distribution of responses that was indistinguishable from the sham group, suggesting network-wide down-scaling and connectional diaschisis after stroke. When connections within the peri-infarct were isolated, we did not observe equal down-scaling of responses after stroke. Our findings suggest that during recovery, most cortical areas undergo homeostatic upscaling, resulting in a relative distribution of responses that is similar to the pre-stroke (sham) network, albeit still depressed. However, recovery within the peri-infarct zone is heterogeneous and these cortical points do not follow the recovery scaling factor expected for the entire network.

Preface

Portions of this thesis have been published.

Chapter 1, section 1.3.3 and a portion of Chapter 4, section 4.2 is based on a review article published in Frontiers in Neuroscience:

Lim DH, LeDue J, Mohajerani MH, Vanni MP, Murphy TH (2013). Optogenetic approaches for functional mouse brain mapping. Front Neurosci 7:54.

I wrote the manuscript with editing assistance from the co-authors. Figures in this section (1.3.3) are as originally published.

Chapter 2 is based on a publication in Frontiers in Neural Circuits:

Lim DH*, Mohajerani MH*, LeDue J, Boyd J, Chen S, Murphy TH (2012). In vivo Large-Scale Cortical Mapping Using Channelrhodopsin-2 Stimulation in Transgenic Mice Reveals Asymmetric and Reciprocal Relationships between Cortical Areas. Front Neural Circuits 6:11. (*Equal contributors).

Together with Dr. Majid Mohajerani, I designed the experiments, collected and analyzed the data, and wrote the manuscript. Jeff LeDue contributed greatly to data colleciton, data analysis, and editing the manuscript. Dr. Jamie Boyd developed the software. Dr. Shangbin Chen contributed MatLab programs for analysis. Dr. Tim Murphy supervised the project and contributed greatly to the manuscript. Figures in this chapter are as originally published.

Chapter 3 is based on a manuscript in the Journal of Neuroscience:

Lim DH, LeDue J, Mohajernai MH, Murphy TH (2014). Optogenetic mapping after stroke reveals network-wide scaling of functional connections and heterogenous recovery of the peri-infarct. J Neurosci 34(49):16455-16466.

I designed the experiments, collected and analyzed the data, and wrote the manuscript. Jeff LeDue contributed greatly to data collection, data analysis, and editing the manuscript. Dr. Majid Mohajerani contributed to experimental design. Dr. Tim Murphy supervised the project and contributed greatly to the manuscript. Figures in this chapter are as originally published.

All animal experiments were approved by the Animal Care Committee of the University of British Columbia (Protocols A09-0665 and A10-0140) and in accordance with guidelines set forth by the Canadian Council for Animal Care.

Table of contents

Abstract ii

Preface iii

Table of contents v

List of tables viii

List of figures ix

List of abbreviations x

Acknowledgments xiii

1. Introduction 1

1.1 THE IMPORTANCE OF MAPPING IN THE BRAIN 1

1.1.1 The balance between structure and function 1

1.1.2 General cortical organization and cartography 3

1.1.3 The brain as a network 6

1.2 VOLTAGE-SENSITIVE DYE IMAGING 9

1.2.1 A short history of voltage-sensitive dye imaging in neuroscience 9

1.2.2 Properties of voltage-sensitive dyes 11

1.2.3 In vivo applications and recent findings with voltage-sensitive dye imaging 14

1.3 OPTOGENETIC MAPPING 16

1.3.1 A short history of optogenetics 16

1.3.2 Optogenetic variants 19

1.3.3 Optogenetic approaches for functional mouse brain mapping 20

1.4 STROKE 35

1.4.1 Stroke: an important disease 35

1.4.2 Plasticity after stroke 36

1.4.3 Animal models of ischemic stroke 39

1.5 RESEARCH AIMS AND HYPOTHESES 41

2. In vivo large-scale cortical mapping using channelrhodopsin-2 stimulation in transgenic mice reveals asymmetric and reciprocal relationships between cortical areas 43

2.1 INTRODUCTION 43

2.2 MATERIALS AND METHODS 44

2.2.1 Animals 44

2.2.2 Surgery 45

2.2.4 Cortical electroencephologram (EEG) recording 45

2.2.5 VSD imaging 45

2.2.6 Sensory stimulation 47

2.2.7 Photostimulation 47

2.2.8 Data analysis 50

2.2.9 Pharmacology 50

2.2.10 Network analysis 50

2.2.11 Histology 52

2.2.12 Statistical analyses 52

2.3 RESULTS 53

2.3.1 Assessment of channelrhodopsin-evoked cortical activity through qualitative comparison to sensory-evoked cortical activity 53
2.3.2 Quantitative comparison between sensory and Channelrhodopsin-2-evoked VSD responses 55
2.3.3 Assessment of the inter- and intracortical network trends from connectivity matrices 59
2.3.4 Analysis of VSD responses after channelrhodopsin-2 stimulation in control animals 61
2.3.5 Intrahemispheric network analysis of regional activity evoked by Channelrhodopsin-2 stimulation 62
2.4 DISCUSSION 67
2.4.1 Self-assembly of functional cortical circuits through stimulation of neuronal subsets 67
2.4.2 Possible limitations of simultaneous voltage sensitive dye imaging and channelrhodopsin-2 stimulation in vivo 68
2.4.3 Network analysis of reciprocal connections and identification of hub regions reveals asymmetry in large-scale cortical organization 70
2.4.4 Outlook for large-scale functional mapping in vivo 72
2.5 SUPPLEMENTARY MATERIALS 73
2.5.1 Optrode recording 73
2.5.2 Network analysis of sensory stimulation 73
2.5.3 Supplementary figures 74

3. Optogenetic mapping after stroke reveals network-wide scaling of functional connections and heterogeneous recovery of the peri-infarct 76
3.1 INTRODUCTION 76
3.2 MATERIALS AND METHODS 77
3.2.1 Photothrombotic strokes 77
3.2.2 In vivo VSD imaging 78
3.2.3 Cortical electroencephalogram recordings 78
3.2.4 Sensory stimulation 79
3.2.5 Photostimulation 79
3.2.6 Data analysis 79
3.2.7 Network analysis 80
3.2.8 Histology 81
3.2.9 Statistical analyses 81
3.3 RESULTS 82
3.3.1 Sensory-evoked activity after stroke shows delayed and depressed VSD responses in the injured hemisphere 82
3.3.2 Channelrhodopsin-evoked activity shows depressed, but not delayed VSD responses after stroke in the injured hemisphere 83
3.3.3 Assessment of the inter- and intracortical network trends from connectivity matrices 85
3.3.4 Assessment of the differences between groups using the connectivity matrices 90
3.3.5 Assessment of the peri-infarct using grid photostimulation 92
3.4 DISCUSSION 95
3.4.1 VSD imaging and ChR2 stimulation reveals network-wide plasticity after stroke 95
3.4.2 Non-uniform recovery of peri-infarct connections 96
3.4.3 Implications for future work 98
3.4.4 Conclusion 98

4. General discussion 99
4.1 STRENGTHS AND LIMITATIONS OF THE IMAGING METHOD 99
4.1.1 Strengths of simultaneous VSD imaging and ChR2 stimulation 99
4.1.2 Weaknesses of simultaneous VSD imaging and ChR2 stimulation 101
4.1.3 Channelrhodopsin-2 transgenic mice 102
4.2 FUTURE IMPROVEMENTS AND DIRECTIONS 104

4.2.1 Voltage-sensitive fluorescent proteins and genetically-encoded calcium indicators *105*
4.2.2 Optogenetic expression *106*
4.2.3 Additional testing of the stroke model *107*
4.2.4 Modification of the experimental design for translational relevance *108*
4.2.5 Further applications of the method: beyond stroke models *109*
4.3 TRANSLATION: RELEVANCE TO CLINICAL STUDIES 109
4.3.1 Comparison to clinical techniques of non-invasive stimulation *109*
4.3.2 Translation from basic preclinical to clinical studies *111*
4.4 CONCLUDING REMARKS 113

References 114

List of tables

TABLE 1.1 OPTOGENETIC FUNCTIONAL MAPPING TECHNIQUES 22
TABLE 1.2 PROPERTIES OF AN IDEAL FUNCTIONAL MAPPING TECHNIQUE 34

List of figures

FIGURE 1.1 CONNECTIONS BETWEEN CELLS OF THE DENTATE GYRUS. 3
FIGURE 1.2 EXCITATORY HODOLOGY OF EXCITATORY CELLS IN LAYERS 2-5. 5
FIGURE 1.3 SCHEMATIC ILLUSTRATIONS OF NETWORK MODELS. 7
FIGURE 1.4 VSD IMAGING PRINCIPLE IN THREE STEPS. 10
FIGURE 1.5 HISTOLOGICAL EXAMINATION OF RH1692 VOLTAGE-SENSITIVE DYE DISTRIBUTION *IN VIVO*
FIGURE 1.6 CHANNELRHODOPSIN AS AN OPTOGENETIC TOOL. 17
FIGURE 1.7 USING CHANNELRHODOPSIN-2 STIMULATION TO MAP FUNCTIONAL CONNECTIVITY AT MULTIPLE SCALES OF MOUSE BRAIN ORGANIZATION 26
FIGURE 1.8 CHANNELRHODOPSIN-2 STIMULATION IN THE THY-1 TRANSGENIC MOUSE MAY RESULT IN MORE SPECIFIC ACTIVATION COMPARED TO DIRECT ELECTRICAL STIMULATION 30
FIGURE 1.9 ISCHEMIC CASCADE LEADING TO CEREBRAL DAMAGE. 36
FIGURE 2.1 MAPPING INTERHEMISPHERIC AND INTRAHEMISPHERIC CONNECTIVITY USING CHR2 STIMULATION AND VSD IMAGING. 47
FIGURE 2.2 VOLTAGE-SENSITIVE DYE IMAGING MAPS TO COMPARE SENSORY STIMULATION TO LOCAL PHOTOSTIMULATION. 54
FIGURE 2.3 TEMPORAL CORRELATION BETWEEN SENSORY-EVOKED VSD RESPONSES AND CHR2-EVOKED VSD RESPONSES. 56
FIGURE 2.4 INTERHEMISPHERIC AND INTRAHEMISPHERIC CONNECTIVITY: COMPARISON OF SENSORY-EVOKED CORTICAL MAPS WITH CHR2-EVOKED CORTICAL MAPS. 58
FIGURE 2.5 CHR2 EXPRESSION AND CHR2- EVOKED EEG RESPONSES ACROSS THE ANTERIOR-POSTERIOR AXIS OF CORTEX. 60
FIGURE 2.6 CHR2-EVOKED VSD RESPONSES ARE DEPENDENT ON INTRACORTICAL SYNAPTIC TRANSMISSION AND CHR2. 62
FIGURE 2.7 NETWORK ANALYSIS OF CONNECTIVITY MATRICES REVEALS CORTICAL HUBS. 64
FIGURE 2.8 INTRAHEMISPHERIC CONNECTIVITY CHANGES OVER MILLISECOND TIMESCALES AFTER DIRECT CORTICAL PHOTOSTIMULATION. 66
FIGURE 2.9 OPTRODE RECORDINGS FROM CHR2-EXPRESSING LAYER 5B PYRAMIDAL NEURONS FOLLOWING PHOTOSTIMULATION. 74
FIGURE 2.10 COMPARISON OF THE CHR2-EVOKED NETWORK WITH THE SENSORY-EVOKED NETWORK. 75
FIGURE 3.1 EXPERIMENTAL TIMELINE FOR MAPPING FUNCTIONAL CONNECTIVITY WITH CHANNELRHODOPSIN-2 STIMULATION AND VOLTAGE SENSITIVE DYE IMAGING. 78
FIGURE 3.2 VOLTAGE SENSITIVE DYE IMAGING MAPS OF THE INJURED LIMB SHOWS DELAYED AND DECREASED VSD RESPONSES IN BOTH HEMISPHERES 83
FIGURE 3.3 VOLTAGE SENSITIVE DYE IMAGING MAPS OF PHOTOSTIMULATION OF THE INJURED FORELIMB CORTEX RESULTS IN STRONGER AND FASTER VSD RESPONSES THAN EXPECTED FROM SENSORY STIMULATION. 84
FIGURE 3.4 CONNECTIVITY CHANGES OVER TIME REVEAL ASYMMETRIES AFTER STROKE 89
FIGURE 3.5 REGIONAL NETWORK-WIDE SCALING OF THE CONNECTIVITY MATRIX LEADS TO RELATIVE CONNECTIVITY STRENGTHS SIMILAR TO SHAM 89
FIGURE 3.6 NODE STRENGTH FROM THE SHAM NETWORK PREDICTS WHICH SITES WILL BE MOST-AFFECTED AND LEAST-AFFECTED AFTER STROKE. 91
FIGURE 3.7 SCALING THE RESPONSES IN THE PERI-INFARCT ZONE DOES NOT LEAD TO RELATIVE CONNECTIVITY STRENGTH SIMILAR TO SHAMS. 93
FIGURE 3.8 RESPONSE STRENGTH WITHIN THE PERI-INFARCT AND HOMOTOPIC FL REVEALS THAT THE WEAKEST PRE-STROKE SITES HAVE THE GREATEST RELATIVE GAINS POST-STROKE, RESULTING IN HETEROGENEOUS RECOVERY. 94

List of abbreviations

A1	Primary auditory cortex
AAV	Adeno-associated virus
ANOVA	Analysis of variance
AP5	(2R)-amino-5-phosphonovaleric acid
BC	In graph theory, betweenness centrality
BCS1	Barrel cortex area of the primary somatosensory cortex
BOLD	Blood-oxygenation level-dependent
C	In graph theory, clustering coefficient
C1V1	A chimeric channelrhodopsin composed of channelrhodopsin-1 parts from *Chlamydomonas reinhardtii* and *Volvox carteri*
CA	Cornu ammonis
CA3	Cornu ammonis area 3
CaMKII	Calcium/calmodulin-dependent protein kinase II
CaSD	Calcium sensitive dye
CCAO	Common carotid artery occlusion
CG	Cingulate cortex
ChETA	Ultrafast mutants of ChR2-E123T
ChR	Channelrhodopsin
ChR2	Channelrhodopsin -2
CIMT	Constraint-induced movement therapy
CNQX	6-cyano-7-nitroquinoxaline-2,3-dione
CRACM	Channelrhodopsin-2 assisted circuit mapping
CT	Corticothalamic
DC	Direct current
DNQX	Dinitroquinoxaline-2,3-dione
DTI	Diffusion tensor imaging
EEG	Electroencephalogram
Et-1	Endothelin-1
FL	Forelimb

FLS1	Forelimb area of the primary somatosensory cortex
fcOIS	Functional connectivity optical intrinsic signal imaging
fMRI	Functional magnetic resonance imaging
FRET	Fluorescence resonance energy transfer
FS	Fast-spiking
GABA	ϒ amino butyric acid
GCaMP	A type of genetically encoded calcium indicator, made of a fusion of green fluorescent protein, calmodulin, and M13
GECI	Genetically encoded calcium indicators
GFP	Green fluorescent protein
HEK293 cells	Human embryonic kidney 293 cells
HL	Hindlimb
HLS1	Hindlimb area of the primary somatosensory cortex
ICMS	Intracortical microstimulation
IT	Intratelencephalic
L	In graph theory, characteristic path length
LASER	Light amplification by the stimulated emission of radiation
LBM	Light based mapping
LFP	Local field potential
LSPS	Laser scanning photostimulation
M1	Primary motor cortex
M2	Secondary motor cortex
MCAO	Middle cerebral artery occlusion
NFS	Non fast-spiking
NpHR	*Natonomonas phargonis* halorhodopsin
OGB-1	Oregon green BAPTA-1
Opto-fMRI	Optogenetic functional magnetic resonance imaging
PT	Pyramidal tract
PTA	Primary association area
ROI	Region of interest
RS	Retrosplenial cortex

S/N	Signal to noise ratio
S1	Primary sensory cortex
S2	Secondary sensory cortex
SEM	Standard error of the mean
TMS	Transcranial magnetic stimulation
tDCS	Transcranial direct current stimulation
tPA	Tissue plasminogen activator
V1	Primary visual cortex
V2L	Lateral secondary visual cortex
V2M	Medial secondary visual cortex
VChR1	*Volvox caeri* channelrhodopsin-1
VSD	Voltage-sensitive dye
VSFP	Voltage-sensitive fluorescent protein
VSFP2	Second generation voltage-sensitive fluorescent protein
WK	C2 whisker

Acknowledgments

There are a number of people who made this journey possible.

Thank you to my supervisor, Dr. Tim Murphy, for the support though my program and for allowing me the freedom to explore new and exciting areas of neuroscience.

Thank you to my committee members, Dr. Lara Boyd, Dr. Kurt Haas, and Dr. Wolfram Tetzlaff, for your time and guidance throughout the years.

I am grateful for the funding support I received during my studies. I was supported by a Canada Graduate Scholarship from the Natural Sciences and Engineering Research Council of Canada (NSERC) and an Isaak Walton Killam Memorial Pre-doctoral Fellowship. Thank you to these agencies for supporting science in Canada.

Thank you to the past and present members of the Murphy Lab for your camaraderie and good humor in this crazy game we call "science". Thank you especially to Dr. Majid Mohajerani, whose mentorship was invaluable, and to Jeff LeDue whose technical expertise and optimism was greatly appreciated throughout the years. This work would not have been possible without the technical assistance of Cindy Jiang and Pumin Wang – thank you for being so generous with your time and meticulous with your work.

And finally, thank you to my friends and family for your unfailing support and encouragement. The journey was easier and far more enjoyable with you by my side.

1. Introduction

1.1 The importance of mapping in the brain

1.1.1 The balance between structure and function

One of the major goals in neuroscience has been to map the connectivity of the brain. From the classical structural studies by Ramon y Cajal, which hypothesized connections between pairs of neurons (reviewed by Sotelo, 2003) to the more recent endeavours to reverse-engineer the brain in the mouse (Lein et al., 2007; Oh et al., 2014), the rat (Hjornevik et al., 2007), and even the human (Markram, 2006), it is clear that understanding the brain and it's connections has been long sought-after in the field of neuroscience. With these recent efforts, the term "connectome" was coined, meaning "the complete description of structural connections between elements of a nervous system" (Bullmore and Sporns, 2009). Within the mouse, ultra-high-resolution structural mapping has taken place that has allowed researchers to reconstruct every cell and every connection within a sample of tissue at a microscale level, however, these mapping studies are so exhaustive that even within the relatively-simple mouse brain these reconstructions are only on the order of 1 mm^3 (Lichtman and Denk, 2011). While the highest resolution connectome possible is preferred, this is not always practical, especially when dealing with more complex brains. Techniques exist to map the structure of the human brain at a macroscale level, with a lower level of resolution. Diffusion Tensor Imaging (DTI) is a useful and noninvasive tool for characterizing structure and is often used for mapping major pathways within the human brain (Sporns et al., 2005). Although DTI does not give information with the resolution of a single axon, it can be used to identify major anatomical tracts and show gross structural connectivity between brain areas (Sporns et al., 2005). Functional mapping using functional magnetic resonance imaging (fMRI) can be used to identify which areas of the brain are functionally connected with each other, and from these correlations, a functional connectome can be derived (Biswal et al., 2010). While a functional connectome does not necessarily provide any information about the underlying anatomical structure (and vice

versa), it has been shown that structure and function often correlate (Honey et al., 2010). For this reason, it is optimal to consider and integrate both structure and function when mapping brain connectivity and to consider multiple levels of organization (from microscale to macroscale).

Historically, connectivity mapping started with the structural drawings and hypotheses of Ramon y Cajal (Sotelo, 2003). Based on his detailed drawings, he hypothesized the flow of information along neurons and between cells (Figure 1.1). These were the first depictions, and the first explanation of how information could travel within the brain. Since this time, anatomical tracing has been used to further elucidate the structural connectivity in the brain (Lanciego and Wouterlood, 2011). These studies have been important in developing our understanding of how the brain is organized and have been especially important in revealing which properties are conserved across animal models. Based on the structural framework that has been defined based on decades of work, we can now use functional mapping experiments to understand how the brain operates within its structural framework (Honey et al., 2010). Functional mapping adds another layer of complexity because functional maps can vary depending on the developmental stage of the animal (i.e. Juvenile or adult), the behavioural state of the animal (i.e. Awake vs. anesthetised), and depending on the task at hand (i.e. A cognitive task, a sensory recognition task or sensory stimulus). Based on the multitude of possible functional maps that could be present within the brain, it is useful to understand the underlying structural framework. It should be noted, however, that brain structure is not static; the brain is plastic and while major brain regions and anatomical pathways are less prone to plastic changes, fine-resolution structural changes (i.e. Dendritic spines) are in a constant state of flux (Kolb and Whishaw, 1998). Clearly, with all of these competing factors and all of this complexity, mapping the brain is no small feat.

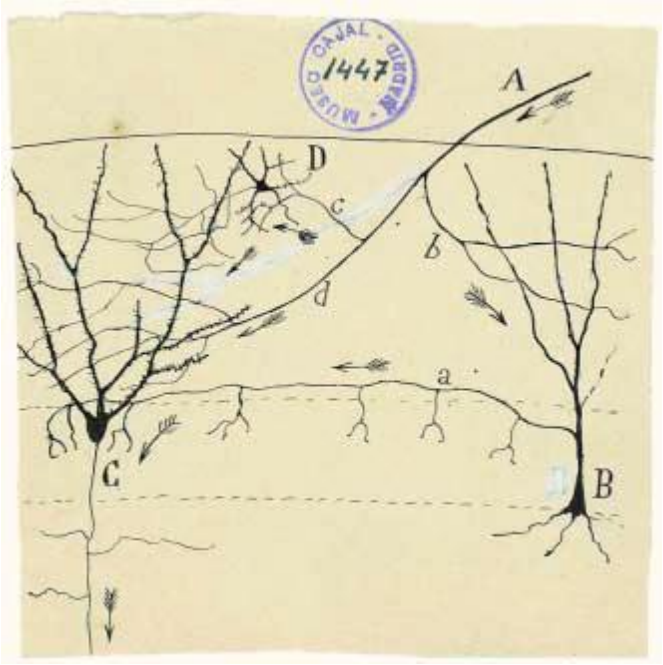

Figure 1.1 Connections between cells of the dentate gyrus. This drawing by Cajal shows the hypothesized flow of information in the dentate gyrus. A single afferent fibre (A) has connections with a pyramidal cell (B), granule cell (C), and stellate cell (D). Reprinted with permission from Macmillan Publishers Ltd: Nature Reviews Neuroscience (Sotelo 2003. Viewing the brain through the master hand of Ramon y Cajal), Copyright (2003).

1.1.2 General cortical organization and cartography

The brain is an intricately organized and wonderfully complex organ. The human cortex alone is made up of 10 billion neurons, and these neurons are organized into specialized cortical areas to process specific information and carry out particular functions. Broadly speaking, the rostral areas are responsible for motor movements and higher-level cognitive functions, while the caudal areas are responsible for sensory inputs (such as visual information) and sensory integration. This general spatial organization is relatively consistent across mammals (O'Leary et al., 2007). The development and initial organization of these cortical areas begins early in prenatal development, with different signalling centres generating signalling molecules (transcription factors) that guide proper development by stimulating proliferation, migration, and connectivity. As the brain continues to develop, subcortical regions establish connections with the cortex, forming topographic connections between areas of the thalamus and the cortex. From here, areal topography will be further refined through neuronal activity where “cells that

fire together, wire together" (i.e. Hebbian plasticity). Cortical areas will become specialized and further organizational patterns within each area may develop (for example, ocular dominance columns) (Sur and Rubenstein, 2005; Majewska and Sur, 2006). While the brain has many complex regions, the mammalian cortex is by far the most complex and is the focus for this thesis.

The classical view of the mammalian neocortex is that it is arranged in six layers (for a review, see Thomson and Bannister, 2003; Thomson and Lamy, 2007), although this view of laminar organization is oversimplified. One obvious caveat is that laminar structure and organization varies throughout the cortex – the laminar structure of motor cortex is very different compared to the visual cortex (Thomson and Bannister, 2003; Thomson and Lamy, 2007). Thus, a recent view of laminar organization divides excitatory cells in the cortex based on their axonal projections (Harris and Shepherd, 2015):

Intratelencephalic (IT) neurons are pyramidal neurons found in layers 2-6 and project strictly within the telencephalon (neocortex and striatum). Within the IT neurons, distinct subclasses can be identified. Layer 4 IT neurons receive inputs primarily from the thalamus with few inputs from the other cortical layers, and project primarily to layer 2/3, with very few long-range projections. IT neurons found in the other cortical layers (2/3, 5A, 5B, 6) have many local inputs (from other IT neurons) and long-range inputs (from the thalamus), as well as many long-range projections within the telencephalon. These IT neurons may send long-range efferent projections to the contralateral cortex via the corpus callosum or anterior commissure. It has been suggested that the subclasses of IT neurons may explain inter-areal connectivity patterns (Harris and Shepherd, 2015).

Pyramidal tract (PT) neurons are thick-tufted large pyramidal neurons found in layer 5B. These large pyramidal cells receive inputs from IT cells, the thalamus, and higher and lower order cortex. They have many long-range subcortical and subcerebral projections to areas such as the brainstem, spinal cord, and thalamus. These neurons are thought to integrate cortical and thalmocortical inputs, and then send information to subcerebral areas.

Corticothalamic (CT) neurons are pyramidal neurons found in layer 6. These cells receive inputs primarily from the higher order cortex (and, to a lesser degree, from deep-layer IT neurons) and send projections to the thalamus, as well as the ipsilateral cortex and striatum. The function of these neurons remains unclear, although modulation of thalmocortical activity has been suggested (Harris and Shepherd, 2015).

Using this framework, there is dense interconnectivity within a cortical circuit with multiple entry and exit points rather than a linear, sequential pathway (Figure 1.2). This basic excitatory circuit seems to be repeated across neocortical areas and across a number of species, however, area- and species-specific variations exist (Harris and Shepherd, 2015) and questions remain about how this excitatory circuit is influenced by or interacts with inhibitory circuits, and how cortical organization affects behaviour. Nonetheless, cytoarchitecture represents an important platform for understanding how different areas of the brain may function and how areas of the brain are connected, providing a mesoscale perspective of brain connectivity (Silasi and Murphy 2014).

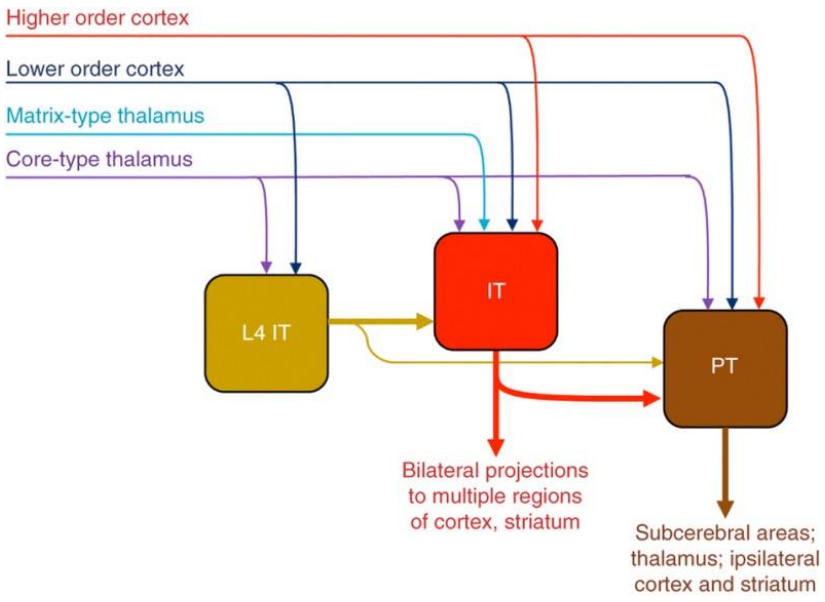

Figure 1.2 Excitatory hodology of excitatory cells in layers 2-5. Intratelencephalic neurons in layer 4 (L4 IT) neurons project mostly unidirectionally to other IT neurons (layers 2/3, 5A, 5B; grouped as IT here), which in turn project mostly unidirectionally to pyramidal tract (PT) neurons. Each class receives extrinsic inputs, but information flows across classes in a largely directional manner owing to asymmetric interclass connectivity. All classes have recurrent connections with other members of their own class (not shown). The relationship of CT neurons and IT

neurons in layer 6 to this stratified hodology is not yet established. Reprinted with permission from Macmillan Publishers Ltd: Nature Neuroscience (Harris and Shepherd 2015. The neocortical circuit: themes and variations), Copyright (2015).

1.1.3 The brain as a network

Studies of the brain's structure and function have been important in developing our understanding of the brain's connectivity. Through these studies, we have come to recognize that the brain is a complex system with many overlapping maps – there is redundancy in the circuitry, a myriad of feedback and feed-forward loops, long-range corticocortical connections, and neurons, while specialized for a particular function, may be distributed in multiple cortical areas. Thus, in order to fully map the connectivity of the brain, it may be useful to expand our perspective and start defining networks within the brain and how networks may interact together.

Recently, graph theory has been applied to brain connectivity datasets to mathematically describe the elements of the system and the interactions occurring within the system in a consistent and quantifiable way (Bullmore and Sporns, 2009; van den Heuvel and Hulshoff Pol, 2010; Feldt et al., 2011; Cheng et al., 2012). Graph theory is the mathematical description and analysis of graphs and is particularly useful when dealing with large and complex datasets. Such graphs are made up of nodes (vertices) and connections (edges). Networks can be broadly defined according to how the nodes and edges are distributed, and network analysis has been used to describe a number of types of networks, ranging from social media networks to biological networks within the brain. There are several general classes of networks that have been defined (for a review see Strogatz, 2001), (Figure 1.3).

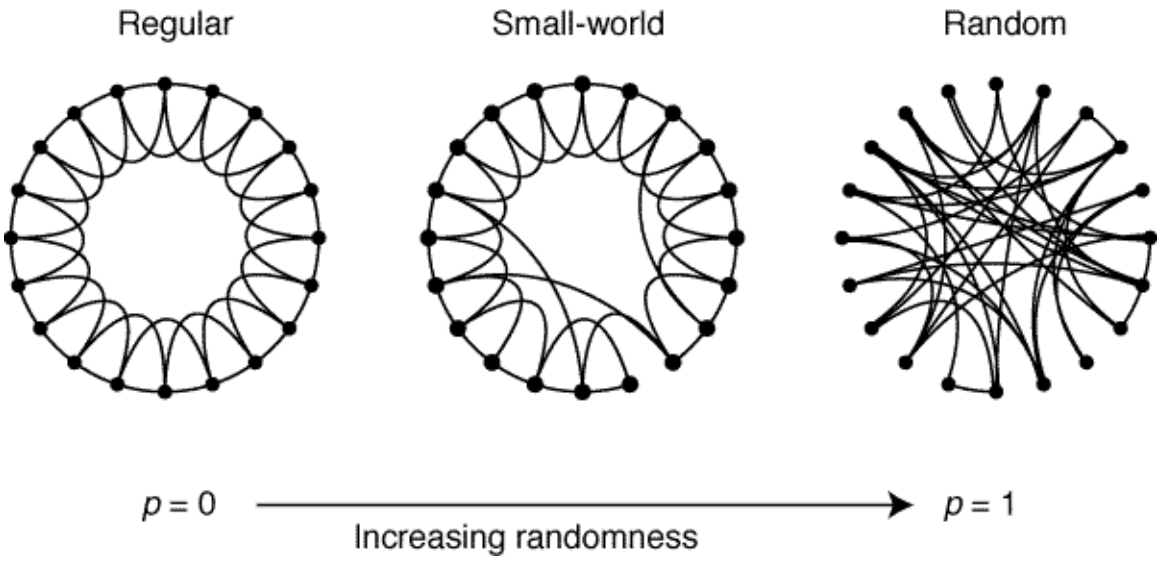

Figure 1.3 Schematic illustrations of network models. Example networks with 20 nodes and 80 edges, using various probability *p* to determine the placement of the edges. In the regular network each node is connected to its four nearest neighbours resulting in high clustering but low efficiency in the network. The random graph has the same number of edges but has a random wiring, resulting in high efficiency but low clustering. The small-world network is highly clustered like the regular graph, but has small characteristic path length, like the random graph. Reprinted with permission from Macmillan Publishers Ltd: Nature (Watts and Strogatz, 1998. Collective dynamics of 'small world' networks), Copyright (1998).

A regular network or lattice network is one where all nodes have the same number of connections (i.e. they have the same node degree) and, in a weighted graph, all nodes have the same number of incoming edges as outgoing edges (i.e. each node has equal in-coming strength and out-going strength). Often, nodes are only connected to their nearest neighbour. This creates a network that is highly clustered and resistant to damage to a single node, but is costly in terms of wiring and efficiency – information cannot pass from one node to any other given node quickly, especially if they are spatially far apart.

A random network has a Gaussian degree distribution and every pair of nodes in the graph has an equal probability of being connected (Bullmore and Sporns, 2009). Random graphs are most often used for mathematical modeling and are seldom seen in nature. They have been compared to a road map of North America: roads (edges) are scattered throughout the entire network, connecting various cities (nodes).

The "small-world" network, which is the most common type of network for brain networks, is one that has a high degree of local clustering (forming community clusters where a group of nodes is highly connected to each other), while also having a number of

short paths between clusters (Watts and Strogatz, 1998). In this type of network, all nodes are connected to one another through a relatively short path, so while they may not be directly connected to one another, there are only a few nodes between them. Small world networks are often found in nature as they represent complex networks. They have been compared to an airline map of North America: flight routes (edges) cover the entire network, and most cities (nodes) have a small number of connections, yet certain cities have a dense number of flights that come and go (like Toronto's Pearson airport or Chicago's O'Hare airport). These are termed 'hub nodes'. In this network, the network is resistant to random attack of a single node but vulnerable to targeted attack of a hub node.

Classifying the type of network has proven to be useful in describing complex networks (Strogatz, 2001). The investigation of a number of important network properties can further describe network characteristics (for a review, see Rubinov and Sporns, 2010).

Node degree: the number of connections that link a given node to the rest of the network. A higher node degree indicates high importance within the network.
Betweenness centrality (BC): the number of shortest paths that pass through a given node. A higher centrality indicates a 'hub' node. Nodes with high centrality are highly important for network efficiency and integration.
Clustering coefficient (C): Used for measuring segregation within the network; the fraction of triangles around an individual node (i.e. The fraction of the node's neighbours that are also neighbours of each other)
Characteristic path length (L): Used for measuring integration within the network; the average shortest path between all pairs of nodes in the network.
Connection density: the mean network degree, sometimes used to describe the 'wiring cost' of the network.
Modularity: a measure of how easily the network can be subdivided into clearly delineated and non-overlapping groups (i.e. Non-overlapping communities or clusters within the network).

Using these network properties, we now have a set of terms and measures to describe and differentiate brain networks. These analyses open exciting possibilities for experiments using modeling approaches (Bullmore and Sporns, 2009; Feldt et al., 2011), and have proven useful for investigating questions about how brain injury affects the network structure and function (Cheng et al., 2012).

1.2 Voltage-sensitive dye imaging

1.2.1 A short history of voltage-sensitive dye imaging in neuroscience

In order to answer questions about brain networks and network properties, it would be ideal to have a technique that is capable of investigating neuronal ensembles (i.e. spatial resolution on the order of 10s of micrometers), and has high temporal resolution to capture neuronal activity in real-time (i.e. temporal resolution on the order of milliseconds). Voltage-sensitive dye (VSD) imaging is one tool that is suitable for these purposes.

Grinvald et al. (2004) define VSDs as organic molecules with a hydrophobic portion that binds to the cell membrane, and a charged chromophore portion that prevents the dye from inserting fully into the membrane. The dyes have a high absorption coefficient and can change their optical properties in response to a change in membrane potential of the cell. The VSDs bind to the external surface of the cell membrane without disrupting the normal cellular function (Chemla and Chavane, 2010), and then act as a molecular transducer to transform changes in membrane potential to an optical signal that can be imaged (Grinvald and Hildesheim, 2004)
Figure 1.4). The fluorescent signal from the dye is linearly correlated with the membrane potential of the stained cells (Grinvald and Hildesheim, 2004).

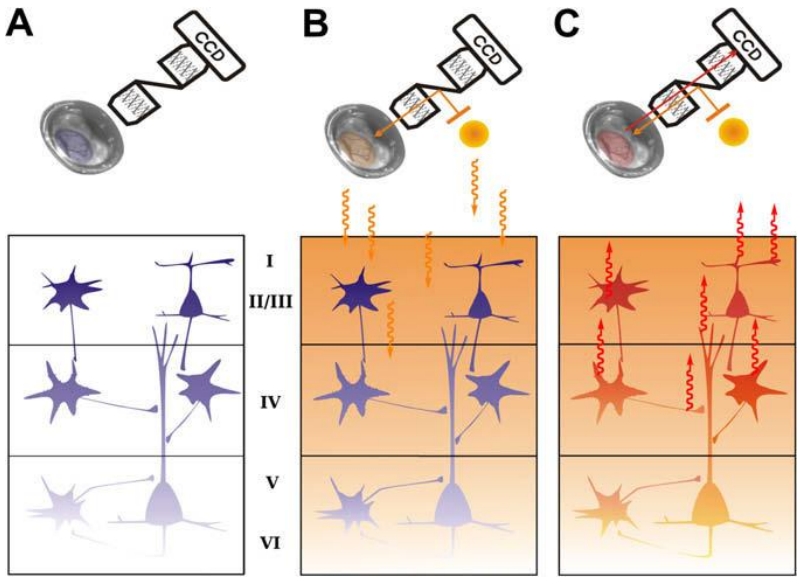

Figure 1.4 VSD imaging principle in three steps. (A) Voltage-sensitive dye is applied on the surface of the cortex (A) and penetrates through all six cortical layers and stains all neuronal and non-neuronal cells. When the cortex is illuminated (B), the dye molecules act as molecular transducers to transform changes in membrane potential into optical signals (C). The fluorescent signal (red arrows) is recorded by a CCD camera. Reprinted from Journal of Physiology-Paris, 104, 1-2. Chemla S and Chavane F. Voltage-sensitive dye imaging: Technique review and models, 40-50. Copyright (2010), with permission from Elsevier.

VSD was first applied in neuroscience by Tasaki et al. in 1968, who applied VSD in the squid giant axon in cultured cells and collected optical recordings (Tasaki et al., 1968a; Tasaki et al., 1968b). Soon after, VSD was used on brain slices in the rodent hippocampus (Grinvald et al., 1982). These early studies demonstrated that VSD imaging was a viable technique for use in mammalian neurons *in vitro*, and suggested that VSD could be applied in *in vivo* experiments. However, these early dyes generated very small signals, and the signal to noise ratio (S/N) was poor. Because of this, these experiments required extensive sampling and averaging to obtain reliable data. This was challenging, as extensive sampling meant extensive illumination time, increasing the possibility of photobleaching and phototoxicity (Shoham et al., 1999). The risk of phototoxicity is especially problematic for *in vivo* experiments. Nonetheless, in 1983 VSD was successfully applied *in vivo* in the salamander olfactory bulb (Orbach and Cohen, 1983).

As more and more *in vivo* studies began to take place using VSD imaging, it became apparent that the largest source of noise in the *in vivo* preparations was the heartbeat, which created significant artefacts even when a subtraction procedure was applied to remove the heartbeat signal (Orbach and Cohen, 1983). It was hypothesized

that changes in hemoglobin concentration were contributing to the noise, since the excitation wavelength of the dye being used at that time matched the peak absorption of hemoglobin. However, it was not until the late 1990s that Shoham et al. (1999) set out to improve the S/N by developing improved blue-shifted dyes with the excitation wavelength outside of the peak absorption of hemoglobin (above 620 nm). From the dye screening process, Shoham et al. found that one dye was particularly successful: RH-1692. This dye showed a 10-fold decrease in the heartbeat noise and a 2- to 3-fold increase in the signal size from increased dye sensitivity. This improved S/N meant that fewer trials were necessary to obtain a reliable signal. Tests revealed no negative pharmacological side effects of the dye, although continuous illumination did result in photobleaching over time (Shoham et al., 1999). The development of these blue-shifted VSDs created opportunities to study functional cortical activity *in vivo* with high spatial and temporal resolution that could not be matched by other imaging techniques. Since then, VSD imaging has been used to investigate many aspects of *in vivo* cortical activity, including sensory processing (Ferezou et al., 2006; Ferezou et al., 2007) and sensory processing after a cortical stroke (Brown et al., 2009; Mohajerani et al., 2011). VSD has also been used extensively to study the visual cortex in cats (Sharon and Grinvald, 2002), ferrets (Chapman et al., 1996), and monkeys (Shoham et al., 1999; Arieli et al., 2002; Slovin et al., 2002).

1.2.2 Properties of voltage-sensitive dyes

One of the primary advantages of using VSD imaging is that the VSD response time is on the order of microseconds and the spatial resolution is on the order of 10s of micrometers, only limited by the quality of the optics and light scattering within the tissue (Grinvald and Hildesheim, 2004). This means that it is possible to investigate spatiotemporal dynamics within networks of cells to create precise and high-resolution functional maps of cortical systems, such as the barrel columns within the barrel cortex (Petersen et al., 2003b), and the ocular-dominance columns in the visual cortex (Shoham et al., 1999).

The VSD signal has been shown to precisely correlate with the changes in membrane potential (Petersen et al., 2003b), however it is important to note that VSDs bind to the membrane of neurons and glial cells alike, thus glial depolarization may

contribute to the signal (Konnerth and Orkand, 1986; Grinvald and Hildesheim, 2004). Despite this, a recent review suggests that glial contribution is unlikely to affect the collected VSD signal since most VSD imaging protocols only use the first 1000 ms of the signal and the time scale for glial activation is much slower (on the order of seconds) compared to the time scale for neuronal activations (Chemla and Chavane, 2010). Similarly, it is important to note that VSD stains both excitatory and inhibitory cells in the cortex, so the VSD signal may include contributions from both populations of cells (Grinvald and Hildesheim, 2004). While VSD stains both excitatory and inhibitory cells in the cortex, excitatory cells represent approximately 80% of the cortical cells while inhibitory cells represent only 20% of the cortical cells (Douglas and Martin, 1991), thus it has been suggested that the contribution from inhibitory cells is minimal (Chemla and Chavane, 2010). However, without cell-specific labeling, it is challenging to determine how much different types of cells are contributing to the VSD signal.

Another important consideration in the VSD signal is the contribution of various subcellular components – the VSD can bind to any area of the membrane, thus it will bind to the soma (where the action potential is generated), the dendrites, and the axon (Chemla and Chavane, 2010). Because the surface area of the dendrites is much larger than the surface area of the axons or the soma, most of the VSD signal will originate from the cortical dendrites (Chemla and Chavane, 2010). The specific contributions of neuron vs. glia, excitatory vs. inhibitory neurons, soma vs. axon vs. dendrite to the VSD signal remain unclear, and is one of the greatest limitations with VSD imaging.

When the VSD is applied in a bath preparation to the cortex, it stains the surface of the cortex. The dye can penetrate through all cortical layers, however, the intensity of the signal peaks at approximately 0.5 mm deep (Ferezou et al., 2006; Mohajerani et al., 2010). Therefore, most of the VSD signal comes from the superficial layers of the cortex rather than the deeper layers (Figure 1.5). Despite this, there still may be contribution to the VSD from the deeper cortical layers (Chemla and Chavane, 2010), as the large pyramidal cells in layer 5 have apical dendrites that reach the superficial layers (as described in section 1.1.2). The same could be said for subcortical contribution to the signal – although the dye only binds on the cortical surface, the cells on the cortical surface may be affected by subcortical or even horizontal inputs from other cortical areas

(Berger et al., 2007). These various contributions are important to consider when interpreting the VSD signal.

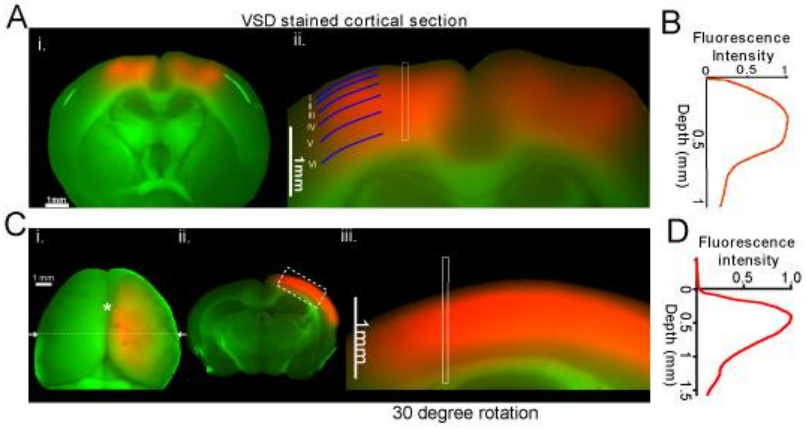

Figure 1.5 Histological examination of RH1692 voltage-sensitive dye distribution *in vivo.* (A) After functional VSD imaging in a bilateral craniotomy preparation (5 x 6 mm). 100 µm coronal sections (i) and magnified image (ii) show VSD staining in all neocortical layers. (B) Depth dependence of VSD fluorescence intensity from histological examination for the bilateral preparation. (C) RH1692 staining after functional VSD imaging in a large unilateral craniotomy preparation (7x5 mm), whole brain (i), 100 µm coronal sections (ii) and magnified image with 30^{o} rotation (iii). (D) Depth dependence of VSD fluorescence intensity from histological examination for the unilateral preparation. * indicates Bregma. Reprinted with permission from the Society for Neuroscience: Journal of Neuroscience (Mohajerani et al., 2010. Mirrored bilateral slow-wave cortical activity within local circuits revealed by fast bihemispheric voltage-sensitive dye imaging in anesthetized and awake mice), Copyright (2010).

A final point on VSD imaging – since the dye binds to the membrane and acts as a transducer to change the membrane potential into an optical signal in a linear fashion, the VSD signal does not distinguish between subthreshold and suprathreshold potentials and does not necessarily indicate spiking activity. This is perhaps one reason why a number of VSD imaging studies have shown the signal to spread over a large cortical area, crossing both anatomical and functional boundaries (Brown et al., 2009; Mohajerani et al., 2010; Lim et al., 2012). While the large spread of VSD signal has been criticized, the signal spread has been tested using other methodologies including anatomy (Ferezou et al., 2007) and calcium imaging (Berger et al., 2007). The results from these other modalities are consistent with the VSD response and show that large areas of the cortex appear to be activated in response to a single sensory stimulus, such as a whisker tap (Ferezou et al., 2006).

1.2.3 In vivo applications and recent findings with voltage-sensitive dye imaging

Recent studies have applied VSD imaging to *in vivo* studies of the organization of the somatosensory cortex (Ferezou et al., 2006; Aronoff et al., 2010), early post-natal brain development (McVea et al., 2012), cortical remapping after injury such as stroke (Brown et al., 2009; Sigler et al., 2009), and to deduce functional activity patterns from spontaneous cortical activity, in a way that is similar to resting-state fMRI (Mohajerani et al., 2013). Several of these experiments have been particularly important in defining how VSD can be used.

Work from Carl Petersen's lab (Ferezou et al. 2006, 2007) has shown that VSD imaging can be used to map the relationship between the primary sensory cortex (S1) and the primary motor cortex (M1). Elegant experiments using both anesthetized and awake, behaving mice have provided us with a greater understanding of the spatiotemporal dynamics of the sensory response. In these studies, Ferezou et al (2006, 2007) did a series of experiments that included active vs. passive whisker sensation as well as collecting spontaneous cortical activity in awake and anesthetized mice. The VSD imaging showed a very consistent and reliable response to whisker stimulation: a primary VSD response was centred over the barrel cortex, and a second response appeared approximately 8 ms later in the primary motor cortex in the hemisphere contralateral to whisker stimulation. These VSD responses then spread across the cortex, and a weaker VSD signal appeared in the ipsilateral hemisphere. To further investigate this connection, Ferezou et al (2007) completed anatomical tracing experiments using a lentivirus (GFP under the CaMKII promoter) to determine whether there was any underlying structure to support the VSD signal spread. A small amount of virus (50 nl) was injected into the somatosensory cortex. Three weeks later, the brain slices show dense axonal labeling from the somatosensory cortex to the primary motor cortex, indicating a monosynaptic connection. Weaker labelling was also seen in the ipsilateral-to-stimulation hemisphere, which agreed with the weaker and delayed VSD signal that was recorded in this hemisphere. Together, these anatomical results demonstrated a functional and structural connection between S1 and M1.

Perhaps the most important aspect of these studies was the comparison of the VSD response in an anaesthetized vs. awake mouse. To investigate the VSD response in

the anesthetized state compared to the awake state, Ferezou et al., (2006, 2007) trained mice for head fixation, and then completed VSD imaging while filming whisking movements and/or while stimulating the whiskers. While the VSD response had a longer duration in the awake animals compared to the animals under isoflurane anaesthesia, the patterns of cortical activity and the spread of the VSD signal over a large area of the cortex was similar in both cases. From this, they suggest that the large cortical activation seen after whisker stimulation is therefore not an effect of anaesthesia, but is rather a product of normal brain function and perhaps sensory integration within the cortex (Ferezou et al., 2007). This is an important finding, because experiments with awake animals are much more technically challenging, and may be more stressful for the animals. To be able to record similar VSD responses in the anesthetized preparation is a great advantage to VSD imaging.

VSD has also been used in combination with other techniques in order to rigorously map the brain *in vivo*. Recently, VSD imaging (using RH1691) was combined with calcium sensitive dye (CaSD) imaging (using Oregon Green BAPTA-1; OGB-1) in *in vitro* and *in vivo* conditions in order to quantify and compare how these techniques capture cortical activity (Berger et al., 2007). Using a series of experiments, Berger et al. (2007) demonstrated that VSD signals were predominantly correlated to subthreshold membrane potential changes (and the post-synaptic potentials), while the CaSD signals were predominantly correlated to the suprathreshold action potentials. This was true both in cell cultures and *in vivo.* While these two signals were closely related *in vivo,* they found that the VSD signal was slightly faster than the CaSD signal, and the CaSD signal lasted longer compared to the VSD signal. Furthermore, they saw that the CaSD signal was more localized, and was less affected by long-range axonal signals from other cortical areas or from subcortical structures, such as the thalamus. In contrast, the VSD signal was driven by post-synaptic potentials and could be affected by long-range connections from other structures. Based on this, Berger et al. hypothesize that the VSD signal may provide us with an idea of how (and where) cortical integration occurs. For example, if a single whisker is stimulated, the action potential may originate in a single barrel column, yet this could evoke a wave of subthreshold activity to allow for multiwhisker integration (Berger et al., 2007). Berger et al. (2007) conclude that VSD

and CaSD signals can be measured simultaneously *in vitro* and *in vivo*, and demonstrate that these signals are representative of different aspects of the neuronal signal and of cortical function. While it could be argued that it would be best to measure both VSD and CaSD rather than VSD alone, the CaSD imaging adds technical challenges to the experiment, especially since the CaSDs need to be injected into the cortex for *in vivo* imaging, causing potential cortical damage but also restricting the CaSD signal to the injected cortical areas (Berger et al., 2007). In contrast, VSD can be bath-applied to the exposed cortex with a less-invasive procedure. For this reason, many experiments use only one technique or the other (VSD or CaSD).

While recent studies using VSD imaging have demonstrated the feasibility of using VSD imaging to measure responses over large areas of cortex *in vivo*, these studies have been somewhat limited in what they are able to map because they have relied on peripheral stimulation or single-point cortical stimulation. Because of this, many VSD studies have been restricted to studying sensory systems (such as the barrel cortex) and have neglected to investigate lesser-studied regions such as associational areas or secondary sensory areas. From a macroscopic perspective, this means that there are unresolved questions about the connectivity of the cortical network. VSD imaging is a powerful mapping method for looking at cortical connectivity over a wide-scale, however, to be truly thorough in understanding cortical connectivity it will be necessary to stimulate all areas of the cortex, including the associational areas, and examine the resulting response patterns.

1.3 Optogenetic mapping

1.3.1 A short history of optogenetics

Optogenetics – the combination of light-based and genetic methods – is a fairly recent development in neuroscience. The term optogenetics was coined in 2005 (Deisseroth et al., 2006), however, it was Nagel et al. (2003) who first described channelrhodopsin-2 (ChR2) as a tool to depolarize the cell membrane and drive cellular activity in a mammalian cell (Figure 1.6). ChR2 is a light-sensitive protein from the alga *Chlamydomonas reinhardtii* (Nagel et al., 2003). While the idea of controlling specific

neuronal cells with light had been previously predicted in the fruit fly (Zemelman et al., 2002), Nagel et al. were the first group to successfully control mammalian cells with light by inserting ChR2 into HEK293 cells (Nagel et al., 2003). Using patch clamp experiments, they found that the channel opened rapidly upon blue light illumination (~470 nm), and established that it is a passive and non-selective cation channel.

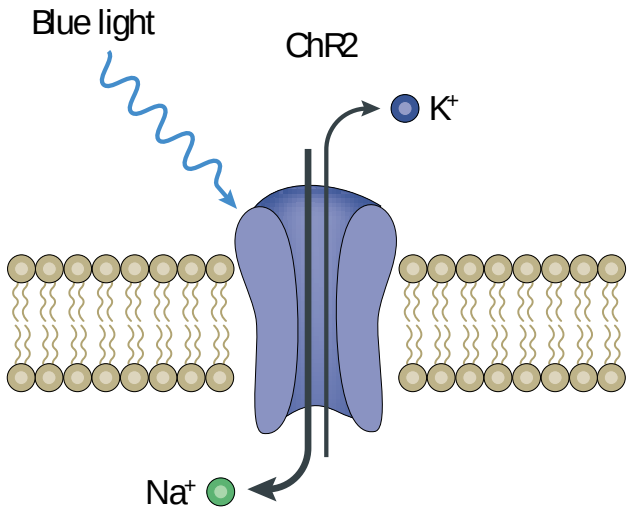

Figure 1.6 Channelrhodopsin as an optogenetic tool. Schematic of channelrhodopsin-2 (ChR2). Following illumination with blue light (activation maximum ~ 470 nm), ChR2 allows the entry of cations (mostly Na^+ and very low levels of Ca^{2+}) into the cell. Reprinted with permission from Macmillan Publishers Ltd: Nature Reviews Neuroscience (Zhang et al., 2007. Circuit-breakers: optical technologies for probing neural signals and systems), Copyright (2007).

In 2005, Boyden et al. took the same ChR2 and inserted it into rodent hippocampal neurons using a lentivirus (Boyden et al., 2005). While previous methods such as glutamate uncaging had been used to control neuronal firing (Shepherd et al., 2003), these methods did not have the temporal resolution to control neurons at the resolution of single spikes, and the neuronal kinetics of these methods (i.e. the depolarization, recovery, and desensitization of the cells) were very slow. With this in mind, Boyden et al. (2005) set out to use ChR2 as a way to genetically target and control neurons at a timescale that is on par with *in vivo* neuronal firing (that is, with a temporal resolution on the order of milliseconds). ChR2 offered the perfect substance for this, as it had already been shown that inward currents could be evoked within 50 µs of illuminating the channel (Nagel et al., 2003).

Using cultured hippocampal neurons, Boyden et al. (2005) demonstrated that neurons expressing ChR2 could be controlled with light at the resolution of a single

spike: both a single pulse of light and a series of light pulses (designed to act like a realistic spike train), reliably resulted in spiking with fast on and off kinetics. Furthermore, Boyden et al. (2005) demonstrated that it was possible to activate ChR2 in mammalian neurons without requiring additional retinal cofactor. This study was important because it was the first to demonstrate the ChR2 could be used for precise voltage control of mammalian neurons without the need for additional chemical substances. In this paper, Boyden et al. discuss the exciting possibility of targeting ChR2 to specific classes or types of cells for even more precise control of neuronal circuits. Only months after this paper was published in Nature Neuroscience, several other papers were published confirming that ChR2 could be used in neurons without added retinal cofactor, and demonstrating that ChR2 could be used *in vivo* in various animal models (Nagel et al., 2005; Bi et al., 2006).

The next breakthrough in the field of optogenetics was the creation of transgenic mice expressing ChR2 in a subset of neurons. In 2007, Arenkiel et al. and Wang et al. used the *Thy1* promoter, specific for neurons, to drive expression of a YFP-tagged ChR2 construct. Transgenic mice were generated and a number of founder lines were established. Line 18 showed high levels of ChR2-YFP expression in the cortex (specifically layer 5B cells), mitral cells of the olfactory cells, CA and CA3 pyramidal neurons in the hippocampus, and cerebellum (Arenkiel et al., 2007). ChR2 was seen in the plasma membrane and could be found in both dendrites and axons (Wang et al., 2007a). These mice were viable and showed no behavioural deficits and no abnormalities in brain structure (Arenkiel et al., 2007). Wang et al. (2007) used cortical slices from these transgenic mice to map neural connectivity in the mouse brain. They found that ChR2 photostimulation was a reliable tool for circuit mapping, resulting in strong and reliable responses with high spatial resolution and millisecond precision, as measured with patch clamp. They suggest that targeting ChR2 to a restricted population of neurons would allow for interesting experimental questions. Arenkiel et al. (2007) used the transgenic mice *in vivo* to investigate questions about complex cortical circuits within the olfactory bulb. They investigated the level of mitral cell convergence and synaptic integration required to elicit an action potential in the piriform cortex, and used simultaneous focal light stimulation in the olfactory bulb and electrophysiological

recordings in the bulb and piriform cortex. While Arenkiel et al. focus on the olfactory bulb for *in vivo* demonstrations, the authors underscore that this approach could be widely applied to any cortical area or neuronal population. The generation of transgenic mice, and the subsequent availability of these mice for other labs opened a world of possibilities for researchers who wanted to study cortical circuits *in vitro* and *in vivo.* Indeed, today these mice can be purchased from Jackson Laboratories (strain name: B6.Cg-Tg(Thy1-COP4/EYFP)18Gfng/J), making it easy for researchers to access and utilize this remarkable tool.

Not all subsequent ChR2 experiments have used transgenic mice, as these mice primarily show ChR2-YFP expression in cortical layer 5B cells. Other studies have instead opted to perform lentiviral injections (Boyden et al., 2005; Cardin et al., 2010), or *in utero* electroporation (Lin, 2012), to target a specific region or cell population for ChR2 expression, related to the experimental questioned being investigated. Nonetheless, it is clear that ChR2 is a viable tool for both *in vitro* and *in vivo* experiments, and gives the experimenter spatial, temporal and even cell-specific precision and control.

1.3.2 Optogenetic variants

After the initial discovery that ChR2 was a viable tool for use in mammalian neurons and *in vivo* experiments, the pursuit for the optimization of ChR2 and newer, faster, red-shifted variants for enhanced control and improved kinetics began. To this day, several labs are actively engineering and distributing improved opsins with the goal of having better, faster, more precise control over cell populations within the brain. Further efforts have gone into finding optogenetic tools that could be used in conjunction with ChR2 so that two or more populations of cells could be simultaneously controlled with different opsins. There are a number of important properties to be considered in evaluating optogenetic variants, as outlined by Lin (2009): 1) Channel conductance; 2) Ion selectivity; 3) Channel kinetics; 4) Desensitization and recovery from the desensitized state; 5) Light sensitivity; 6) Spectral response; 7) Membrane trafficking and expression. A number of channelrhodopsin variants have been engineered, however, many of them are limited in one or more of these properties and still need to be optimized to generate better results (Lin et al., 2009).

One of the most sought-after tools is a red-shifted channelrhodopsin (ChR) variant to be used for simultaneous imaging with calcium imaging dyes or another ChR variant, allowing multiple cell populations to be controlled and imaged in the same experiment (Lin, 2011). To this end, *Volvox cateri* channelrhodopsin-1 (VChR1) was created. VChR1 has a wide spectral excitation (400 to 600 nm), but has poor expression, slow kinetics, and incomplete recovery of the desensitized response (Zhang et al., 2008), and has not been used widely for these reasons. Another red-shifted variant that was created is ChR2+E123T (ChETA) – this variant has a E123T mutation resulting in fast kinetics but reduced light sensitivity and smaller photocurrents (Gunaydin et al., 2010). While these red-shifted variants have been developed, they have not been widely accepted for use and the quest to create a red-shifted ChR variant continues.

Another highly desirable tool is an opsin that can inhibit rather than excite. Soon after ChR2 was introduced in neurons, Han et al. introduced halorhodopsin (NpHR), from *Natronomonas pharaonis,* into neurons (Han and Boyden, 2007). NpHR is a chloride pump that responds to yellow light (~580 nm). It was hoped that the spectra for NpHR and ChR2 were far enough apart that photostimulation of one opsin would not activate the other. In this way, it would be possible to simultaneously but independently have the ability to excite and inhibit cells within the same brain region simply by using different wavelengths of light. Han and Boyden (2007) reported simultaneous ChR2 and NpHR activation within cultured hippocampal neurons, giving them bidirectional control of membrane voltage in the same preparation. However, halorhodopsins have intrinsic kinetic limitations – while they are activated quickly they have a very slow decay time (on the order of minutes) (Chow et al., 2012). This decay time is orders of magnitude slower than the decay time for ChR2 (Chow et al., 2012). Therefore, despite the initial success utilizing ChR2 and NpHR in the same preparation demonstrated by Han and Boyden (2007), there have been few subsequent publications using ChR2 with NpHR due to the slow desensitization and recovery period.

1.3.3 Optogenetic approaches for functional mouse brain mapping

A number of functional mapping techniques use ChR2 to interrogate cortical activity at multiple levels of organization and at multiple spatial scales. While the purpose of this thesis was not to utilize and compare an extensive number of mapping

techniques per se, it is useful to understand the scope of the techniques available for use in functional mapping (Table 1.1). These were taken into careful consideration before we designed our own novel method for optogenetic mapping (Chapter 2). A brief review of some current optogenetic approaches to mapping functional connectivity in the rodent brain is outlined below, ranging from microscale mapping (at the level of the synapse) to macroscale mapping (at the level of the connectome).

Technique	Spatial and temporal resolution	Advantages	Limitations	Future directions	Select references
Single-cell E.phys and ChR2 stimulation / CRACM	- Single synapse or microcircuit (μm) spatial resolution - Microsecond (μs) temporal resolution	- High temporal resolution - Can define layer-specific connections (CRACM)	- Sparse spatial sampling - Not suitable for chronic studies	- Assess response using optical tools (i.e. GECIs)	Petreanu et al., 2007 Avermann et al., 2010 Mateo et al., 2011
ChR2-mediated light based motor mapping	- Regional (<1mm) spatial resolution - Millisecond (ms) temporal resolution	- Relatively non-invasive for chronic studies	- Motor output, not cortical output measured - Limited to motor cortex	- Red-shifted opsins to minimize light scattering in tissue - Tracking disease progression	Ayling et al., 2009 Hira et al., 2009 Harrison et al., 2012
VSD imaging and ChR2 stimulation *NB: see Chapter 2 for details on this method*	- Regional (100s of μm - mm) spatial resolution - Millisecond (ms) temporal resolution	- VSD (RH1692)excitation does not activate ChR2 - Can map cortical areas independent of behavior or sensory processing	- Phototoxicity/ not suitable for chronic studies - Limited to cortex - Nonspecific dye targeting - Images during photostimulation are saturated and cannot be used	- Cell-specific targeting and chronic imaging (i.e. VSFPs)	Lim et al., 2012
Opto-fMRI	- Global (mm) spatial resolution - Second (s) temporal resolution	- Relatively non-invasive for chronic studies - Can be done in awake or anesthetized animals	- Relatively undefined BOLD signal - Animals must be head-fixed - Poor temporal resolution	- Multiple sites of stimulation - Longitudinal studies of disease and/or plasticity	Desai et al., 2010 Lee et al., 2010 Kahn et al., 2011

Table 1.1 Optogenetic functional mapping techniques. CRACM: channelrhodopsin-assisted circuit mapping; E.Phys: electrophysiology; GECI: genetically encoded calcium imaging; LBM: light based motor mapping; Opto-fMRI: optogenetic functional magnetic resonance imaging; VSD-ChR2: voltage-sensitive dye imaging using channelrhodopsin-2 stimulation; VSFPs: Voltage-sensitive fluorescent proteins. Table as originally published in Lim et al. (2013) Optogenetic approaches for functional mouse brain mapping. Front. Neurosci. 7:54. doi: 10.3389/fnins.2013.00054

1.3.3.1 Functional mapping of synaptic and columnar architecture using optogenetic stimulation in brain slices

Initially, electrophysiological recordings were used to investigate functional properties of individual and groups of neurons in response to single-point electrical stimulation (Scanziani and Hausser, 2009) or glutamate uncaging (Callaway and Katz, 1993; Katz and Dalva, 1994; Hooks et al., 2011). These techniques offer excellent temporal resolution at the level of the single cell and have been used to create layer-specific wiring diagrams of the rodent sensory and motor cortex (Weiler et al., 2008; Anderson et al., 2010). Although these are labour-intensive experiments, they provide detailed data on synaptic connectivity and the temporal dynamics of the response. Such mapping studies are best applied in brain slices and typically have not evaluated *in vivo* connectivity. These techniques complement emerging high-throughput structural mapping techniques (Denk and Horstmann, 2004; Lu et al., 2009; Kleinfeld et al., 2011; Gong et al., 2013).

Recently, electrophysiological recordings have been applied in combination with optogenetics to investigate cell-type-specific responses within a small network (Figure 1.7 A). Avermann and colleagues investigated synaptic connectivity in the mouse barrel cortex *in vitro* by comparing synaptic responses from different neuronal types (Avermann et al., 2012). Layer 2/3 excitatory neurons expressing ChR2 were photostimulated, and responses were measured from GABAergic fast-spiking (FS) and GABAergic non-fast-spiking (NFS) cells through multiple simultaneous whole-cell recordings. Stimulation of the layer 2/3 neurons resulted in large-amplitude depolarizing postsynaptic potentials in FS GABAergic neurons, but small-amplitude subthreshold postsynaptic potentials in NFS GABAergic neurons. The authors suggest that FS GABAergic neurons play a large role in excitatory neuron inhibition within the barrel cortex. This study demonstrates the use of optogenetic methods in an *in vitro* brain slice preparation and the ability to monitor functional synaptic connectivity.

An important topic in brain connectivity is understanding how neurons can integrate multiple inputs, and the function of a neuron within the larger scope of a circuit. Optogenetic techniques have been applied to questions concerning circuit-level connectivity in mouse brain by targeting multiple sites for photostimulation at the level of

the sub-cellular compartments, such as afferent axons (Petreanu et al., 2009), (Figure 1.7 B). ChR2 assisted circuit mapping (CRACM) combines photostimulation of multiple points in the sample with post-synaptic recording to investigate cortical circuits in brain slices (Petreanu et al., 2007; Atasoy et al., 2008; Petreanu et al., 2009; Haubensak et al., 2010). Similar to laser scanning photostimulation (LSPS), which maps excitatory connections within a network through glutamate uncaging and post-synaptic recordings (Callaway and Katz, 1993; Katz and Dalva, 1994), CRACM maps excitatory connections through optogenetic stimulation. However, unlike LSPS, which excites all cells but not axons of passage (Katz and Dalva, 1994; Petreanu et al., 2007), CRACM excites only ChR2-expressing cells, allowing for cell-type-specific mapping of local and long-range cortical circuits, such as those found within a cortical column (Petreanu et al., 2007; Petreanu et al., 2009; Mao et al., 2011; Hooks et al., 2013). For example, using CRACM in the somatosensory cortex of the mouse, layer-specific projections were identified and quantified (Petreanu et al., 2007). Layer 2/3 axons had the strongest connection with layer 5 neurons, followed by layer 2/3 and layer 6 neurons, but not layer 4 neurons. This laminar specificity was similar in ipsilateral (local) and contralateral (callosal) projections. Such microcircuits are presumed to be stereotypical within a certain cortical area and form the foundation of cortical function (Douglas and Martin, 2004), making the investigation of these circuits central to our understanding brain connectivity. In the future, it is expected that photostimulation and cellular optical recording using organic or genetic voltage or calcium sensors (Grinvald and Hildesheim, 2004; Knopfel, 2012) will be combined to allow the recording of signals from large ensembles of cells. Moreover, the recent advance of two-photon-mediated excitation of ChR2 (Papagiakoumou et al., 2010; Packer et al., 2012; Rickgauer and Tank, 2012) may help to produce more discrete activation in future studies.

The CRACM technique is desirable because it can isolate the specific contribution of each cell within the slice, avoiding long-range connections and subcortical contributions. At the same time, however, this technique cannot be used for within-animal longitudinal studies because it is limited to brain slices. Furthermore, while patterns of photostimulation using various sequences and rapid scanning can be used to investigate the basic connectivity within a circuit, it is unlikely that it can effectively

mimic the numerous inputs, various sequences of activation, and temporal relationships between multiple neurons that are constantly contributing to the function of the circuit *in vivo* (Katz and Dalva, 1994). For this reason, it is important to consider both *in vitro* and *in vivo* experiments in order to understand functional brain connectivity.

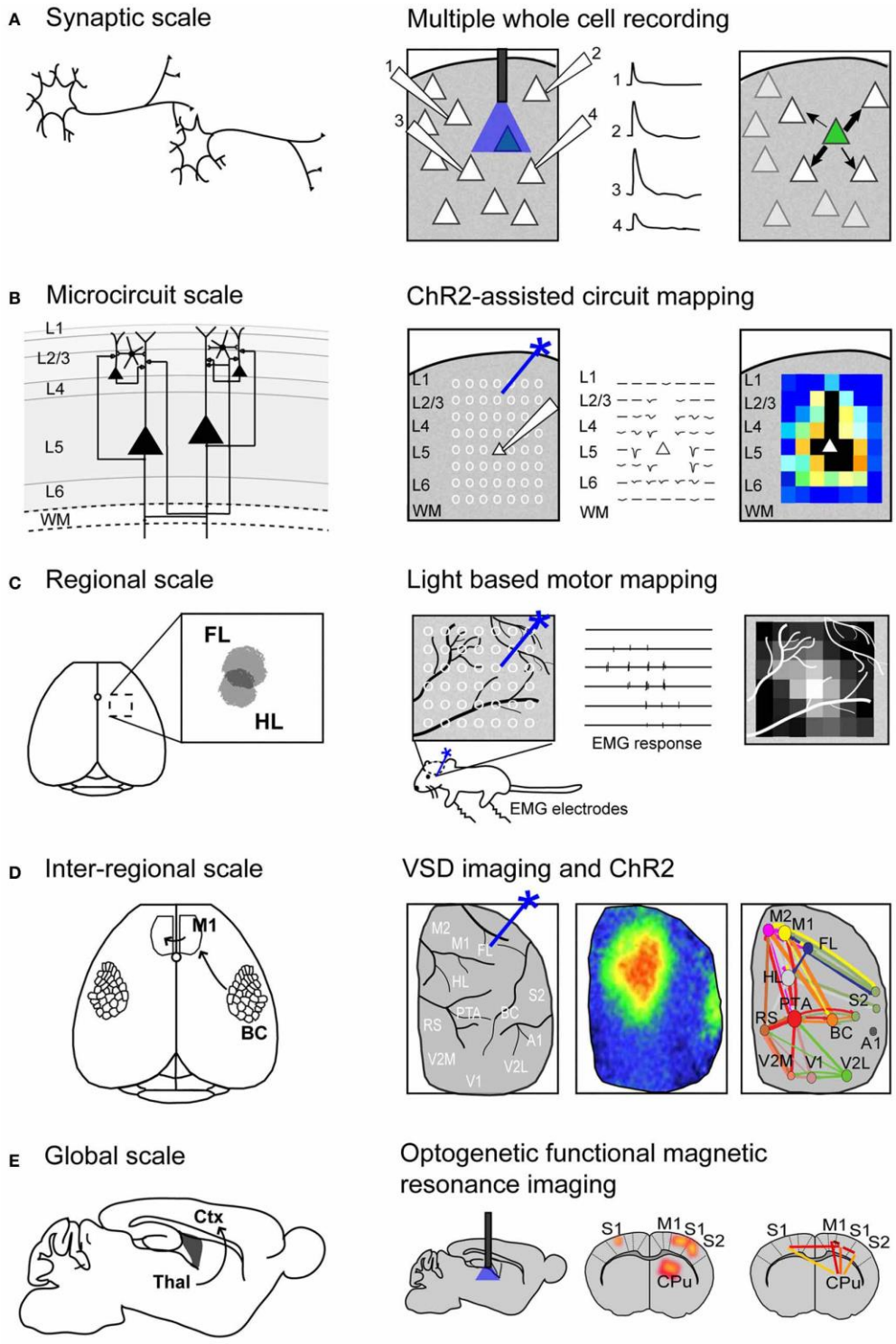

Figure 1.7 Using channelrhodopsin-2 stimulation to map functional connectivity at multiple scales of mouse brain organization. (A) Mapping functional synaptic connectivity between individual neurons (left) using multiple whole-cell recordings (right). ChR2-expressing neurons (indicated in green) are photostimulated and the electrophysiological response is recorded in one or more target neurons (numbered 1-4). (B) Mapping functional connectivity within a column of neurons or a microcircuit (left) using ChR2-assisted circuit mapping (right). Multiple regions within the column are photostimulated (indicated by the white circles) and the response is recorded from a

(Figure 1.7 continued) single target neuron (white triangle). L = layer; WM = white matter. (C) Mapping functional connectivity within a region of cortex (left) using light-based motor mapping (right). A number of regions within the motor cortex are targeted for photostimulation (indicated by white circles) and the resulting motor responses are recorded through electromyograms (EMG) to determine function. mFL = forelimb area of the sensorimotor cortex; mHL = hindlimb area of the sensorimotor cortex (D) Mapping inter-regional functional connectivity (left) using VSD imaging and ChR2 stimulation (right). Multiple regions of interest are targeted for photostimulation and the resulting VSD response (change in fluorescence) is recorded to indicate strength of connections between functional regions. A1 = auditory cortex; BC = barrel cortex; FL = forelimb area of the primary somatosensory cortex; HL = hindlimb area of the primary somatosensory cortex; M1 = primary motor cortex; M2 = secondary motor cortex; PTA = partial association cortex; RS = retrosplenial cortex; V1 = primary visual cortex; V2L = lateral secondary visual cortex; V2M = medial secondary visual cortex. (E) Mapping global functional connectivity (left) using optogenetic functional magnetic resonance imaging (right). ChR2-expressing neurons are photostimulated with an optical fiber and the resulting BOLD signal is recorded over the whole brain. CPu = caudate putamen; Ctx = cortex; M1 = motor cortex; S1 = somatosensory cortex; S2 = secondary somatosensory cortex; Thal = thalamus. Figure as originally published in Lim et al. (2013) Optogenetic approaches for functional mouse brain mapping. Front. Neurosci. 7:54. doi: 10.3389/fnins.2013.00054

1.3.3.2 Functional mapping of the sensorimotor cortex using optogenetic stimulation in vivo

Early maps of the human cortex were based on structure and relied on cytoarchitecture to define boundaries between cortical areas (Garey, 2006; Triarhou, 2007). In order to create an organizational map based on function rather than structure, a method is required that has the ability to stimulate the cortex and a means of measuring the output. Historically, this has been achieved in humans by observing behavioural output following cortical stimulation with single penetrating electrodes (Penfield and Boldrey, 1937; Penfield, 1950), or in animal models by measuring motor output following intracortical microstimulation (ICMS) at multiple sites of the sensorimotor cortex (Neafsey et al., 1986; Mitz and Wise, 1987).

We and others have developed a new method – light based mapping (LBM) – for *in vivo* sensorimotor cortex mapping in the mouse (Ayling et al., 2009; Hira et al., 2009; Komiyama et al., 2010). This method uses optogenetics to stimulate the sensorimotor cortex with high spatiotemporal resolution while recording evoked motor movements to determine cortical function (Figure 1.7 C). A grid of stimulation points was targeted over the sensorimotor cortex of transgenic mice (line 18, from Jackson labs) predominantly expressing ChR2 in the layer 5 pyramidal cells in the cortex (Arenkiel et al., 2007). Sites were photostimulated with 473nm light to selectively activate ChR2-expressing cells, and the evoked motor responses (electromyograms) were recorded. ICMS can be used in a similar fashion to map the topography of the motor cortex (Neafsey et al., 1986; Mitz and Wise, 1987), however, electrical stimulation will activate all cells and axons of passage

without discrimination (Asanuma et al., 1976) and will stimulate both orthrodromic and antridromic activity (Tehovnik, 1996; Histed et al., 2009; Griffin et al., 2011) (Figure 1.8 A)**,** bringing in to question how well the stimulated activity resembles endogenous cortical activity. Moreover, ICMS is not suitable for longitudinal studies. In contrast, LBM selectively stimulates ChR2-expressing neurons, allowing for more precise control of which connections are being stimulated (Figure 1.8 B). While ICMS can be used to map the sensorimotor cortex with relatively high precision, there is a time-cost involved in raising and lowering the stimulating electrode at each site, and electrode insertion will cause tissue damage and could alter cortical function. In comparison, hundreds of cortical sites can be optically stimulated (in a randomized order), in a matter of minutes with LBM, and the stimulation is less invasive, allowing for repeated mapping over time without the risk of tissue damage associated with ICMS (Harrison et al., 2012). Repeated sampling using LBM may result in maps with fewer artefacts and higher definition. Furthermore, rapid stimulation is important for *in vivo* anesthetized experiments since cortical activity is affected by time-dependent changes in the depth of anesthesia (Erchova et al., 2002).

While LBM has several advantages over ICMS, the spatial resolution using LBM will be limited due to overlapping dendritic arbors and light scattering in the tissue (Ayling et al., 2009). A red-shifted ChR2 (Zhang et al., 2008), may be an advantage as red light will not scatter as much as blue light in the tissue. Another limiting factor for ChR2-mediated LBM is the limited availability of animal models, other than rodents, that express ChR2 over wide regions of cortex. Thus far, LBM has only been applied in the mouse (Ayling et al., 2009; Hira et al., 2009; Komiyama et al., 2010; Harrison et al., 2012; Hira et al., 2013) and the spatial resolution of LBM may be insufficient to map the finest details of the relatively small mouse motor cortex. Advancements in the generation of transgenic species, such as the rat (Tomita et al., 2009), or in ChR2 expression through *in utero* electroporation (Huber et al., 2008), would allow this technique to be applied to an animal model with a relatively larger motor cortex (Jazayeri et al., 2012), which may increase the method's relative resolution assuming factors such as light scattering are relatively constant across animals with variable motor cortex size (Aravanis et al., 2007). Furthermore, improvements in cell-specific ChR2 expression (Madisen et al., 2012) may

allow for the generation of cell-specific maps within the sensorimotor cortex. Recently, we have applied LBM to investigate complex forelimb movements (Harrison et al., 2012). We found that prolonged stimulation of the sensorimotor cortex reliably evoked two types of forelimb movements – abduction and adduction movements – and these were generally organized within the sensorimotor cortex with the abduction movement representation anterior to the adduction movement representation. LBM has also been applied to identify tongue motor cortical areas for subsequent calcium imaging during a licking task in awake, head-fixed mice (Komiyama et al., 2010). Together, these studies demonstrate that LBM can be applied to map complex motor movements, and may allow us to draw conclusions about the organization of the sensorimotor cortex. In the future, LBM may be useful for the investigation of cortical map dynamics over time in a disease model (Carmichael, 2003; Dancause and Nudo, 2011), or after motor learning (Kleim et al., 1998).

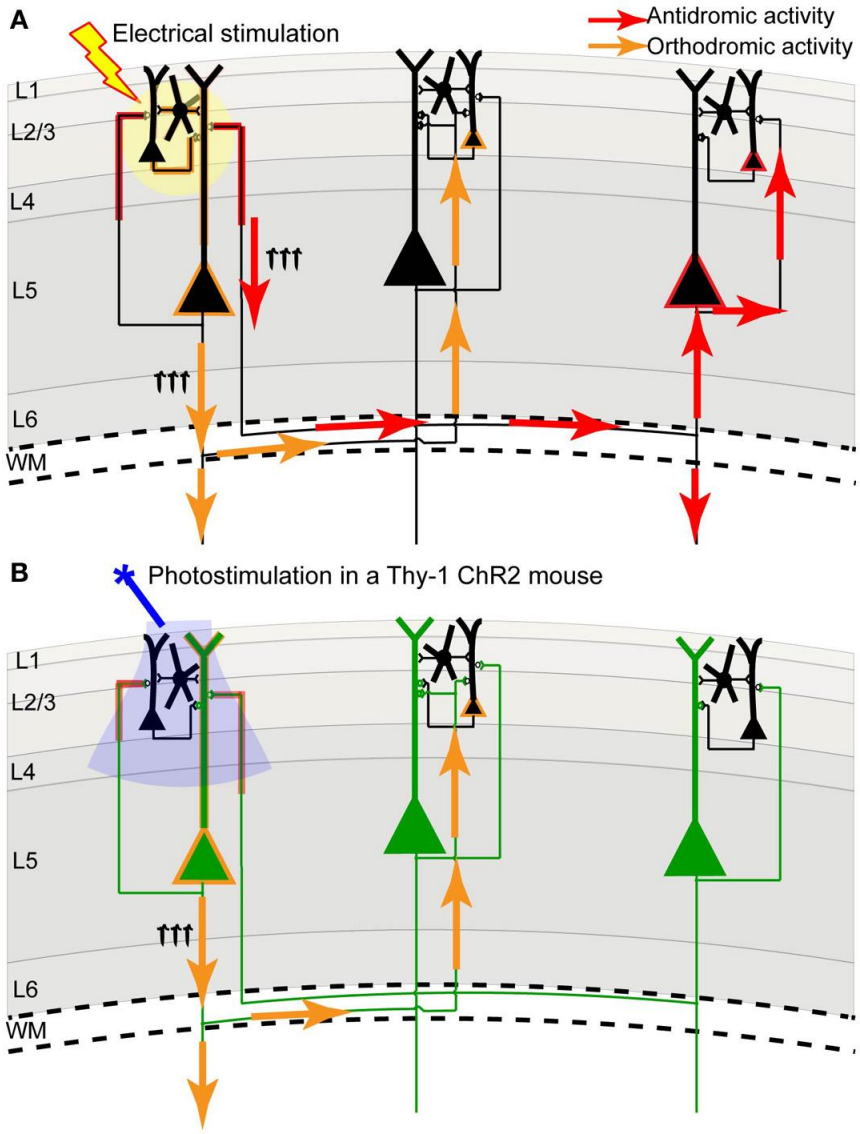

Figure 1.8 Channelrhodopsin-2 stimulation in the Thy-1 transgenic mouse may result in more specific activation compared to direct electrical stimulation. (A) In direct electrical stimulation all cellular components and all cell types within the area of electrical stimulation (indicated by the yellow circle) are activated, inducing both antidromic (axon to soma/dendrite; red arrows) and orthodromic (dendrite/soma to axon; orange arrows) activation. Because electrical stimulation can activate axons (including axons of passage), it may reveal the source of a projection and not its target. (B) In photostimulation of the Thy-1 line 18 transgenic mouse (Arienkiel et al., 2007), predominantly layer-5 ChR2-expressing neurons (indicated in green) are directly activated. While ChR2 is expressed in both axons and dendrites, we suggest that the tuft dendrites of layer 5 neurons are more prominent near the brain surface (where light stimulation is directed) and more likely to become activated, inducing primarily orthodromic synaptic stimulation of distant targets (as determined by antagonist sensitivity; Lim et al., 2012). Figure as originally published in Lim et al. (2013) Optogenetic approaches for functional mouse brain mapping. Front. Neurosci. 7:54. doi: 10.3389/fnins.2013.00054

1.3.3.3 Functional regional mapping using optogenetic stimulation in vivo

Light-based mapping is an effective method for determining the organization of the sensorimotor cortex, yet because it is based on motor output rather than cortical output, it is limited to the sensorimotor cortex. Questions remain about the cortical connections and their function, such as: what are the cortical connections to and from a particular region of interest? Are other cortical regions involved in downstream processing? In order to answer these questions, a method capable of addressing the wide spatial scope of cortical activity is necessary. VSD imaging has already been demonstrated to be a useful tool for large-scale *in vivo* imaging in the rodent brain (see section 1.2), but has had limited scope because most studies are restricted to peripheral stimulation (using well-known sensory systems such as the barrel cortex or visual cortex). This was the driving force behind the development of a novel method for optogenetic mapping using voltage-sensitive dye (VSD) imaging in combination with ChR2 stimulation (VSD-ChR2) (Figure 1.7 D), which is detailed in Chapter 2. The combination of these two methods, which had never been accomplished before *in vivo*, allowed for unprecedented stimulation and recording of a large-scale cortical response, resulting in functional regional cortical maps (see Chapter 2 for complete details).

1.3.3.4 Functional global mapping using optogenetic stimulation in vivo

Thus far, the methods described are effective for determining synaptic or even regional connectivity within the cortex, however, they are not capable of answering questions about global connectivity and the contribution of subcortical structures. Blood oxygenation level dependent (BOLD) functional magnetic resonance imaging (fMRI) is a widely used technique for non-invasive, whole-brain imaging in animal and human studies. Although the relationship between BOLD signals and neuronal coupling is still incompletely understood (Logothetis and Pfeuffer, 2004; Logothetis, 2007), fMRI is an attractive technique for investigating the distribution of neuronal activity within the brain because it is non-invasive. Recently, fMRI has been combined with optogenetics (Lee et al., 2010; Desai et al., 2011; Kahn et al., 2011; Abe et al., 2012) to study the distribution of cortical and subcortical activity following cell-type-specific stimulation (Figure 1.7 E). These studies demonstrated that optogenetic fMRI (opto-fMRI) could be used to stimulate network activity and identify long-range projections on a global scale.

The first study to employ opto-fMRI was by Lee et al. (2010). They used a rat model expressing ChR2 in the excitatory neurons of the motor cortex (M1) and observed activity in the thalamus after light stimulation of ChR2-expressing neurons in M1. Light pulses delivered via an optical fiber were able to reliably drive neuronal firing in ChR2-expressing neurons and in areas distal to the stimulation site, suggesting connectivity between the stimulation site and these distant areas. They further explored global cortical connections through optogenetic stimulation of different thalamic nuclei. Optogenetic stimulation of the posterior thalamic nucleus resulted in a BOLD response in the ipsilateral somatosensory cortex, while stimulation of the anterior thalamic nucleus resulted in a bilateral motor cortex BOLD response, suggesting that thalamic projections differ between the somatosensory cortex and the motor cortex, consistent with previous neuronal tracing reports (Alloway et al., 2008).

Opto-fMRI has also been applied in transgenic mice expressing ChR2 primarily in the layer 5 pyramidal neurons. Here, both the BOLD signal and the local field potential (LFP) responses to photostimulation were recorded (Lee et al., 2010; Kahn et al., 2011). ChR2 stimulation in the barrel cortex was shown to elicit similar regions of BOLD activity compared to sensory stimulation of the whiskers (Kahn et al., 2011), suggesting optogenetic stimulation is a feasible alternative for eliciting BOLD responses and determining global functional connections. In an awake mouse model, opto-fMRI was used to show connectivity between the primary barrel cortex (BCS1) and structures that are known to be connected to the primary somatosensory cortex, including secondary sensory areas and subcortical areas such as the striatum (Desai et al., 2011). ChR2 stimulation was able to reliably elicit a hemodynamic response (BOLD signal) in the local region of stimulation as well as downstream areas, consistent with BOLD fluctuations observed in human studies (Fox and Raichle, 2007; Fox et al., 2007). This correlation, combined with the ability to use opto-fMRI in an awake animal model, will make opto-fMRI an important technique for translational studies of disease, learning or plasticity. However, because of technical constraints, it is not yet possible to produce multi-site high definition photostimulation as presented for other optogenetic mapping techniques (see above).

Opto-fMRI is limited by the incomplete understanding of the relationship between neural activity and cerebral blood flow. Previous reports have demonstrated that ChR2 activation in an *in vivo* mouse model results in increases in blood flow and oxygenation that can occur independent of ionotropic glutamatergic synaptic transmission (Scott and Murphy, 2012), presumably due to direct activation of neurons and secondary non-synaptic activation of other cells. Indeed, Lee et al. caution that the ChR2-evoked BOLD response may include contributions from cells other than those optically stimulated (Lee et al., 2010), as is likely the case for any active network of cells. Furthermore, a recent study suggests that light stimulation may affect the BOLD signal even in a naïve brain (Christie et al., 2012). Despite this incomplete understanding, some conclusions from opto-fMRI may be supported through additional measures, such as structural mapping (Assaf and Pasternak, 2008; Damoiseaux and Greicius, 2009) and due to the relatively non-invasive nature of opto-fMRI it remains a valuable platform for translational studies involving brain connectivity.

1.3.3.5 Future prospects for optogenetic mapping in vivo

The techniques reviewed here could be used to deduce impaired functional relationships between various cortical areas in disease models, especially for diseases such as autism where the underlying mechanism is poorly understood (Qiu et al., 2011), or could be used to examine and monitor recovery after brain injury, such as stroke (Murphy and Corbett, 2009; Krakauer et al., 2012). It is even possible that neuronal connectivity maps will be someday paired with maps of the cerebrovasculature (Tsai et al., 2009), to understand the effects of perturbations to flow during even relatively small strokes (Shih et al., 2013). Clearly, developing comprehensive maps is going to be a significant task due to the complexity of the brain and the number of variables that need to be considered. While there has yet to be developed a single perfect method for *in vivo* arbitrary point functional mapping (

Table 1.2), through combining information gathered from a variety of techniques and by taking advantage of technological advancements such as optogenetics, we will continue to gain important insights on cortical organization and function.

Property	Description	Suitable techniques	Unsuitable techniques
Longitudinal assessment	Relatively non-invasive and non-toxic for longitudinal (chronic) studies	LBM VSFPs GECI-C1V1 Opto-fMRI	VSD-ChR2 CRACM
High temporal resolution	Relatively fast kinetics (on the order of milliseconds); on par with action potentials	CRACM LBM VSD-ChR2 GECI-C1V1	Opto-fMRI
Wide spatial scale	Can map activity over a large field of view; can track long-range projections	VSD-ChR2 Opto-fMRI	CRACM LBM
Arbitrary point stimulation	Can stimulate defined sites in rapid succession	CRACM VSD-ChR2 GECI-C1V1	Opto-fMRI
Reports neuronal activity	Reports membrane potential changes	CRACM VSD-ChR2 GECI-C1V1	Opto-fMRI
Cell-specific reporting	Reports activity from a defined cell population	CRACM GECI-C1V1	Opto-fMRI

Table 1.2 Properties of an ideal functional mapping technique. CRACM: channelrhodopsin-assisted circuit mapping (Petreanu et al., 2007); GECI-C1V1, genetically encoded calcium imaging using red-shifted channelrhodopsin (C1V1) stimulation (Rickgauer and Tank, 2012); LBM: light based motor mapping (Ayling et al., 2009); Opto-fMRI, optogenetic functional magnetic resonance imaging (Lee et al., 2010); VSD-ChR2: voltage-sensitive dye imaging using channelrhodopsin-2 stimulation (Lim et al., 2012); VSFPs: Voltage-sensitive fluorescent proteins (Akemann et al., 2010). Table as originally published in Lim et al. (2013) Optogenetic approaches for functional mouse brain mapping. Front. Neurosci. 7:54. doi: 10.3389/fnins.2013.00054

1.4 Stroke

1.4.1 Stroke: an important disease

Stroke can be defined as any interruption of blood flow, either through a blocked vessel (in this case, an ischemic stroke), or an uncontrolled bleed (in this case, a haemorrhagic stroke). The brain requires a significant amount of oxygen to maintain function, thus, any interruption of blood flow is dangerous. Within minutes of oxygen deprivation, a whole cascade of events will occur (Figure 1.9), (Lakhan et al., 2009). The cells within the core area of oxygen deprivation (known as the infarct zone), begin to die due to a lack of oxygen, and ionic and neurochemical balance is disrupted (Durukan and Tatlisumak, 2007). Cells neighbouring the infarct zone (known as the peri-infarct), begin to degenerate and retract, and over time these axons will re-route (Murphy and Corbett, 2009). Axons and dendrites swell, taking on abnormal morphology (Brown et al., 2008). The inflammatory response begins, eliciting a whole host of reactions (Carmichael, 2006). Depending on where the stroke is located within the brain, functional deficits and behavioural changes may be evident, and these may change in the days and weeks post-stroke (Murphy and Corbett, 2009).

While it is generally understood that the location and size of a stroke will determine the specific type and degree of behavioural impairment(s), the recovery process remains unclear, and there is no cure for stroke patients. Recovery is variable, and understanding this process and how to improve it remains one of the most important questions in stroke research.

In Canada, stroke is the third leading cause of death, with an estimated incidence of 50,000 strokes per year, or approximately one stroke every 10 minutes (Heart and Stroke (Foundation, 2014). While there have been great strides in stroke management and the mortality rate amongst stroke patients is declining (Canada, 2011; Go et al., 2014), many stroke survivors will experience some sort of long-term disability requiring rehabilitation and/or long-term care, and up to 1/3 will experience post-stroke depression (Go et al., 2014). Taken together, the cost of stroke in Canada in 2010 (including immediate and follow-up care), was estimated to be $2.7 billion (Go et al., 2014). As our population ages, stroke-related costs are expected to increase substantially, with costs estimated to triple by 2030 (Go et al., 2014).

These points highlight the importance of understanding stroke as a disease. As our population ages and the incidence of stroke increases, we will need to find better treatment and rehabilitation strategies to cope with the burden this will place on the health care system and on our families and communities.

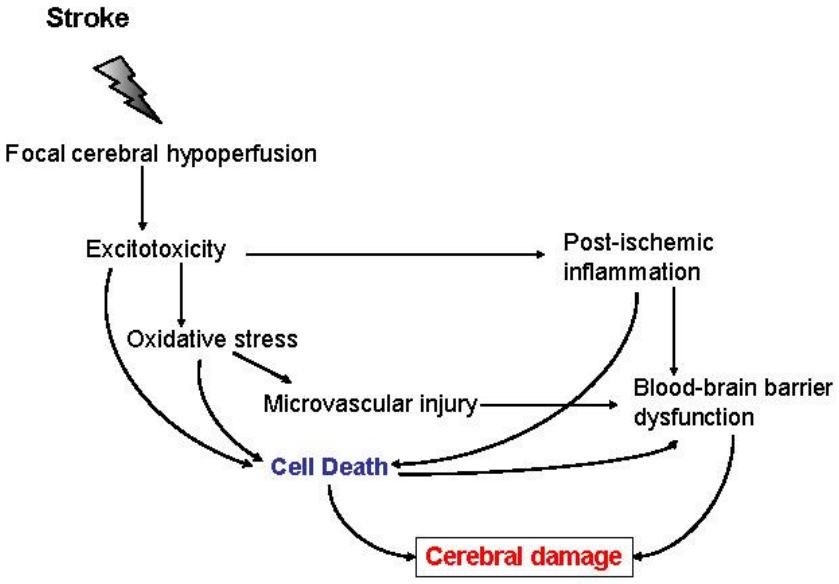

Figure 1.9 Ischemic cascade leading to cerebral damage. Ischemic stroke leads to hypoperfusion of a brain area that initiates a complex series of events. Excitotoxicity, oxidative stress, microvascular injury, blood-brain barrier dysfunction and postischemic inflammation lead ultimately to cell death of neurons, glia and endothelial cells. The degree and duration of ischemia determines the extent of cerebral damage. Reprinted with permission from BioMed Central: Journal of translational medicine (Lakhan 2009. Inflammatory mechanisms in ischemic stroke: therapeutic approaches), Copyright (2009).

1.4.2 Plasticity after stroke

As of yet, there is no cure for stroke, though many patients show some degree of functional recovery after stroke. This recovery has been attributed to neuroplasticity, which can be broadly defined as the constant changes to synaptic strength and synaptic connections that occur in the brain in response to stimuli, including brain injury such as stroke. More specifically, plasticity after brain injury is the ability of the brain to compensate for functional loss through both structural and functional adaptations (for a review, see Murphy and Corbett 2009).

Following a focal stroke, there are two main areas of injury. The infarct core is the area that is irreversibly damaged due to ischemia. Within the infarct core, blood flow falls below 20% of baseline blood flow and cellular function ceases (Heiss, 2012). Within minutes, hypoxic death occurs, and even with reperfusion, this area remains damaged (Brown et al., 2007; Li and

Murphy, 2008). The surrounding area, known as the penumbra or peri-infarct, is tissue that is ischemic but may not be fully or permanently damaged. Here, blood flow falls between 25% and 50% of pre-occlusion levels (Heiss, 2012). It is possible for damage within the peri-infarct zone to be reduced or even reversed depending on whether the region has adequate collateral arteries and/or if reperfusion is established soon after ischemia. In a clinical setting, the survival of the penumbra varies from patient to patient, however the more time passes after the stroke onset, the less likely that the penumbral tissue can be salvaged (Bivard et al., 2011). Thus, the peri-infarct zone is the area that is the target of many acute pharmacologic interventions, with the hope of reperfusing this tissue to minimize cell death and ischemic damage.

While these are the main areas that are affected by stroke, numerous studies have reported that stroke can affect more than just the ischemic area –distal areas that may have connections to the infarcted area (for example, homotopic areas) can show deficits after stroke despite being removed from the ischemic territory (Dancause et al., 2005), subcortical areas may experience retrograde damage resulting from a cortical stroke (Iizuka et al., 1990; Dancause et al., 2005; Jablonka et al., 2010), and even healthy tissue in the ipsilesional hemisphere may experience reduced metabolic activity and be affected (Dancause et al., 2005). From a cortical mapping perspective, two processes occur after stroke: diaschisis and vicariation.

The term diaschisis, meaning "shocked throughout", was first coined by Von Monakow in 1914 to describe post-stroke dysfunction in an intact region that was separate from the stroke core. Recently, a number of different classes of diaschisis have been described and reviewed (for a full review, see Carerra and Tononi 2014). Focal diaschisis (Feeney and Baron, 1986) may include a loss of excitability or change in functional responsiveness at a region distant to the lesion. A more recent description of diaschisis takes a broader perspective – connectional diaschisis describes a change in coupling between two nodes within a defined network, likely due to lost afferents from the lesioned node (Campo et al., 2012). Finally, the broadest perspective of diaschisis is connectomal diaschisis, which describes changes in the structural and/or functional connectome as a result of stroke. This includes disconnections or reorganizations between different networks or different clusters, which may be distant from the lesion itself (Carrera and Tononi, 2014). In the past, focal diaschisis had limited clinical evidence, but improved imaging techniques and a better understanding of brain networks has led to an increase in the investigation of connectional and connectomal diaschisis after stroke. While

still a relatively new area of research, connectional and connectomal diaschisis seems to have more consistent clinical relevance (compared to focal diaschisis), with some evidence for the best recovery after stroke correlating to normalization of remote connectivity changes (Carrera and Tononi, 2014). For a better understanding of connectional and connectomal diaschisis after stroke, it will be essential to take a macroscopic approach in experimental stroke studies. Thus, the global network will need to be considered after stroke, rather than just local changes.

Vicariation is a process of remapping or reorganization after stroke, where healthy cortical tissue will assume the function of the infarcted area. Such remapping was first described in the 1980s (Kaas et al., 1983; Merzenich et al., 1983). In these classic studies, the authors mapped the somatosensory cortex of monkeys following peripheral damage and found that the somatosensory cortex subsequently underwent dramatic structural and physiological reorganization. These studies showed that the cortical map was plastic, even in adult monkeys, and showed that dis-use or behavioural training had an effect on remapping. Furthermore, these studies showed that this type of plasticity was a normal function of the cortex because somatosensory cortex reorganization occurred with or without intervention. Such reorganization or remapping has since been described in both animal models of stroke (Brown et al., 2009) and in clinical studies of human stroke patients (Gerloff et al., 2006; Xerri, 2012). Remapping can take place in both the contralesional and ipsilesional hemisphere (Dancause, 2006), and has been measured both structurally and functionally: there is evidence for increased axonal sprouting in the contralesional hemisphere (Overman et al., 2012), and evidence of functional remapping as measured through intracortical microstimulation (Nudo and Milliken, 1996), intrinsic optical signal imaging (Frostig et al., 2008; Scott and Murphy, 2012; Anenberg et al., 2014), or VSD imaging (Brown et al., 2009; Mohajerani et al., 2011) in animal studies, or through fMRI in clinical studies (Grefkes and Fink, 2011). While the concept of remapping following stroke is now generally accepted, even after small focal lesions (Mohajerani et al., 2011), questions remain about whether post-stroke changes to functional maps are adaptive or maladaptive, and whether we can shape the course of this remapping using strategies such as targeted stimulation (i.e. transcranial magnetic stimulation; TMS) or rehabilitation (i.e. enriched environments, constraint-induced movement therapy etc.).

1.4.3 Animal models of ischemic stroke

Based on clinical studies of stroke, a limited amount of progress has been made in understanding the mechanism underlying stroke and in understanding the immediate effects of stroke. This is mainly due to the fact that strokes between patients are quite variable (based on size, location, type of stroke, age of patients, health of patients etc.) and because many patients do not arrive at the hospital immediately after a stroke. This means that there is limited controlled data from clinical studies. There are many case studies of stroke, and many studies that take place in the days, weeks, and months after stroke, but few that take place in the hours or minutes after stroke. This is where animal models of stroke have become increasingly useful.

Primate models of stroke are most desirable for translational research because the primate brain is most similar to the human brain in terms of complexity and functional organization, however, experimental research on primates is challenging because of strict ethical guidelines and increased costs. Thus, rodent models have been the predominant animal model of stroke (Carmichael, 2005), and there are a number of models available. Some models have been designed to specifically model a certain condition or to test a specific therapy. Rodent models of stroke have been criticized for using young animals or using models of stroke that are dissimilar from what is typically seen in the clinical setting (Cheng 2004). Several models of stroke are described below.

1.4.3.1 Middle cerebral artery occlusion

One of the most common models of stroke is the middle cerebral artery occlusion (MCAO). This technique creates large cortical stroke, and can be either permanent or temporary (allowing reperfusion). The middle cerebral artery is occluded using a suture to block the vessel (Longa et al., 1989) or by using microvascular clips (Carmichael, 2005), and may be left in place for a permanent MCAO, or may be removed after a set period of time to cause reperfusion and a temporary MCAO. This model is beneficial because it does not require a craniotomy and produces large lesions (up to 45% of the injured hemisphere) and includes damage to subcortical regions such as the striatum, as well as the cortex in areas like the parietal cortex (Carmichael, 2005). Because it creates extensive damage to a number of regions, it also is associated with a large number of deficits including motor, sensory and cognitive impairments. While this model represents a relatively good model of human strokes because it avoids craniotomy, it causes damage beyond what is considered treatable in human stroke patients; the majority of treatable

strokes in humans are less than 14% of the affected hemisphere (Roome et al., 2014). This makes the clinical relevance of the MCAO model debatable. However, a similar model exists which creates less damage called the common carotid artery occlusion (CCAO) – here the common carotid is occluded using a suture. It is possible to do a bilateral CCAO for a global model of ischemia or a unilateral CCAO for a focal model of ischemia. While the artery occlusion models are consistent in generating lesions in rats, they are less consistent between various strains of mice (Carmichael, 2005). It has been shown that the C57BL/6 strain, which has poor development of the circle of Willis, is the most susceptible to this model of stroke, as measured by neurological signs, histology, and India ink perfusion patterns (Yang et al., 1997; Kitagawa et al., 1998). This makes the MCAO somewhat less reliable when it comes to mouse models of stroke.

1.4.3.2 Photothrombotic stroke

A common method for inducing targeted cortical strokes is the photothrombotic stroke model. Here, Rose Bengal, a photosensitive dye, is injected intravenously or intraperitoneally into the animal, and the cortical region of interest is irradiated with a green laser or epifluorescent light source through the intact skull (Watson et al., 1985). The irradiation creates singlet oxygen species that causes platelet activation and a microvascular occlusion (Carmichael, 2005; Murphy and Corbett, 2009). The primary benefit of this model is that the occlusion can be targeted anywhere on the cortex – the light simply needs to be targeted to the desired area – and these strokes are consistent and reproducible between animals. Similarly, this method allows for greater control over the size of the stroke (both in depth and in width) by varying the amount of cortex that is exposed to irradiation or by varying the duration of light irradiation; longer duration creates deeper lesions, in some cases all the way down to the white matter. The downside of this model is that it is limited to creating cortical strokes. Because of this, it has been criticized as having limited clinical relevance. Nonetheless, compared to other stroke models, this model is relatively non-invasive because the skull can remain intact, and is also gives the experimenter a high degree of control over the stroke size and location, with the precision of targeting a single microvessel (Sigler et al., 2009; Shih et al., 2013).

1.4.3.3 Endothelin-1 injections

Another method for creating focal strokes is through the injection of endothelin-1 (ET-1). Endothelin-1 is a vasoconstrictor peptide that can be injected intracerebrally using stereotaxic coordinates to occlude the MCA or to occlude other blood vessels of interest (Sharkey and Butcher, 1995). The ET-1 injection is relatively fast and is less technically challenging compared to the MCAO. It is better for creating small, targeted strokes rather than large cerebral strokes (Horie et al., 2008). A major disadvantage of this method is that while it consistently produces ischemic lesions in rats, it does not have a consistent effect on mice, even at large doses (Horie et al., 2008). The discrepancy between rats and mice remains unclear (Horie et al., 2008), and while there is some indication that ET-1 could be used in combination with other methods to create lesions (Wang et al., 2007b; Horie et al., 2008), this method is not a popular choice as a mouse model of stroke (however, see Roome et al., 2014).

1.4.3.4 Embolic stroke models

There are various models of embolic stroke. These may include the injection of microspheres (Miyake et al., 1993) or macrospheres (Gerriets et al., 2003), or thrombotic clot embolization (Overgaard et al., 1992). Macrospheres (300-400 μm in diameter) or microspheres (approximately 50 μm in diameter) can be injected into the internal carotid artery where they will travel to the brain and lodge in the middle cerebral artery (macrospheres) or in various places in the brain (microspheres), creating diffuse and distal infarcts and a number of possible behavioural impairments. Recently, microspheres have been used for modelling vascular dementia (Jiwa et al., 2010). The spheres are injected and may lodge anywhere in the brain, creating microinfarcts throughout the brain. Thrombotic blood clot emboli can also be pre-formed and injected into the internal carotid artery (Overgaard et al., 1992). While the embolic stroke models represent a good model of human stroke and vascular dementia, these methods produce highly variable infarcts in terms of number of infarcts, location of infarcts, and size of infarcts, and the mortality rate is high (Carmichael, 2005). Nonetheless, this model of stroke has been very beneficial in testing thrombolytic therapies (Carmichael, 2005).

1.5 Research aims and hypotheses

Research using cortical mapping methods have made enormous progress over the past several years, however, there is a lack of knowledge about functional cortical mapping at the

regional level, especially in areas outside of the primary sensory and motor cortices. As we begin to understand more and more about how the brain functions as a network, we see that any change or injury within the network may have broad effects on network properties or on the network as a whole. This is an important perspective to consider when examining the effects of a brain injury or when creating treatment strategies. With this in mind, this thesis was directed towards precise functional mapping *in vivo,* and then applying this mapping in an animal model of stroke.

Aim 1: Establish large-scale VSD imaging and ChR2 stimulation as a method for mapping and identifying functional circuits within the mouse brain *in vivo*.

Aim 2: Use VSD imaging and ChR2 stimulation in a mouse model of focal stroke to evaluate spatial and temporal changes to cortical circuits post-stroke. Assess network properties after stroke at multiple time-points, considering both global and local connections, and determine whether cortical changes after stroke can be predicted based on network properties.

Hypotheses:

1) Optogenetic mapping combined with VSD imaging will be a useful technique for functional mapping of both local and long-range cortical circuits in the mouse. The combination of these methods will give unprecedented control of cortical stimulation (through cell-specific ChR2 stimulation) and a measure of large-scale cortical responses (through VSD imaging).

2) Cortical stroke will result in network-wide cortical changes (suggesting connectional or connectomal diaschisis), which can be ideally measured using optogenetic mapping combined with VSD imaging.

2. In vivo large-scale cortical mapping using channelrhodopsin-2 stimulation in transgenic mice reveals asymmetric and reciprocal relationships between cortical areas

2.1 Introduction

Functional relationships between brain areas have been deduced through an elegant combination of structural, electrophysiological, and lesion/inactivation studies (Shepherd et al., 2005; Douglas and Martin, 2007). Recently, efforts have begun to exhaustively sample cortical structure at the synaptic, cellular, and regional level to derive maps of cortical wiring (Bohland et al., 2009). In contrast to structural analysis, functional connectivity studies *in vivo* are often restricted to evaluating areas with well-documented sensory input or behavioral links, and have not necessarily sampled connections between multiple arbitrary locations. In brain slices, arbitrary point microstimulation mapping techniques involving glutamate uncaging (Callaway and Katz, 1993; Fino and Yuste, 2011), or channelrhodopsin-2 (ChR2), have been employed to elucidate laminar (Weiler et al., 2008), and transcallosal (Petreanu et al., 2007) relationships in neocortex. Functional mapping between specific sites has been performed *in vivo* through electrical microstimulation (Ferezou et al., 2007; Histed et al., 2009), and combining optogenetic stimulation with functional magnetic resonance imaging (fMRI) (Lee et al., 2010; Logothetis, 2010; Desai et al.; Kahn et al., 2011), yet electrical microstimulation is limited in the number of regions that can be sampled quickly, and fMRI has limited temporal resolution. With these limitations in mind, our goal was to develop an approach that would allow for arbitrary point functional mapping *in vivo* while maintaining relatively high spatiotemporal resolution.

Here we describe an automated approach to assess intrahemispheric and interhemispheric functional relationships by the activation of a subset of ChR2-expressing deep layer cortical neurons in transgenic mice (Arenkiel et al., 2007; Ayling et al., 2009). These mice represent the best current model for reproducible arbitrary point cortical activation over wide spatial scales. Previous work by our lab (Ayling et al., 2009) using comparisons to other well-known mouse strains such as the YFP-H line (Feng et al., 2000), and work from the original developers (Wang et al., 2007a) has shown that these transgenic animals robustly express ChR2 within layer 5 pyramidal neurons, as well as other minority cell populations throughout the neocortex.

Although ChR2 is expressed in axons of passage and exhibits some variability in expression levels across the cortex (Wang et al., 2007a; Ayling et al., 2009), these transgenic mice may have advantages over multiple viral injections due to incomplete sampling and potential for tissue damage at each injection site.

To monitor intracortical activity, fluorescent calcium indicator proteins (Mank et al., 2008; Tian et al., 2009; Lutcke et al., 2010) or recombinant voltage sensors (Perron et al., 2009; Akemann et al., 2010; Borghuis et al.; Minderer et al., 2012) provide the potential to record cell-specific signals. However, these recombinant sensors do not currently offer the ability to monitor activity over large spatial scales (up to 50 mm^2) and with high time resolution without regional variation being introduced due to differences in virus-injection dependent sensor expression. Small molecule calcium indicators have provided much insight into developmental and local synchronized activity (Golshani et al., 2009), but due to the need to apply bolus loading techniques have been restricted to smaller fields of view (0.3 mm^2). Therefore, we have chosen to monitor regional cortical activity using organic voltage sensitive dyes (VSD) (London et al., 1989; Kleinfeld and Delaney, 1996; Shoham et al., 1999; Petersen et al., 2003a). Using this approach, we show that point photostimulation of deep layer pyramidal neuronal subsets in functionally identified primary sensory cortices reveals cortical maps which are archetypal of the maps obtained via sensory stimulation. We extend the point stimulation to arbitrary areas targeting association cortices and secondary somatosensory regions that are inaccessible to direct stimulation via the senses. We apply graph theory and complex network analysis to connection matrices derived from these self-assembled, functional maps to elucidate reciprocal connections between primary and secondary sensory areas, identify network hubs, and determine asymmetries in intracortical connectivity.

2.2 Materials and Methods

2.2.1 Animals

ChR2 transgenic mice were obtained from the Jackson Laboratory (line 18, stock 007612, strain B6.Cg-Tg (Thy1-COP4/EYFP) 18Gfng/J). Mice were approximately 16 weeks old and weighed ~30 g and were housed in clear plastic cages in groups of two to five, under a 12:12 hour light/dark cycle. Mice were given *ad libitum* access to water and standard laboratory mouse diet at all times. All experiments were conducted with approval from the University of British

Columbia Animal Care Committee and in accordance with guidelines set forth by the Canadian Council for Animal Care.

2.2.2 Surgery

At approximately 16 weeks of age, mice were given a craniotomy. During craniotomy surgery, mice were anesthetized with isoflurane (1.0%), for induction, and urethane (15% w/v, dissolved in distilled water; 1.25 g/kg), for the bilateral craniotomy, or were anesthetized with isoflurane (1.0%), for the duration of the experiment for the unilateral craniotomy. Mice were placed on a metal plate that could be mounted onto the stage of the upright microscope and the skull was fastened to a steel plate. A 7x8 mm bilateral craniotomy (Bregma 2.5 to -4.5 mm, lateral 0 to 4 mm), or 7x6 mm unilateral craniotomy (Bregma 2.5 to -4.5 mm, lateral 0 to 6 mm), was made and the underlying dura was removed, as described previously (Mohajerani et al., 2010). Throughout surgery and imaging, body temperature was maintained at 37 degrees C using a heating pad with a feedback thermistor. In some cases, mice were also given a tracheotomy to assist with breathing.

2.2.4 Cortical electroencephologram (EEG) recording

In order to monitor EEG activity throughout the experiment, two Teflon coated chlorided silver wires (0.125 mm), were placed on the left and right edge of the craniotomy. A reference electrode was placed on the nasal bone. The cortical signal was amplified and filtered (0.1–1000 Hz), using an A-M Systems (Sequim, WA) Model 1700 AC amplifier.

2.2.5 VSD imaging

For *in vivo* VSD imaging, the dye RH1692 (Optical Imaging, New York, NY) (Shoham et al., 1999), was dissolved in HEPES-buffered saline solution (to a final optical density of 5–7, measured at 550 nm) and applied to the exposed cortex for 60-90 min, staining all neocortical layers, as reported previously (Mohajerani et al., 2010). To minimize movement artifacts due to respiration, the brain was covered with 1.5% agarose made in HEPES-buffered saline and sealed with a glass coverslip. For VSD data collection, 12-bit images were captured with 6.67 ms resolution with a CCD camera (1M60 Pantera, Dalsa, Waterloo, ON), and EPIX E4DB frame grabber with XCAP 2.2 imaging software (EPIX, Inc., Buffalo Grove IL). VSD was excited with a red LED (Luxeon K2, 627 nm center), and fluorescence filters as described (Mohajerani et al., 2010). An Olympus BX51WI microscope and XLFluor 2X/340 (0.14 NA), objective provided a

6.4x6.4 mm field of view. The depth of field was 1.20 mm. and was defined by the distance along the optical axis where the resolution was better than 10 lines per mm, corresponding to a maximum blur of 2 pixels. VSD fluorescence was filtered using a 673-703 nm bandpass (Semrock, New York, NY), after reflection by a dichroic mirror (510 dcspxr; 400-495 transmission reflection 550-725 nm, Chroma, Bellows Falls VT), that separated the ChR2 stimulation and VSD imaging light paths (Figure 2.1 A). For each trial, 108 frames were collected at 150 Hz (6.67 ms/frame). Since animals under anesthesia typically exhibit spontaneous cortical activity (Mohajerani et al., 2010), we averaged 4-10 trials of stimulus presentation to reduce these effects. To correct for time-dependent changes in VSD signals that accompany all imaging, we also collected a number of non-stimulation trials that were used for normalization of stimulated data. To reduce potential VSD signal distortion caused by the presence of large cortical blood vessels, we focused into the cortex to a depth of ~0.7 mm. Previous work from our lab has measured VSD fluorescence across the cortex using histology and demonstrated relatively high labelling at even ~750 μm in depth (Mohajerani et al., 2010). Nonetheless, to reduce regional bias in VSD signal caused by uneven dye loading or due to brain curvature, all VSD responses were expressed as a percent change relative to baseline VSD responses ($\Delta F/F_0$*100%).

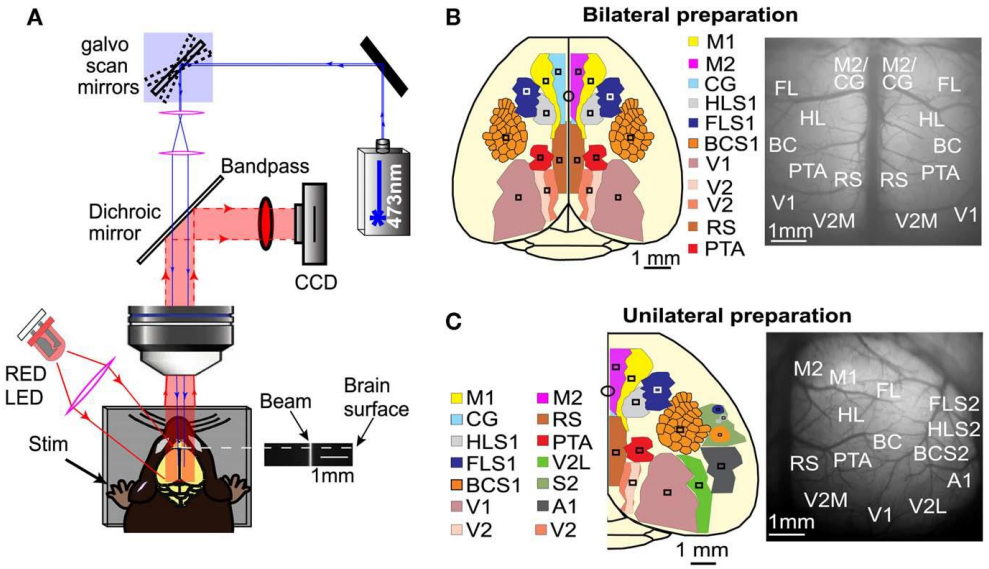

Figure 2.1 Mapping interhemispheric and intrahemispheric connectivity using ChR2 stimulation and VSD imaging. (A) Experimental set up for simultaneous ChR2-photoactivation and VSD imaging. Galvanometer scan mirrors position a 473 nm laser at specific cortical locations while VSd fluorescence is monitored in fluorescence mode. An image of the laser beam demonstrates that it is relatively collimated. (B) Schematic of the bilateral craniotomy preparation showing the 16 different ROIs that were used for photostimulation and simultaneous monitoring of VSD fluorescence. (C) Schematic of the unilateral craniotomy preparation showing the 14 different areas that were stimulated and assayed to examine intrahemispheric connectivity.

2.2.6 Sensory stimulation

Sensory stimuli were used to generate maps of the primary sensory cortical areas - forelimb (FLS1), hindlimb (HLS1) and barrel cortex area (BCS1) of the primary somatosensory cortex, primary visual cortex (V1), and auditory cortex (A1) - in order to compare these responses to ChR2-evoked responses. To map FLS1 and HLS1, probes were inserted into the paws and a 1 mA, 1 ms electrical pulse was delivered. To map BCS1, a single whisker (C2), was attached to a piezoelectric device (Q220-A4-203YB, Piezo Systems, Inc., Woburn, MA), and given a single 1 ms tap using a square pulse. The piezoelectric device was attached ~2 mm from the base of the C2 whisker. The whisker was moved at most 90 µm in an anterior to posterior direction, which corresponds to a 2.6º angle of deflection. A 1 ms pulse of combined green and blue light was delivered in order to map V1. A single 5 ms tone was used to map A1. Visual and auditory stimuli were only used in the unilateral craniotomy, as these areas are difficult to examine in the bilateral craniotomy given the relatively smaller lateral field of view.

2.2.7 Photostimulation

A 473 nm diode pumped solid state laser (CNI Optoelectronics, Changchun, China), was used to stimulate ChR2-expressing neurons. The beam was positioned on the cortex using

custom software written in IGOR PRO (Portland, OR), which controlled galvanometer scan mirrors (Cambridge Tech, Lexington, MA), via analog output voltage from PCI-6115 DAQ (National Instruments, Austin, TX). The beam diameter measured through the objective was 85 μm and was nearly collimated (f-number = 34) due to the relatively small size of the laser beam compared to the back aperture of the objective. This degree of collimation reduced the potential effect of differences in path length due to brain curvature and ensured that the area of photostimulation was limited by light scattering in the tissue (Ayling et al., 2009) rather than the geometry of the laser beam. In the present study, the photostimulation area is comparable to the size of the pixels used for regional voltage sensitive dye imaging (Grinvald and Hildesheim, 2004). The IGOR program controlled the overall timing of individual stimulation trials with TTL triggers to XCAP from a second DAQ (PCI-6036E). Stimuli were delayed relative to the onset of image acquisition by an A-M Systems (Sequim, WA) Isolated Pulse Stimulator (Model 2100).

The intensity and duration of the photostimulation was based on its ability to evoke EEG responses in a ChR2 mouse. We found that relatively low amplitude and short duration single laser pulses were optimal to ensure sufficient activation and a low laser stimulus artifact (typically a 5 mW, 1 ms pulse). Consistent with previous data, this brief activation led to depolarization of the cortex as measured by EEG (Ayling et al., 2009) Further analysis of neuronal activity using optrode recordings after layer 5 ChR2 photostimulation demonstrated that a 1 ms 5 mW laser pulse was able to elicit robust intracortical spiking, and the highest firing rate occurred within 20 ms of photostimulation (See supplementary materials and supplementary Figure 2.9).

During data acquisition for both preparations, stimulation of the photostimulation points was given in an interleaved manner to reduce the effect of time-dependent changes in cortical excitability or depth of anesthesia. Stimuli were given in a semi-random order designed to reduce sequential stimulation at neighboring cortical sites. The site of optical stimulation was not used for ROI quantification due to a transient optical artifact; the VSD was bleached at the site of stimulation, but recovered within 500 ms. A 10 s interval between each photostimulation ensured full recovery of VSD fluorescence before the next trial was collected. Analysis of EEG recordings showed significant EEG depolarizations at all photostimulation sites (data not shown). To reduce the possible effect of unequal ChR2 activation between stimulation sites due

to possible variability in regional ChR2 expression, VSD responses were normalized to the maximum VSD response per stimulation site.

To quantify the spread of evoked signal over the cortex, regions of interest (ROIs) for both stimulation and analysis were determined per animal and located based on relative stereotaxic location (Paxinos and Franklin, 2001) from functionally-defined HLS1 and FLS1 areas. For the bilateral craniotomy, both cortical hemispheres were divided into 9 distinct ROIs (square regions, 0.0625 mm^2). The ROIs for photostimulation and VSD response in the bilateral craniotomy included: (1) secondary motor cortex (M2) and anterior segment of cingulate cortex (CG), (2) primary motor cortex (M1), (3) forelimb area of the primary somatosensory cortex (FLS1), (4) hindlimb area of the primary somatosensory cortex (HLS1), (5) barrel cortex area of the primary somatosensory cortex (BCS1), (6) parietal association area (PTA), (7) retrosplenial cortex (RS), (8) primary visual cortex (V1), and (9) medial secondary visual cortex (V2M) (Figure 2.1 B). VSD responses were measured from all regions for a total of 18 response sites across both hemispheres. All regions were targeted for photostimulation, excluding M1, for a total of 16 photostimulation sites across both hemispheres. For each photostimulation site, VSD responses were collected from all other ROIs. Each site was stimulated 10 times and replicate responses were averaged together.

For the unilateral craniotomy, fourteen ROIs were selected for photostimulation. Sensory stimulation was used to determine the coordinates for the primary sensory areas (HLS1, FLS1, BCS1, V1, and A1) and secondary somatosensory areas (HLS2, FLS2, and BCS2). From these primary sensory coordinates, the relative locations of additional associational areas were estimated. The ROIs for the unilateral craniotomy include: (1) secondary motor cortex (M2) and anterior segment of cingulate cortex (CG), (2) primary motor cortex (M1), (3) forelimb area of the primary somatosensory cortex (FLS1), (4) hindlimb area of the primary somatosensory cortex (HLS1), (5) secondary forelimb cortex (FLS2), (6) secondary hindlimb cortex (HLS2), (7) barrel cortex area of the primary somatosensory cortex (BCS1), (8) auditory cortex (A1), (9) secondary barrel cortex (BCS2), (10) parietal association area (PTA), (11) retrosplenial cortex (RS), (12) medial secondary visual cortex (V2M), (13) primary visual cortex (V1), and (14) lateral secondary visual cortex (V2L) (Figure 2.1 C). VSD responses were measured from all regions for a total of 14 intrahemispheric response sites. All regions were targeted for semi-

random photostimulation for a total of 14 stimulation sites in one hemisphere. Each site was stimulated 2-4 times and replicate responses were averaged together.

2.2.8 Data analysis

VSD responses to stimulation were calculated in MatLab (Mathworks, Natick, MA) as the normalized difference to the average baseline recorded before stimulation ($\Delta F/F_0*100$). VSD data occurring at a frame rate of 150 Hz were interpolated in MatLab (1000 Hz) for ROI analysis to better match sampling rates of other signals (i.e. EEG). Responses were quantified at all ROIs listed above (square regions 0.0625 mm^2) at 6 ms, 12 ms, and 20 ms after stimulation. In order to create the connectivity matrices for network analysis and average data from multiple animals, VSD responses from each animal were normalized to the maximum response per stimulation site, reducing the effect of between animal differences in absolute response that could arise from VSD labelling, variable ChR2 expression between animals, or other factors. In order to assess spatial bias in VSD response due to brain curvature, we calculated the distance from the edge of the craniotomy for each ROI and then compared this to the mean VSD response at 20 ms after stimulation using a Pearson's correlation coefficient.

2.2.9 Pharmacology

In cases where antagonists of synaptic transmission were used, the cortex was covered with HEPES-buffered saline solution to allow for later topical application of AMPA/NMDA glutamate receptor antagonists: 200 µM 6,7-dinitroquinoxaline-2,3-dione (DNQX), and 500 µM (2R)-amino-5-phosphonovaleric acid (AP5). The cortex was incubated with antagonists for 30 min prior to further imaging.

2.2.10 Network analysis

We used custom-written MatLab programs to create a connectivity matrix using ChR2-evoked VSD responses from each ROI. We chose to represent the data as a weighted, directed network (as opposed to the more common binary, undirected network) in order to preserve the information regarding reciprocal connections and their relative importance. Each node in our network corresponds to one ROI in the unilateral preparation and they are connected by edges with weights proportional to the VSD signal observed in the remaining ROIs when each ROI is stimulated in turn. We used functions from the MatLab Bioinformatics toolbox to draw the network diagram and functions from the Brain Connectivity Toolbox (http://www.brain-

connectivity-toolbox.net described by (Rubinov and Sporns, 2010) to calculate network properties. These properties include strength (both in-strength and out-strength), betweenness centrality (BC), characteristic path length (L), and the mean clustering coefficient (C).

Both BC and node strength were calculated per animal and averaged. Node strength is the sum of the edge weights of a given node (i.e. row and column sum of the connectivity matrix). It quantifies how strongly connected a particular node is to the other nodes (if at all). In a weighted, directed network, out-strength and in-strength separately quantify the strength of out-going and in-coming connections of a particular node. Here, out-strength is determined by the VSD response recorded at the other ROIs following the stimulation of a given node (a column sum in our connectivity matrix) and in-strength is determined by the VSD response at a given node following photostimulation at the other ROIs (a row sum in our connectivity matrix). Node out-strength was calculated on the sub-network of primary (S1) and secondary sensory (S2) nodes to investigate reciprocal connections between them. To determine which nodes were highly connected we calculated BC for each node. A high BC indicates that, given the random selection of two other nodes within the network selection, there is a high probability that the shortest path between these two nodes passes through the node of interest. BC is a common metric in network analysis, indicating hub regions within the network. In order to assess spatial bias in network measures due to possible edge effects, we calculated the distance from the edge of the craniotomy for each node and then compared this to the node strength and the BC using a Pearson's correlation coefficient. Distance from the edge of the craniotomy was calculated per animal by creating a mask of the craniotomy and calculating the minimum distance from the mask to each ROI.

Using the connectivity matrix, where VSD responses were normalized per stimulation site, per animal, before averaging (see Data Analysis), we applied a threshold to highlight the strongest connections within the network. This threshold was applied for display only (in Figure 2.7 and Figure 2.8) as it is difficult to visually assess trends within the diagram due to the large number of connections present. In order to test the effects of isolating the strongest connections within the network on the overall network properties, we computed global network properties, L and C, as a function of variable threshold levels. L measures compactness of the network by calculating the average shortest path between pairs of nodes, while C gives a measure of the local connectivity by quantifying groups of interconnected nodes. We chose a threshold level

which removed a large number of connections while having a negligible influence on L and C. Connectivity matrices and network diagrams were then constructed for ROI data at 6 ms, 12 ms, and 20 ms to illustrate the integrated response of the network over time.

2.2.11 Histology

To investigate ChR2 expression in the cortex (expressed as a YFP fusion protein) (Wang et al., 2007a), mice were deeply anesthetized and perfused transcardially with 10 ml of PBS followed by 10 ml of 4% paraformaldehyde in PBS. The brain was removed and immersed in 4% paraformaldehyde overnight before being transferred to a 30% sucrose solution in PBS for cryoprotection. Sagittal sections (50 μm) were cut on a frozen microtome and imaged using a Zeiss LSM 510 Meta confocal microscope with a multi-line argon laser and a Plan-Neofluar 5X (0.15 NA) or Plan-Neofluar 20X (0.50 NA) objective. Fluorescence was excited using the 488 nm line of the argon laser and was filtered using a 505-530 nm bandpass. Tiled scans (12-bit; 512 x 512 pixels per tile for 5X images; 460 x 460 pixels per tile for 20X images) were collected using LSM-510 software (Version 3.2 SP2). To determine ChR2 expression from anterior to posterior across the section a Gaussian filter was applied (6.0 pixel radius) and a freehand line (100 pixel thickness) was drawn to plot the fluorescence profile of the layer 5 region using NIH ImageJ software (Version 1.42q). This was done in 3 animals from sections ranging from 2.28 – 2.32 mm lateral from Bregma, each being normalized relative to its mean fluorescence.

2.2.12 Statistical analyses

Statistical analyses were completed using GraphPad Prism version 4.03 (GraphPad Software, San Diego, CA) or custom codes written in MatLab. In order to determine the relationship between sensory-evoked responses and ChR2-evoked responses, a repeated measures two-way ANOVA was conducted, followed by Bonferroni post-tests, for each type of stimulation. All p values ≤ 0.05 were considered statistically significant, and all data are expressed as the mean ± standard error of the mean (SEM). Sensory and ChR2-evoked stimuli were paired together (ex. FL sensory stimulation was paired with FLS1 photostimulation) in order to determine differences in responses between these stimulation types. Permutation tests (van den Heuvel and Sporns, 2011) were used to evaluate the mean strengths of connections between primary and secondary sensory nodes as well as to test for asymmetry in the outgoing

and incoming connection weights on a node by node basis. Pearson's correlation coefficients were calculated to assess potential spatial bias within the craniotomy window on VSD responses and/or on network properties (strength per node, and BC per node).

2.3 Results

2.3.1 Assessment of channelrhodopsin-evoked cortical activity through qualitative comparison to sensory-evoked cortical activity

Using a ChR2-based intracortical mapping approach (Ayling et al., 2009) with transgenic mice (B6.Cg-Tg(Thy1-COP4/EYFP)18Gfng/J) (Wang et al., 2007a) we were able to activate specific cortical areas while imaging local and regional activity using VSD (RH1692) (Shoham et al., 1999) under urethane or isoflurane anesthesia (Figure 2.1 A). Anesthesia was used to depress the motor system, making muscle twitches and indirect sensory responses less likely (Antognini et al., 1999), and to create a relatively uniform level of background activity for circuit analysis allowing functional relationships between primary sensory areas (including forelimb, hindlimb, barrel, auditory and visual cortex), and other cortical regions (including secondary sensory, motor, and association areas) to be mapped. For all experiments the cortical locations of ChR2 stimulation sites were based on relative position to functional coordinates (defined by sensory stimulation) derived from VSD imaging prior to photostimulation. By using a bilateral (Figure 2.1 B), or a wide unilateral craniotomy preparation (Figure 2.1 C), we have monitored activation of the contralateral hemisphere, indicating interhemispheric relationships, as well as activation of the ipsilateral hemisphere, indicating intrahemispheric connectivity. Given the presence of a transient optical artifact at the stimulation site, we did not use the data from the location or time-point of photostimulation. For example, if photostimulation was targeted to the left hemisphere HLS1, the data from the center of the left hemisphere HLS1 was not used for ROI quantification (due to reversible photobleaching), but the spread of activity within the photostimulated hemisphere and transcallosal responses in the opposite hemisphere were measured. Using the average of photostimulation trials that were normalized to unstimulated trials, we found that a 1 ms electrical stimulation to the right hindlimb led to a localized VSD response at the left hemisphere HLS1 and a discrete activation at the homotopic HLS1 in the right hemisphere (Figure 2.2 A, i). Similarly, a 1 ms 473 nm light pulse delivered to a point centered within the HLS1 led to a ChR2-dependent local spread of activity around the excitation

site and a discrete activation of the homotopic HLS1 in the right hemisphere (Figure 2.2 A, ii). Similar activation patterns were observed when forelimb (FL), C2 whisker (WK), vision, and auditory sensory stimulation were compared to photostimulation of FLS1, BCS1, V1, or A1, respectively (Figure 2.2 B-E). Analysis of correlation over time indicated that the relationship between the forelimb sensory-evoked response (Figure 2.3 A) and the FLS1 (cortex) ChR2-evoked response (Figure 2.3 B) had the highest correlation within 25 ms after stimulation (Figure 2.3 C).

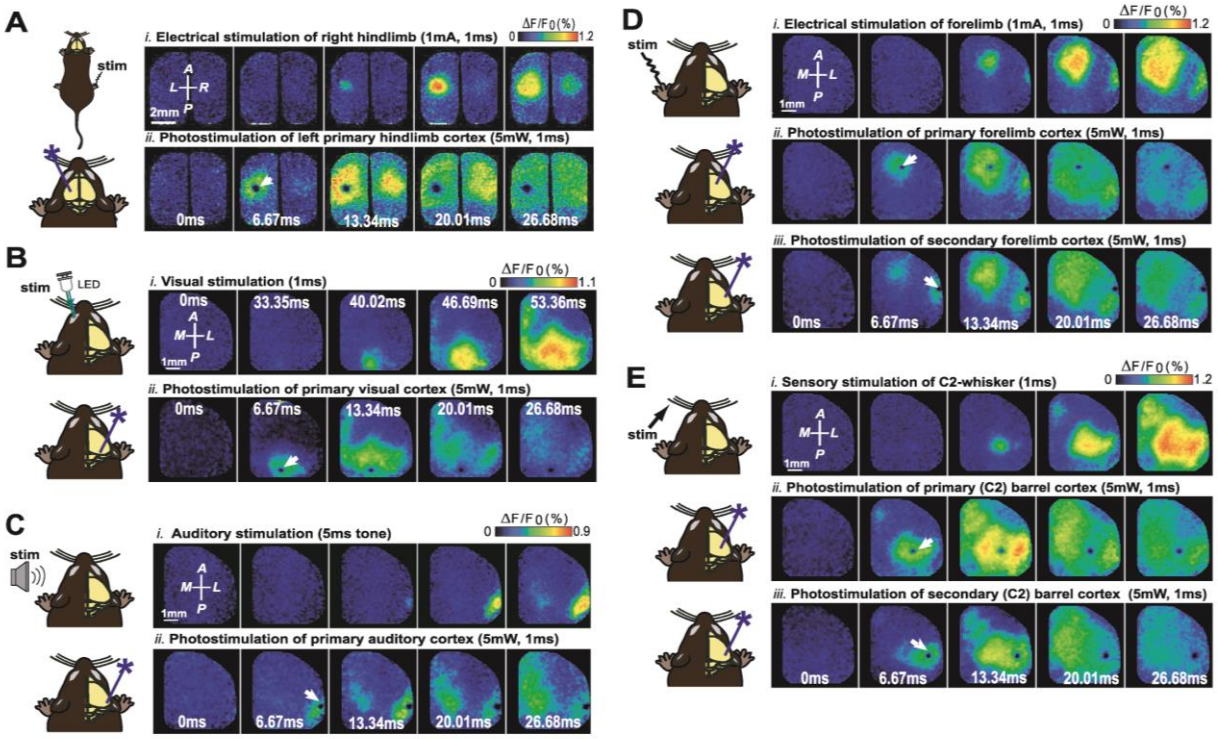

Figure 2.2 Voltage-sensitive dye imaging maps to compare sensory stimulation to local photostimulation. (A) Example of VSD response in a bilateral craniotomy preparation after electrical stimulation of the right hindlimb (i), or direct photostimulation of the left HLS1 (ii). (B) Example of VSD responses in a unilateral craniotomy preparation during visual stimulation of the contralateral (left), eye (i), or direct photostimulation of the right V1 (ii). (C) VSD responses after auditory stimulation using a tone (i), and photostimulation of A1 (ii). (D) VSD responses after electrical stimulation of the contralateral (left), FL (i), direct photostimulation of FLS1 (ii), and direct photostimulation of FLS2 (iii). (E) Example of VSD responses in a unilateral craniotomy preparation during piezoelectric stimulation of a single whisker (C2; i), direct photostimulation of BCS1 (ii), and direct photostimulation of BCS2 (iii). White arrows indicate the site of photostimulation.

2.3.2 Quantitative comparison between sensory and Channelrhodopsin-2-evoked VSD responses

In order to quantify similarities between sensory-evoked responses and photostimulation-evoked responses in both bilateral and unilateral preparations, the VSD responses were compared at each ROI. It is possible our ability to measure the VSD response of the ROI may be influenced by the curvature of the brain surface and the location of the ROI within the craniotomy window. To determine whether this was a major factor we calculated the minimum distance to the edge of the unilateral craniotomy for each ROI and compared this to the mean VSD response from that ROI (across all photostimulation sites). Pearson's correlation coefficient showed no significant correlation between distance from the edge of the craniotomy and mean VSD response for the ROI ($r = 0.30$, $p = 0.29$), suggesting that the location of the ROI within the craniotomy window does not have a significant effect on the VSD response (data not shown). Nonetheless, VSD responses were calculated as a percent change from baseline VSD response ($\Delta F/F_0$*100%) in order to reduce any effects of variable VSD signal strength across the craniotomy window caused by brain curvature. To reduce the possible effect of regional differences in ChR2 expression, the ChR2-evoked responses were normalized to the maximum response for each stimulus site (see Materials and Methods). Sensory responses were normalized to the maximum response obtained for that stimulus.

In the bilateral preparation (n=10 animals), a 2-way repeated measures ANOVA revealed no significant difference when comparing forelimb and whisker sensory-evoked VSD responses to ChR2-evoked VSD responses following photostimulation of FLS1 or BCS1 ($p = 0.50$ and $p = 0.17$, respectively) but did show a significant difference when comparing hindlimb sensory-evoked VSD responses to ChR2-evoked responses after HLS1 photostimulation ($p < 0.01$; Figure 2.4 A). For light or sensory stimulation there was a main effect of ROI ($p < 0.01$ for all pairs), indicating differences in the VSD response levels at certain ROIs rather than an equal and diffuse VSD response at all ROIs. Bonferroni post-tests comparing sensory-evoked versus ChR2-evoked responses at each ROI were also conducted (significant differences indicated in Figure 2.4 A; * = $p < 0.05$). There were very few pairs that were significantly different between the sensory and ChR2-evoked responses indicating a high degree of similarity in activation at each ROI.

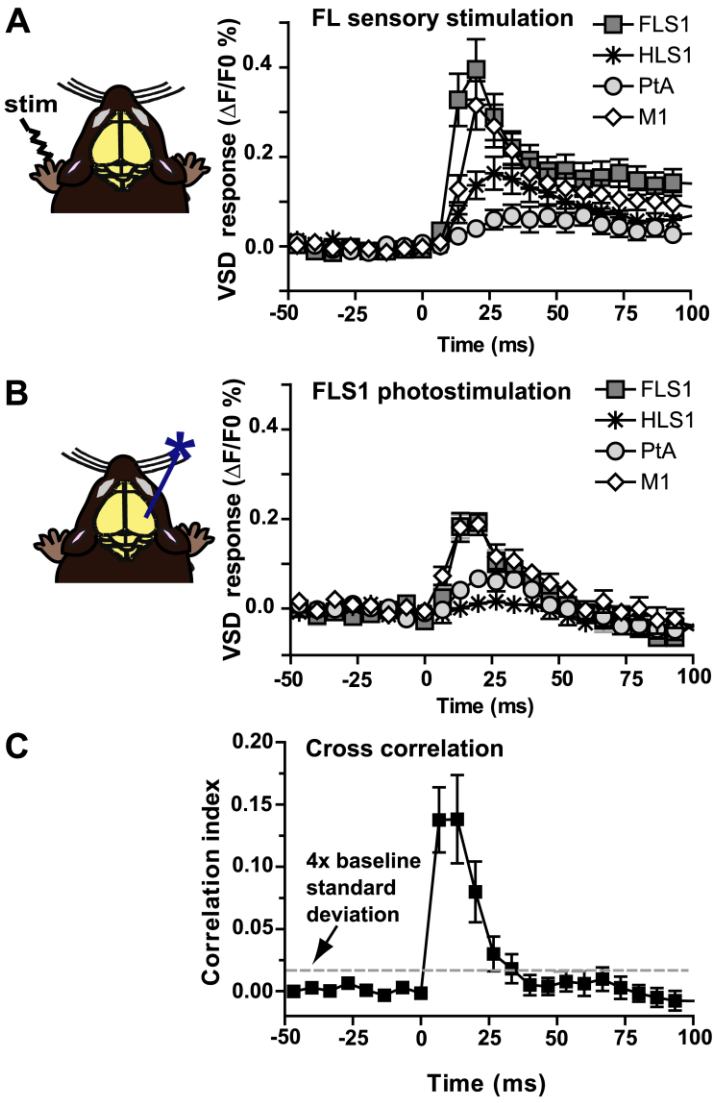

Figure 2.3 Temporal correlation between sensory-evoked VSD responses and ChR2-evoked VSD responses. (A) VSD responses from selected regions in the contralateral hemisphere after electrical stimulation to the forelimb (n=10 mice). (B) VSD responses from selected regions in the contralateral hemisphere after photostimulation of FLS1 (n=10 mice). (C) A Pearson correlation coefficient between sensory and ChR2-evoked responses was computed (n=10 mice) for all pixels and plotted in a frame by frame manner to determine correlation. Note the high correlation index during the first 25 ms after stimulation, where the correlation index is greater than four times the standard deviation of baseline (dashed line).

Within the unilateral preparation (n=6 animals), a 2-way repeated measures ANOVA revealed no main effect when comparing sensory- and ChR2-evoked VSD responses in forelimb, whisker, and visual areas (p = 0.42, p = 0.29, and p = 0.19, respectively) (Figure 2.4 B). While hindlimb sensory stimulation showed similar VSD responses to photostimulation of HLS1 at

some ROIs, ChR2-evoked responses tended to be more diffuse. Although auditory stimulation showed strong similarities to photostimulation at some ROIs (particularly the secondary somatosensory regions), ChR2-evoked activation of A1 also tended to show more diffuse responses than sensory stimulation. Sensory- and ChR2-evoked responses were significantly different by a two-way ANOVA when comparing hindlimb-HLS1 ($p < 0.01$) and when comparing tone-A1 ($p < 0.01$) (Figure 2.4 B). All sensory- and ChR2-evoked pairs (forelimb-FLS1, whisker-BCS1, visual-V1, hindlimb-HLS1, auditory-A1) had a main effect of ROI ($p < 0.01$ for all pairs), indicating variable levels of VSD response rather than equal activation at all ROIs. Bonferroni post-tests were conducted for pairs of ChR2 and sensory stimulation (Figure 2.4 B). There were very few significant differences (* = $p < 0.05$ in Figure 2.4 A,B) between sensory- and ChR2-evoked responses at individual ROIs, suggesting that ChR2 and sensory stimulation elicited similar patterns and amplitudes of responses at each ROI.

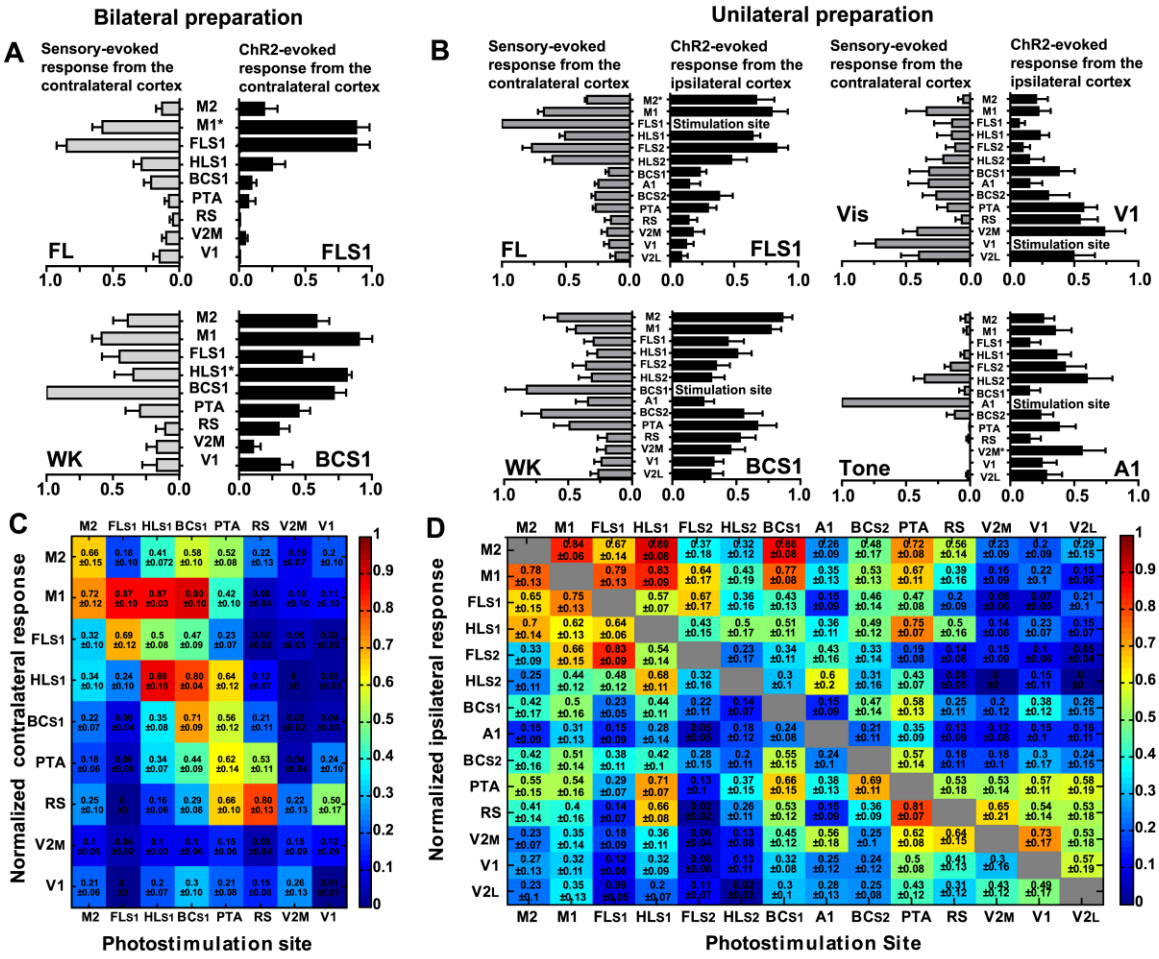

Figure 2.4 Interhemispheric and intrahemispheric connectivity: comparison of sensory-evoked cortical maps with ChR2-evoked cortical maps. (A) Comparison of contralateral sensory-evoked responses (gray bars), to contralateral ChR2-evoked responses (black bars), at 9 ROIs in the bilateral preparation. FL sensory stimulation was compared to direct photostimulation of FLS1 (top), whisker sensory stimulation was compared to direct photostimulation of BCS1 (middle), and HL sensory stimulation was compared to direct photostimulation of HLS1 (bottom) (* = $p < 0.05$, 2-way ANOVA post test). (B) Comparison of contralateral sensory-evoked responses (gray bars), to ipsilateral ChR2-evoked responses (black bars), at 14 ROIs in the unilateral preparation. FL sensory stimulation was compared to FLS1 photostimulation(top, left), whisker sensory stimulation was compared to BCS1 photostimulation (middle, left), HL sensory stimulation was compared to direct photostimulation of HLS1 (bottom, left) visual stimulation was compared to V1 photostimulation (top, right), and auditory stimulation (tone), was compared to A1 photostimulation (middle, right). (* = $p < 0.05$, 2-way ANOVA post test) (C) Connectivity matrix derived from the bilateral preparation. Nine sites of photostimulation are indicated along the X-axis, and nine ROIs are indicated along the Y-axis. M1 was not a photostimulation site (gray column) but was used as a ROI for VSD responses. The responses represent the integrated VSD response in the hemisphere contralateral to photostimulation at 20 ms after photostimulation. Responses were normalized to the maximum response per stimulation site, per animal, and then averaged across 10 animals. In cases where the response was less than four times the standard deviation of the baseline, it was assigned a value of zero indicating no response. (D) Connectivity matrix derived from the unilateral preparation. Fourteen sites of photostimulation are indicated along the X-axis, and fourteen ROIs are indicated along the Y-axis. The responses represent the integrated VSD response at 20 ms after photostimulation within the hemisphere where photostimulation occurred. Responses are not shown for the site of stimulation(gray boxes) Responses were normalized to the maximum response per stimulation site, per animal, and averaged across 6 animals.

2.3.3 Assessment of the inter- and intracortical network trends from connectivity matrices

Pseudo-colored connectivity matrices were created to show relationships between photostimulation sites and VSD responses, both between (Figure 2.4 C) and within (Figure 2.4 D) cortical hemispheres. In assessing ChR2-evoked responses that traveled to the contralateral hemisphere in the bilateral preparation (Figure 2.4 C), strong contralateral activity was usually observed in the homotopic regions (outlined in black in Figure 2.4 C) and neighboring regions. For example, ipsilateral photostimulation of HLS1 produced a strong response in the contralateral HLS1 (0.89 ± 0.10) and the contralateral M1 (0.87 ± 0.03) (Figure 2.4 C). One notable exception where photostimulation did not elicit a strong response at the homotopic site was V1 (0.01 ± 0.01), however photostimulation of V1 did result in excitation of the contralateral retrosplenial cortex (0.50 ± 0.17) (Figure 2.4 C). In the unilateral preparation functionally related HLS1 and FLS1 areas were reciprocally connected and able to excite M1 (Figure 2.4 D). Photostimulation of BCS1 led to secondary activation of M1 (0.86 ± 0.08), consistent with our sensory stimulation data and previous reports (Ferezou et al., 2007). BCS1 photostimulation was able to excite limb sensory areas and M1, yet limb cortical areas were less able to activate BCS1, V1, and A1. Stimulation within posterior cortical areas tended to produce lower levels of both local and regional depolarization as assessed using VSD imaging. It is possible that regional differences in ChR2 expression may have contributed to this pattern (Wang et al., 2007a). However, examination of sagittal sections from the transgenic mice indicated that ChR2 expression within the layer 5 region did not vary by more than 50% across the anterior-posterior axis (Figure 2.5 A-E) and EEG recordings showed that ChR2-evoked depolarization following photostimulation correlated with increases in VSD fluorescence that were still readily detectable, even within posterior regions with relatively lower ChR2 expression (Figure 2.5 F). Region-specific differences in excitability can in part be compensated by examining patterns of relative responsiveness (normalized to the maximum response observed over the ROIs that were assessed) as we have done.

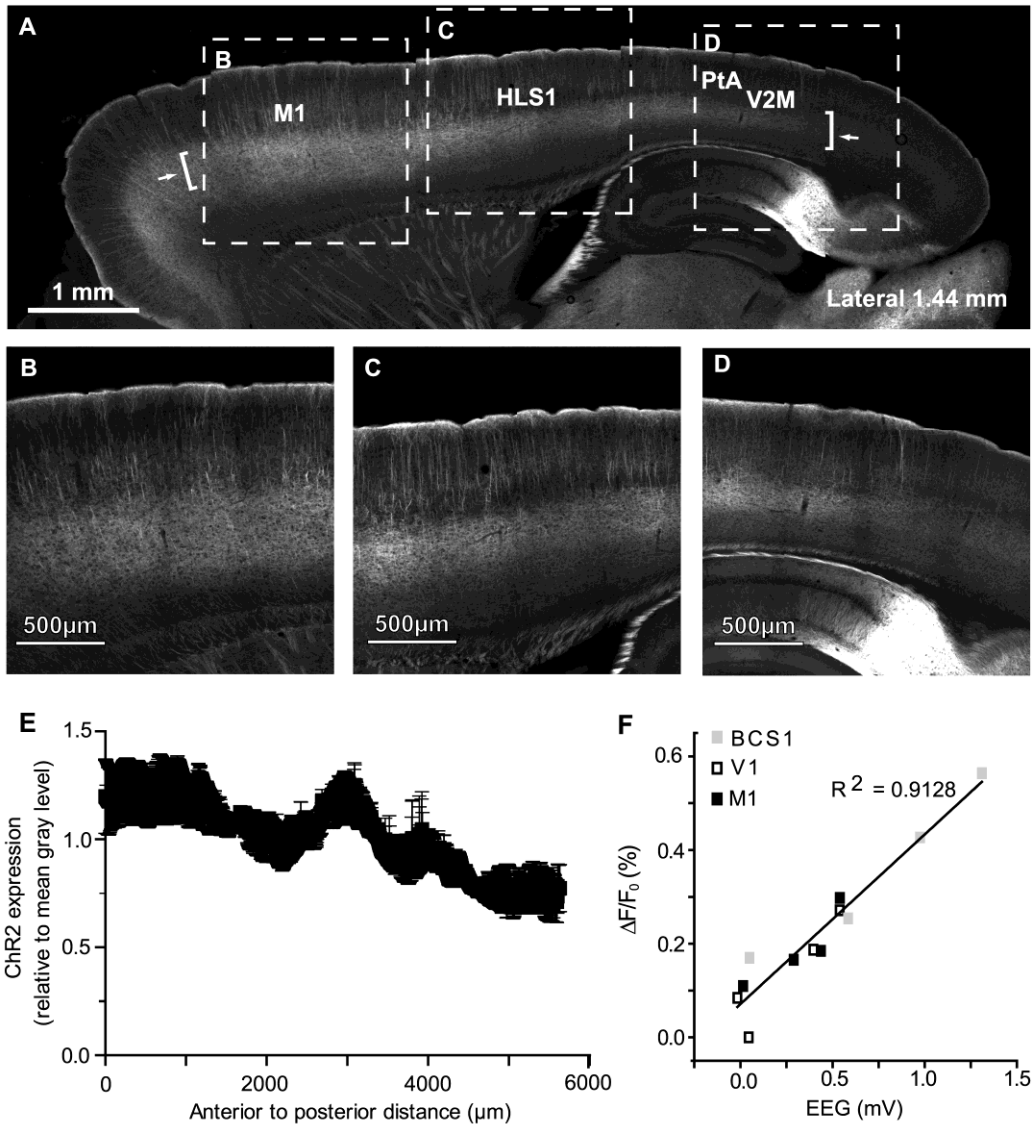

Figure 2.5 ChR2 expression and ChR2- evoked EEG responses across the anterior-posterior axis of cortex. (A) Confocal image of a 50 µm sagittal section (1.44 mm lateral from Bregma) from a ChR2 transgenic mouse (line 18, stock 007612, strain B6.Cg-Tg (Thy1-COP4/EYFP) 18Gfng/J from the Jackson Laboratory); high magnification shown in (B)–(D). Arrows indicate the start and end points of the fluorescence profile in (E). Brackets indicate the approximate location of layer 5 sampled for the profile in (E). (B) High magnification image from the anterior area of the section shown in (A). (C) High magnification image from the section shown in (A). (D) High magnification image from the posterior end of the section shown in (A). E) Anterior to posterior fluorescence profile of average ChR2 expression, quantified relative to mean gray value per animal. Data shown as mean gray value ± SEM (n=3 animals). (F) Relationship between VSD signal strength and EEG depolarization following photostimulation at different ROIs within a single representative animal. Peak VSD responses are plotted against peak EEG depolarizations following photostimulation at different sites.

ChR2 photostimulation allowed us to determine relationships between primary and secondary sensory areas as well as association cortices (RS, PTA, and M2/CG). Stimulation of secondary sensory areas revealed strong reciprocal connections with primary sensory areas (Figure 2.4 D). Some areas, in particular the PTA, appeared to be connected to most cortical

areas (Figure 2.4 D). Reciprocal connections can be seen in the connectivity matrix, especially in neighboring areas such as M1 and M2/CG; the M1 to M2/CG connection weight is 0.84 ± 0.06 while the M2/CG to M1 weight is 0.78 ± 0.13 indicating a nearly symmetric connection between these regions. Conversely, dissimilar connection weights can also be seen between visual cortex stimulation sites. For example, the V2M to V1 weight is 0.30 ± 0.16 while the V1 to V2M weight is 0.73 ± 0.17, indicating an asymmetric reciprocal connection. This implies a weighted directed (i.e. asymmetric) network (Rubinov and Sporns, 2010).

We used a permutation test to compare mean node strength from primary sensory (S1) areas (FLS1, HLS1, BCS1, A1, and V1) to secondary sensory (S2) areas (FLS2, HLS2, BCS2, V2M, and V2L) with the mean node strength from S2 areas to S1 areas (i.e. reciprocal node strengths). The mean strength from S1 to S2 areas was 1.99, while the mean strength from S2 to S1 was 1.36 ($p = 0.03$). This suggests that reciprocal connections between S1 and S2 are not of equivalent strength but are instead biased for network flow from S1 to S2.

2.3.4 Analysis of VSD responses after channelrhodopsin-2 stimulation in control animals

Controls performed using glutamate receptor antagonists (n=3 mice; Figure 2.6 A-B) or wild type mice (n=3; Figure 2.6 C), indicated that the ChR2-evoked VSD responses were dependent on both the presence of ChR2 and intracortical synaptic transmission. A two-way repeated measures ANOVA was completed to compare responses before and after application of glutamate antagonists at HLS1 and BCS1 using connectivity matrices. There was a significant difference in responses before and after antagonist application ($p < 0.01$), indicating that intracortical synaptic transmission is required for the observed spread of activity. In wild type animals that lacked ChR2 expression no consistent photostimulation-evoked responses were observed.

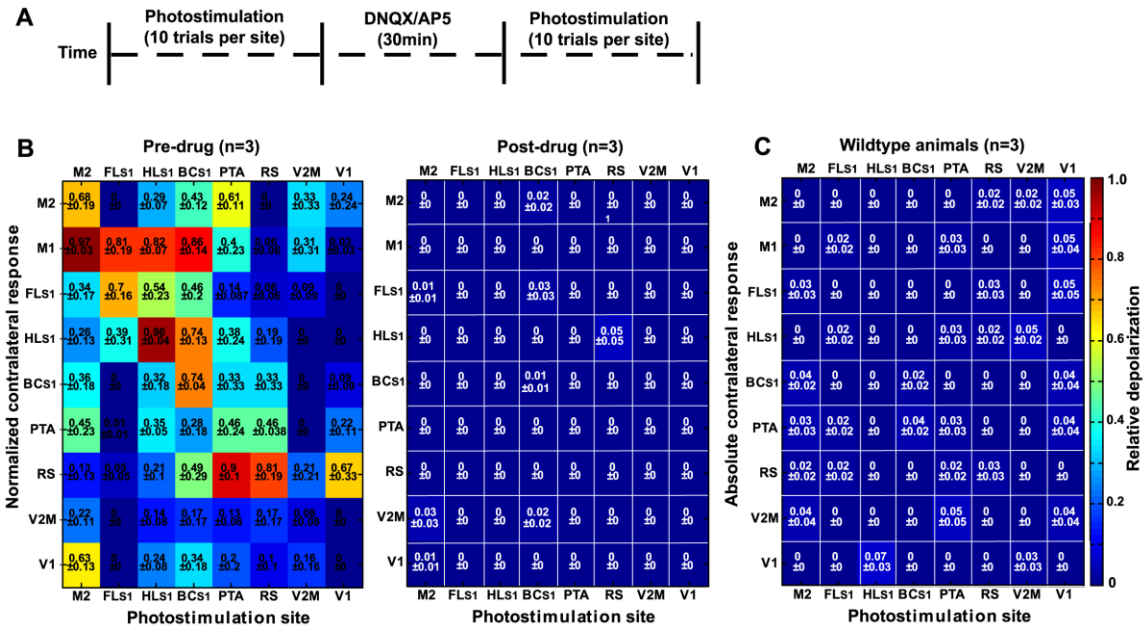

Figure 2.6 ChR2-evoked VSD responses are dependent on intracortical synaptic transmission and ChR2. (A) Schematic showing the experimental timeline for pharmacological blockade of intracortical transmission. (B) Connectivity matrix showing normalized VSD responses before antagonist application. (C) Connectivity matrix showing VSD responses after application of 200 µM DNQX and 200 µM AP5 to the cortical surface (n = 3 mice). VSD responses were normalized to the VSD response before antagonist application. (D) Connectivity matrix showing contralateral responses to photostimulation in the bilateral preparation in wild-type mice (n=3). In ChR2-negative animals we failed to evoke significant regional VSD responses using photostimulation. Responses were assigned a value of zero (0±0), when the response failed to be four times greater than the standard deviation of the baseline. Note for B-D M1 was not a photostimulation site (gray column) but was used as a ROI for VSD responses.

2.3.5 Intrahemispheric network analysis of regional activity evoked by Channelrhodopsin-2 stimulation

In order to better understand intrahemispheric relationships between cortical areas we derived an intracortical network diagram (Figure 2.7 A) using the VSD response at 20 ms after stimulation (from our unilateral connectivity matrix; Figure 2.4 D). For clarity in displaying the network diagrams in Figure 2.7 and Figure 2.8, we applied a threshold to highlight the strongest connections which determine the global network properties. We tested variable threshold levels against two network metrics: characteristic path length (L) (Figure 2.7 B) and mean clustering coefficient (C) (Figure 2.7 C; see Materials and Methods). An absolute threshold of 0.5 (normalized VSD responses of 0.5 and higher were maintained) was applied to the connectivity matrix and had minimal effects on L and C; this threshold changed L by 6% and C by 0.13%. The number of connections in the network after thresholding was reduced from 182 to 55, leaving 30% of the original connections. We used these connections to create the network

diagram, but performed all calculations and statistical testing on the full (unthresholded) connection matrix.

The diagram represents the data as a network of the strongest connections observed in our study, with each stimulation site (ROI) corresponding to a node and average VSD responses corresponding to the weight of the connections between nodes (Figure 2.7 A). The network was drawn such that the node size is proportional to the node strength and the thickness of the connecting lines is proportional to the edge weight of the particular connection. The nodes were positioned based on the average brain coordinates for 6 animals. The diagram allows the reciprocal connections between brain regions to be visualized. For example, the connection from BCS1 to M1 was considerably stronger than the reciprocal direction (compare arrow thickness between these two nodes). Using unthresholded VSD responses from the connectivity matrix, permutation testing was used to test the hypothesis that individual nodes were symmetric in the mean input and output weight of their edges (data not shown). We anticipated that primary sensory nodes would have greater output weights (that is, stronger connections going towards other regions such as S2) compared to input weight (that is, connections coming into the node from other regions), while secondary sensory nodes would have greater input weight compared to output weight. Indeed, for most primary sensory nodes, output weight was significantly greater than input weight (HLS1 $p = 0.03$, BCS1 $p < 0.01$, and A1 $p < 0.01$). Contrary to our hypothesis only some secondary sensory nodes showed a significant difference between input and output weight. FLS2 and V2M had significantly stronger input weight compared to output weight (FLS2 $p = 0.02$, V2M $p < 0.01$), while BCS2 had significantly higher output weight compared to input weight (BCS2 $p = 0.02$). M2/CG and retrosplenial cortex showed significantly greater input weight ($p < 0.01$ and $p = 0.02$, respectively). The other nodes showed no statistical difference in their mean output and input weights.

To further assess the relative importance of individual nodes within the network we calculated the betweenness centrality (BC) for each node (Figure 2.7 D). The BC is the fraction of shortest paths between pairs of nodes in the network that pass through the node of interest. This metric is used to highlight network hubs (Rubinov and Sporns, 2010). We found that PTA had the highest betweenness centrality and a one-way ANOVA of the BC per node revealed a significant main effect of node ($p < 0.05$, n=6 animals) and Bonferroni post-tests were calculated between PTA and the remaining nodes (Figure 2.7 D).

It is possible that differences in node location may influence our ability to measure the strength of the node within the network; a bias may exist in defining hubs for nodes that are near to the edge of the craniotomy because we are unable to measure all connections to and from these nodes. To determine whether this was a major factor we calculated the minimum distance to the edge of the craniotomy for each node and compared this to node strength and BC. Pearson's correlation coefficient showed a significant but modest correlation between node strength and distance to the edge of the craniotomy ($r = 0.66$, $p = 0.01$), with nodes at a greater distance from the edge showing a higher node strength (data not shown). However, there was no significant correlation between distance from the edge of the craniotomy and BC ($r = 0.15$, $p = 0.62$), suggesting that nodes can be defined as hubs irrespective of their spatial location within the craniotomy window (data not shown).

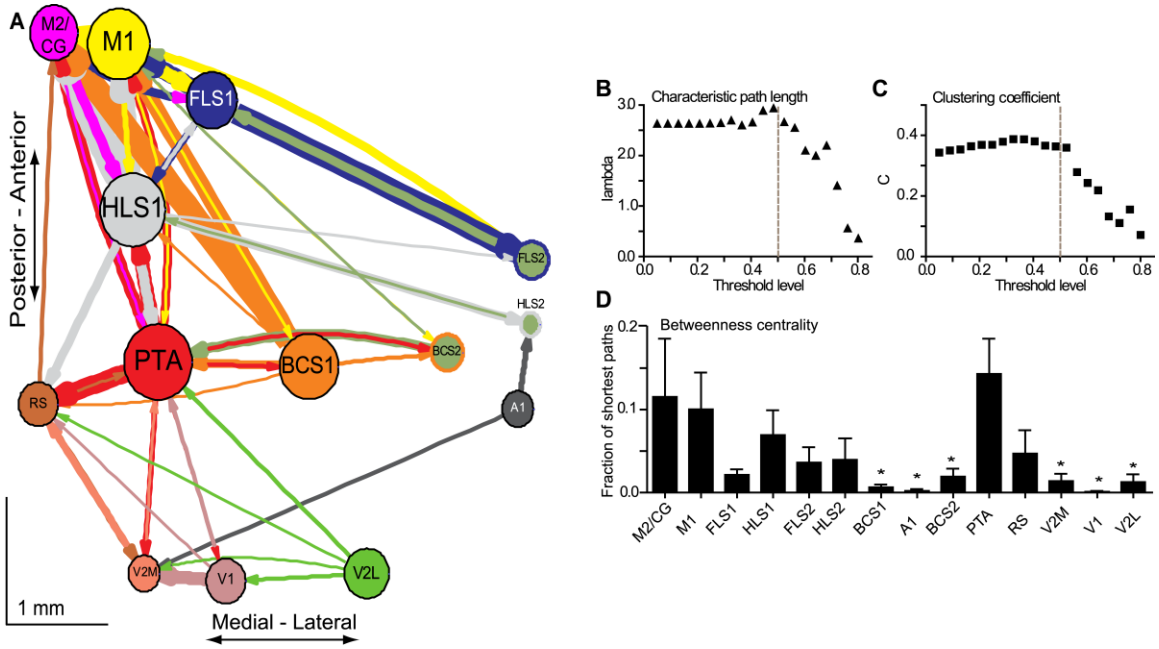

Figure 2.7 Network analysis of connectivity matrices reveals cortical hubs. (A) A weighted, directed network diagram was derived from the unilateral connectivity matrix (n=6 mice) shown in Fig. 4D by thresholding the elements (weights) at a relative response of 0.5. Nodes were placed according to the site of photostimulation with size proportional to the strength of connections per node (sum of weights). Arrow thickness is related to weight of an individual connection. (B) Average characteristic path length as a function of varying thresholds. A threshold of 0.5 (dashed line) results in a 6% decrease in characteristic path length within the network. (C) Average clustering coefficient as a function of varying thresholds. A threshold of 0.5 (dashed line) results in a negligible change (0.13%) to clustering coefficient within the network. (D) Betweenness centrality calculated for each node (stimulation site; n=6 mice) to determine the fraction of shortest paths that pass through a given node and define network hubs. Post-tests were calculated between PTA and all other nodes (* = $p < 0.05$).

In order to assess the spread of the observed VSD signal over time, we analyzed the integrated VSD responses at several time-points after stimulation. We created connectivity

matrices and network diagrams at 6, 12, and 20 ms after photostimulation (Figure 2.8 A-C). At 6 ms after stimulation the areas of activation were localized to the homotopic region (for the bilateral preparation), and areas that are presumably more directly linked to the photostimulation site (for the unilateral preparation; Figure 2.8 A). For example, previous work indicates that excitation can spread through projections from BCS1 to M1 (a distance of ~4 mm) within ~8 ms (Ferezou et al., 2007). At early time-points (6-12 ms), relatively strong connections were found between primary and secondary somatosensory nodes, as well as between areas such as BCS1 and M1 that may have a direct connection, but were less likely to occur between less-related nodes such as A1 and RS (Figure 2.8 B). At 20 ms after photostimulation the number of highly connected nodes increased and relatively strong connections were observed for most nodes, including between V1 and RS or PTA cortex (Figure 2.8 C). This early localization and subsequent spreading of VSD signal to related and more distant nodes is similar to the VSD signal spread that we observed following sensory stimulation (Figure 2.2), and as reported previously (Ferezou et al., 2007; Brown et al., 2009).

A network diagram derived from sensory stimulation was completed to further compare similarities between photostimulation and sensory stimulation (Supplementary Figure 2.10). The sensory diagram is limited in the number of projections it can show because only five of the fourteen ROIs in our unilateral preparation are primary sensory areas that can be activated reliably through peripheral sensory stimulation. For this reason, the sensory network diagram cannot include information about back projections from secondary or associational areas, and will likely contain unknown contribution from subcortical sources.

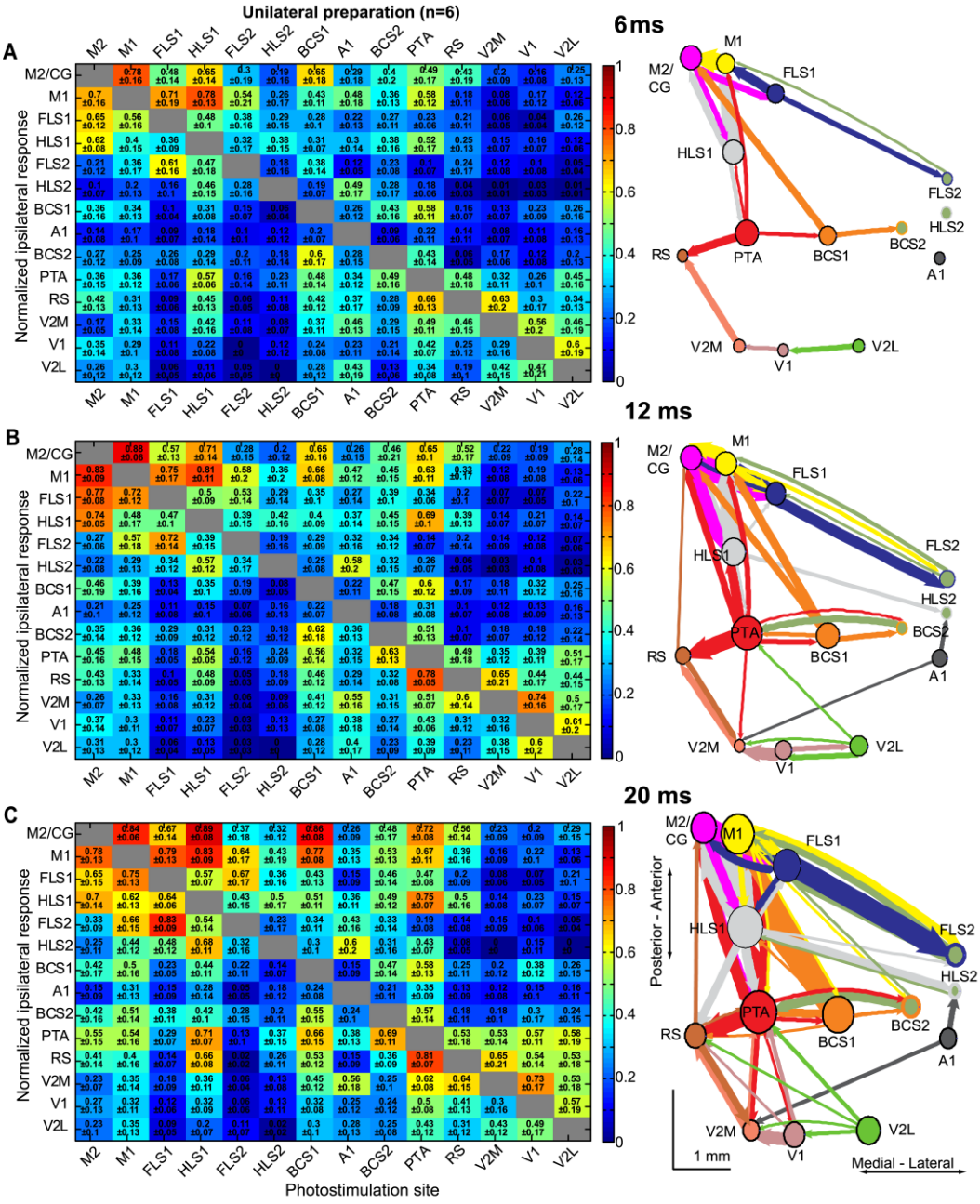

Figure 2.8 Intrahemispheric connectivity changes over millisecond timescales after direct cortical photostimulation. Connectivity matrices and network diagrams derived from the unilateral preparation at 6 ms (A), 12 ms (B) and 20 ms (C) after stimulation. For each time-point, VSD responses were normalized to the maximum response per stimulation site, per animal, and averaged across animals (n=6 mice). VSD responses were integrated to represent the sum of the VSD response from response onset. In each case, a 0.5 threshold was applied for display purposes so only the strongest connections were used to create the network diagrams. Nodes were placed according to the site of photostimulation. The size of node is proportional to the strength of connections per node (sum of weights) and arrow thickness between nodes is proportional to the weight of the connection.

2.4 Discussion

2.4.1 Self-assembly of functional cortical circuits through stimulation of neuronal subsets

Rather than an isotropic spread of activity from the site of photostimulation, single point ChR2 activation of predominantly deep layer cortical pyramidal neurons (Wang et al., 2007a), reconstitutes much of the activity patterns observed with normal sensory activation, thus the map can be said to "self-assemble" after stimulation. This self-assembly was evident in a number of different sensory circuits. For example, photostimulation of the BCS1 produced a characteristic secondary activation of M1, which has been previously reported using electrode stimulation (Ferezou et al., 2007). ChR2 point stimulation can be targeted to arbitrary locations, including secondary sensory and association areas, to generate maps via self-assembly which are inaccessible by normal sensory stimulation. We have used this feature to reveal novel findings regarding reciprocal connections between primary and secondary sensory or association areas, extending previous anatomical work (Aronoff et al., 2010) to function.

Data analysis indicates consensus patterns between sensory-evoked and ChR2-evoked VSD responses for intra-and interhemispheric connectivity, such as expected homotopic connections to the opposite hemisphere. Layer 5B neurons primarily have subcortical connections, such as to the striatum and the posteromedial thalamic nucleus (Hattox and Nelson, 2007). Activity present in the opposite hemisphere following photostimulation of ChR2-expressing layer 5 neurons suggests subsequent activation of cortical neurons with transcallosal homotopic projections (Koralek et al., 1990; Hattox and Nelson, 2007), or may suggest indirect activation of contralateral layer 2/3 by ipsilateral layer 2/3 neurons (Petreanu et al., 2007; Weiler et al., 2008). This suggests a multisynaptic response, which is consistent with our finding that glutamate blockers abolished the ChR2-evoked response. It is possible that axons of passage may be activated by photostimulation (Petreanu et al., 2007), but given the correspondence between ChR2 and sensory-evoked maps these potentially off-target contributions are likely small. The ability of direct cortical stimulation to recapitulate much of sensory map structure was surprising since specific thalamo-cortical or brainstem circuits may be required to ensure the proper topographic mapping of inputs (Kaas, 1999; Kleinfeld et al., 2006; Matyas et al., 2010). Therefore, cortical maps may be both the product of activity-dependent sensory inputs (Fox, 1992), as well as intrinsic cortical circuits (Kenet et al., 2003; Wiemer, 2003; Vincent et al.,

2007; Ringach, 2009; Mohajerani et al., 2010). The role of thalamic feedback loops and the subcortical contribution to the signal remain unclear. Our analysis does not account for subcortical contributions, or propagation of signal in subcortical regions; thus, the network diagrams should be considered a representation of the functional connectivity of mouse dorsal neocortex evoked by a subset of neurons, and should not be considered a comprehensive connectivity map. The self-assembly of map-like representations from single point stimulation has implications for other fields of neuroscience including prosthetic brain stimulation (Nicolelis and Lebedev, 2009). Although there has been clinical success using brain stimulation (Perlmutter and Mink, 2006), or within animal models (Gradinaru et al., 2009), the effect of direct cortical stimulation on brain circuitry remains unclear. Based on our observations of self-organizing maps, optogenetic, or electrode-based stimulation could be used to activate relevant intra-cortical circuitry.

Recently, optogenetic stimulation has been paired with functional magnetic resonance imaging (opto-fMRI) (Lee et al., 2010; Desai et al., 2011; Kahn et al., 2011) and similar blood oxygenation level-dependent (BOLD) signals between photostimulation of BCS1 and sensory stimulation of the whisker have been reported (Kahn et al., 2011). Here, we expand on the suggestion that optogenetic stimulation elicits neuronal activity that is closely matched to sensory stimulation by comparing optogenetic stimulation of cortical sites with a number of different sensory stimuli, while employing an imaging approach that allows us to dynamically follow cortical activity with high spatiotemporal resolution to derive maps of cortical activity.

2.4.2 Possible limitations of simultaneous voltage sensitive dye imaging and channelrhodopsin-2 stimulation in vivo

We used a nearly collimated beam to photostimulate a number of ROIs across the cortical surface. Despite the fact that our beam diameter was 85 μm, we would expect considerable scattering of excitation light at the depth of ChR2-expressing neurons. Previous work in our lab using these ChR2 mice for motor mapping has reported increased beam width at a depth of 250 μm (Ayling et al., 2009). While local insertion of light fibers into the cortex would result in a lesser degree of light scattering and could potentially target smaller populations of neurons, we believe our approach has advantages because repeated placement of light fibers could lead to cortical damage that may result in an immediate redistribution of cortical response (Mohajerani et al., 2011).

We used *in vivo* VSD imaging in anesthetized animals to map large-scale cortical activity patterns. The behavioral state could impact the VSD responses we observe (Ferezou et al., 2007), however previous studies have shown that anesthesia does not prevent cortical responses to sensory stimulation (Hudetz and Imas, 2007). Although ChR2 stimulation revealed the expected intracortical activation patterns, the responses may also reflect activity within more complex pathways through the thalamus (Theyel et al., 2010) or brainstem (Nguyen and Kleinfeld, 2005; Matyas et al., 2010). It is also possible that photostimulation of primary sensory areas may evoke movements, and hence indirectly activate sensory pathways, affecting the VSD responses at motor and sensory ROIs. However, since isoflurane or urethane anesthesia were employed muscle movements are not likely and the VSD signal responses are unlikely to reflect secondary sensory responses triggered by muscle twitches (Altura and Weinberg, 1979; Antognini et al., 1999). We cannot directly address whether activation of target neurons occurs within apical dendrites that reach towards the cortical surface, or within deeper structures. Select expression of ChR2 via local injection or electroporation would not address this problem, as projections from cortical layers to subcortical structures could still cause indirect activation of deeper structures such as the thalamus.

Topical application of VSD causes staining of the cortical surface, which corresponds mainly to the superficial layers (Petersen et al., 2003a; Grinvald and Hildesheim, 2004; Mohajerani et al., 2010). While the optical signals originate mostly from the superficial layers (Ferezou et al., 2007), it is possible that activity in these layers could be driven by deeper layers or even contain optical contributions from them (Chemla and Chavane, 2010). Furthermore, it is possible that ChR2 stimulation could evoke downstream activity that remains in deeper layers (Hooks et al., 2011), and is therefore largely undetectable in the VSD signal. Due to these limitations in VSD imaging, it should be acknowledged that the networks we have shown here are specific to activity from the superficial cortical layers that is evoked following stimulation of a subset of neurons.

VSD imaging reports changes in both supra- and subthreshold membrane potential (Grinvald and Hildesheim, 2004; Ferezou et al., 2007). Although the propagation of the subthreshold VSD signal has been described (Wu et al., 2008) and confirmed with intracellular recordings (Petersen et al., 2003a), and ChR2-evoked VSD responses correlate with EEG depolarizations, the observed response may not necessarily be indicative of action potential

propagation. Nonetheless, subthreshold changes (indicating VSD responses) have been shown to influence interspike interval variance (Stern et al., 1997) and affect subsequent sensory input (Grinvald and Hildesheim, 2004). Ongoing subthreshold activity has been shown to be important in processing sensory information in the network and is correlated to behavioral state and cognitive processes (Arieli et al., 1996; Petersen et al., 2003b). Furthermore, subthreshold activation spread has been described in rat sensorimotor cortex using an electrode array (Frostig et al., 2008), indicating that subthreshold signal spread is not unique to VSD.

Finally, although we can image much of the neocortex using VSDs, we cannot resolve connections to cortical areas outside of the craniotomy and large-scale *in vivo* VSD imaging is not an appropriate method to study deeper cortical structures. For this reason, and due to the limited number of regions sampled, our network diagram should be considered a local connectivity map of mouse dorsal neocortex rather than a comprehensive connectome. Other cortical hub regions could exist outside of our sampling window at more lateral sites, or even in subcortical regions. Hence the network properties reported must be considered relative to the area imaged and ROIs used.

2.4.3 Network analysis of reciprocal connections and identification of hub regions reveals asymmetry in large-scale cortical organization

Although ChR2 stimulation was used to recapitulate cortical sensory maps, its greatest utility may be in probing of non-sensory areas. These areas are usually difficult to selectively activate through sensation or behavioral paradigms and tend to be understudied. Traditionally, they have been studied through anatomical methods, such as tracing of axonal projections (Veenman et al., 1992; Veenman et al., 1995; Reiner et al., 2000; Brown and Dyck, 2005). These methods are informative regarding the structural organization, but they cannot answer functional questions. As our approach allows stimulation and recording from arbitrary cortical areas, we can use our functional VSD data, represented as a weighted, directed network, to investigate reciprocal connections between regions of cortex and examine the connectivity of non-sensory and associational areas in detail. This information will add to our understanding of large-scale cortical organization.

In assessing the organization of our network we examined reciprocal connections between nodes using the connection weights from our connectivity matrix. Although reciprocal connections between cortical areas in the rodent have been previously described in tracing

studies (Fabri and Burton, 1991; Ferezou et al., 2007) and interhemispheric asymmetry between homotopic regions has been described (Chen-Bee and Frostig, 1996), less is known about intrahemispheric reciprocal connections. The strength of the reciprocal connections between M1 and BC has been described using a combination of structural analysis (anterograde and retrograde tracing) and ChR2-assisted circuit mapping (Petreanu et al., 2007; Mao et al., 2011), yet few studies describe intrahemispheric reciprocal connections *in vivo*. We found that intrahemispheric connections tended to be reciprocal, yet analysis of mean out-strength for primary and secondary sensory nodes revealed that the connection strengths between S1 and S2 were unequal; out-strength was biased in the S1 to S2 direction (S1 to S2 connections had stronger out-strength compared to S2 to S1 out-strength). The higher out-strength from S1 to S2 may suggest that S1 nodes tend to stimulate further responses in other nodes or even in sensory feedback loops, including corticothalamic circuits (Kleinfeld et al., 2006). Further analysis of connection bias at individual nodes revealed asymmetry in the out-going and in-coming weights per node (8 out of 14 nodes had asymmetric in and out connection weights), perhaps suggesting different roles in information processing, or even specialization, between nodes. Determining circuit organization at a systems level will be fundamental for our understanding of large-scale cortical processing and will build on previous work at the local cortical level using laser scanning photostimulation and glutamate uncaging in slice to map laminar connectivity (Weiler et al., 2008) and connectivity between cortical areas (Hooks et al., 2011). Both of these studies describe uneven connection strength, suggesting that asymmetrical strength in connectivity exists at multiple levels of cortical organization.

In probing the connectivity of the associational areas within the network, we found that some nodes had relatively few strong connections to or from other nodes, while other nodes had many strong connections. Specifically, we identified PTA as a hub node based on its high BC (Figure 2.7 C). The high BC of PTA indicates that a large number of potentially important connections within the network pass through this region. The PTA has been previously described as an important multisensory association area in the rat (Kolb and Walkey, 1987), monkey (Lynch, 1980), and human (Kertzman et al., 1997; Culham and Kanwisher, 2001). In the rodent, it has been suggested that the PTA is involved in sensory functions, especially due to its proximity to the visual cortices, and in movements in space (Kolb and Walkey, 1987). Lesions to PTA result in spatial navigation deficits in a landmark task in the rat (Kolb and Walkey, 1987),

and a spatial novelty task in the mouse (Thinus-Blanc et al., 1996). Thus, the multimodal nature of the PTA (Andersen, 1997) is consistent with it being defined as a network hub. Unequal connection weights between nodes and the presence of hub areas within our network indicates asymmetry within the network, and implies a scale-free or small-world network, rather than a regular or random network (Feldt et al., 2011).

2.4.4 Outlook for large-scale functional mapping in vivo

Thus far, VSD imaging using RH1692 (Shoham et al., 1999), combined with ChR2 stimulation proves to be a workable solution for *in vivo* imaging of the local and long range activity patterns within the mouse dorsal neocortex, and could be used in the future to reconstitute multisynaptic response patterns through stimulation of putative downstream areas or sequenced co-stimulation of functionally-related areas. While we anticipate that there will be future advances in protein-based voltage sensors (Akemann et al., 2010), these studies will need to involve new red-shifted opsins (Zhang et al., 2008), or voltage sensors to prevent simultaneous activation of ChR2. Our results indicate that cortical functional maps can be evoked from the stimulation of neuronal subsets, even though these neurons may receive only part of the afferent sensory input (Meyer et al., 2010). The ability of subpopulations of neurons to drive relevant downstream connectivity suggests that mechanisms must exist to self-assemble functional maps from off-target connections (Theyel et al., 2010). While we recognize that we have sampled a limited number of areas in this study, this method can be easily applied using alternate regions of interest to investigate specific circuits, or can be expanded to include many more cortical areas or the use of patterned non-point stimulation (Fino and Yuste, 2011). Here, we assume limited lateralization (asymmetry between hemispheres) within the mouse cortex, however, this method could also be used to investigate the lateralization of functional areas in the mouse (Kolb et al., 1982; Lipp et al., 1984; Chen-Bee and Frostig, 1996), expanding recent optogenetic work reporting asymmetry in the mouse hippocampus (Kohl et al., 2011). Circuit connectivity studies have been used to investigate models of disease, such as autism, where the underlying mechanism is poorly understood (Qiu et al., 2011). We anticipate that our *in vivo* approach could be used to deduce functional relationships between cortical areas and large-scale circuit organization in various mouse models of human disease, or to study the recovery after injury such as stroke (Nudo et al., 2001; Murphy and Corbett, 2009). A particular advantage of arbitrary point optogenetic stimulation is that cortical areas disconnected from their normal

functional counterparts by damage from stroke (Feeney and Baron, 1986; Dancause and Nudo, 2011) may be assessed using photostimulation and perhaps conditioned in a manner to participate in sensory or motor processing.

2.5 Supplementary materials

2.5.1 Optrode recording

A silicon optrode with sixteen recording sites (A1x16-3 mm-50-413-Op16, NeuroNexus Technologies) was used for recording of neuronal activity following ChR2 stimulation (Kravitz et al., 2010). The optrode contained sixteen 413 μm^2 recording sites, arranged linearly with 50 µm spacing between each site. The probe was inserted into the forelimb area of the primary sensory cortex (FLS1) in Thy1-ChR2 transgenic mice under urethane anesthesia. A 473 nm visible diode pumped solid state laser (IKE- 473-100-OP, IkeCool) was coupled to the optrode using a fibre-optic patch cord (FC-x.x-NNC, NeuroNexus Technologies). Laser power was adjusted to yield 5 mW at the fibre tip. Broadband signals (1-5000 Hz) from the probe were amplified (1000x), digitized (25 kHz) and stored for offline data analysis. For spike train analysis, the data were first highpass filtered (> 600 Hz). All spike detection and sorting took place offline using open source code in Matlab (Wave_Clus, http://www2.le.ac.uk/departments/engineering/research/bioengineering/neuroengineering-lab/spike-sorting.)

2.5.2 Network analysis of sensory stimulation

As in the network analysis for ChR2 stimulation, we used custom-written MatLab programs to create a connectivity matrix using sensory-evoked VSD responses from each ROI in the unilateral preparation. Here, each node corresponds to one ROI in the unilateral preparation connected by edges with weights proportional to the integrated VSD signal observed at that ROI at 20 ms after sensory stimulation. Sensory stimulation included forelimb, hindlimb, whisker, visual, and auditory stimulation, thus projections were only measured from the corresponding primary sensory areas (FLS1, HLS1, BCS1, V1, and A1). VSD responses were normalized per stimulation site, per animal, before averaging. In this case, we display all of the connections in the network (no threshold was applied).

2.5.3 Supplementary figures

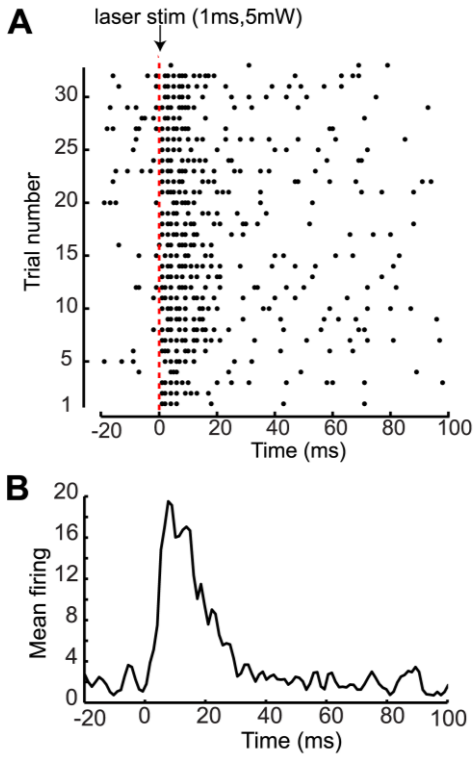

Figure 2.9 Optrode recordings from ChR2-expressing layer 5B pyramidal neurons following photostimulation. (A) Raster plot of neuronal spikes following a 1 ms 5 mW laser pulse. (B) Mean firing rate of spikes in response to laser stimulation.

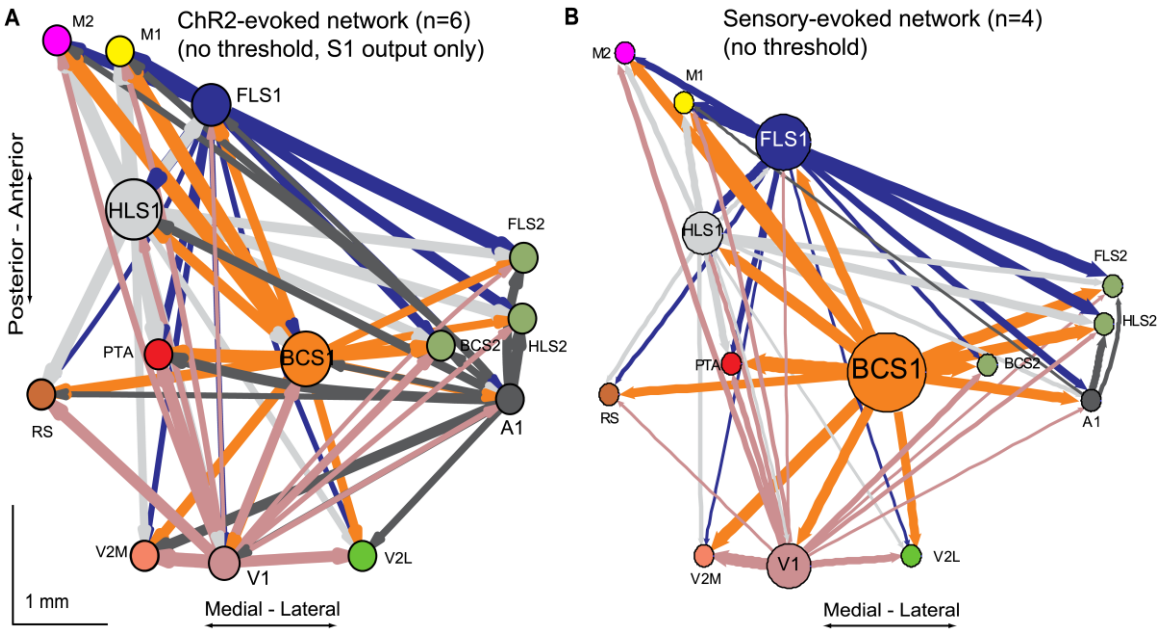

Figure 2.10 Comparison of the ChR2-evoked network with the sensory-evoked network. (A) A weighted, directed network diagram was derived following photostimulation of each ROI in the unilateral preparation by using the unilateral connectivity matrix (n=6 mice) shown in Fig. 4D. Nodes were placed according to the site of photostimulation with size proportional to the strength of connections per node (sum of weights). Arrow thickness is related to weight of an individual connection. Only output from the primary sensory areas (FLS1, HLS1, BCS1, V1, and A1) was used here. The elements (weights) were not thresholded. (B) A weighted, directed network diagram was derived following sensory stimulation of the forelimb, hindlimb, whisker, visual system and auditory system in the unilateral preparation. Node size is proportional to the strength of connections per node (sum of weights). Arrow thickness is proportional to the weight of an individual connection.

3. Optogenetic mapping after stroke reveals network-wide scaling of functional connections and heterogeneous recovery of the peri-infarct

3.1 Introduction

Stroke triggers a cascade of events affecting all levels of cortical organization, from individual neurons and synapses (microscale), to neuronal groups and populations (mesoscale), to distinct regions and inter-regional connections (macroscale) (for a review, see Carmichael, 2003; Grefkes and Fink, 2011; Silasi and Murphy, 2014). At the level of cortex, it has been shown that function is disrupted within minutes of a stroke (Mohajerani et al., 2011) and disrupted circuits can persist for weeks after stroke even in surviving tissues (Nudo and Milliken, 1996; Brown et al., 2009). It has been shown that the effects of cortical damage may extend beyond the stroke core (Buchkremer-Ratzmann et al., 1996; Seitz et al., 1999; Carmichael et al., 2004), however, large-scale functional assessment of the cortex has been challenging. Most methods have relied on peripheral stimulation (Brown et al., 2009), which is limited to sensory or motor cortex activation, or have used invasive cortical stimulation, which provide only limited spatial sampling (Frost et al., 2003; Gharbawie et al., 2005). While blood oxygenation level dependent (BOLD) functional magnetic resonance imaging (fMRI) has been used to describe post-stroke interhemispheric functional connectivity both experimentally (Dijkhuizen et al., 2001; Dijkhuizen et al., 2003; van Meer et al., 2010; van Meer et al., 2012) and clinically (Carter et al., 2010; Grefkes and Fink, 2011), this is potentially an indirect measure of neuronal activity.

We combined channelrhodopsin-2 (ChR2) stimulation with regional voltage sensitive dye (VSD) imaging (Lim et al., 2012) to functionally map the mouse cortex after a targeted photothrombotic stroke. This method has the advantage of high temporal resolution, relatively non-invasive arbitrary point stimulation, and large-scale recording of sub- and supra-threshold neuronal activity (Lim et al., 2013). With these advantages in mind, we assessed macroscale functional connectivity and plasticity after stroke across both hemispheres, and in the peri-infarct area (Figure 3.1).

We found equally scaled network-wide changes in functional connectivity after stroke that extended to the non-injured hemisphere. Network-wide depression observed 1 week after stroke may result from connectional diaschisis (Carrera and Tononi, 2014), where a loss of excitation from infarcted regions affects remote areas. By 8 weeks post-stroke, examination of

connection strength revealed further network-wide scaling, suggesting that the post-stroke network recovers by adjusting towards a pre-stroke pattern of relative connectivity strength between nodes. However, closer inspection of peri-infarct connections revealed a heterogeneous recovery that did not fit the scaling factor of the entire network. This indicates regionally specific plasticity mechanisms, or a failure to overcome the greatest extent of stroke damage.

3.2 Materials and methods

3.2.1 Photothrombotic strokes

We used ChR2 transgenic mice from Jackson Laboratory (line 18, stock 007612, strain B6.Cg-Tg (Thy1-COP4/EYFP) 18Gfng/J). Male mice were approximately 16 weeks old and weighed ~25g and were given a photothrombotic stroke (mean volume = 0.30 ± 0.036 mm^3, n = 15 mice) targeted to the right primary forelimb cortex as described previously (Brown et al., 2009). Consistent with previous reports (Witte et al., 2000; Brown et al., 2009), photothrombotic strokes created lesions that extended through all cortical layers, but without penetrating the underlying white matter (maximal depth from pial surface = 0.791 ± 0.034 mm, present at + 0.14 Bregma, n = 15 mice; see Figure 3.1, i). Previous work in our lab has shown that these strokes are sufficient to cause a significant asymmetry in forelimb use in the cylinder task, with the greatest impairment seen at 1 week post-stroke, and recovery towards baseline levels of performance by 8 weeks post-stroke (Brown et al., 2009). Sham animals underwent sham photothrombosis (no Rose Bengal injection or no laser exposure). All animals were closely monitored for 24 hours following surgery, and then daily for one week thereafter. All experiments were conducted in accordance with the guidelines from the Canadian Council for Animal Care and were conducted with approval from the University of British Columbia Animal Care committee.

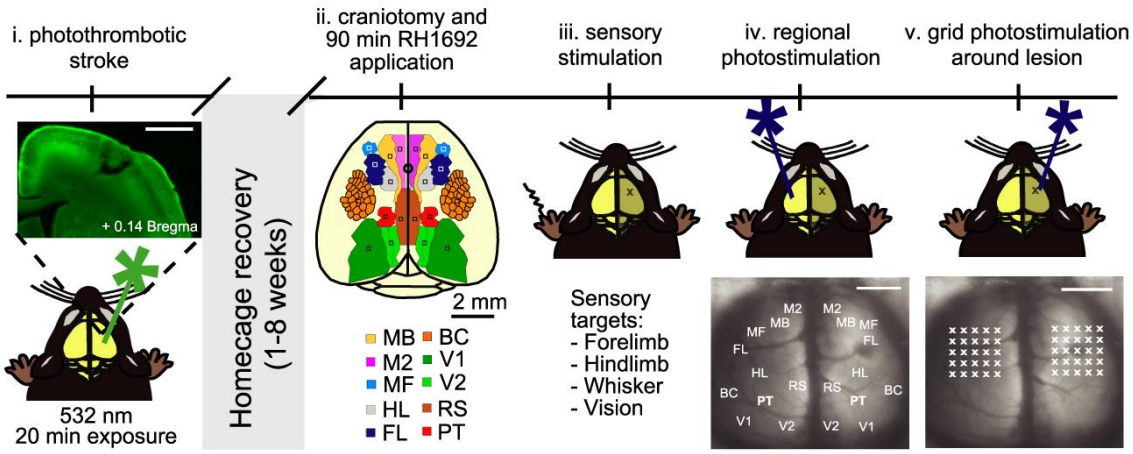

Figure 3.1 Experimental timeline for mapping functional connectivity with channelrhodopsin-2 stimulation and voltage sensitive dye imaging. Schematic illustration of the experimental design. Animals were given a photothrombotic stroke (i) targeted to the forelimb area of the primary somatosensory cortex (FL). The inset shows a coronal section that demonstrates that the stroke damaged the cortical layers without penetrating the underlying white matter (scale bar = 1 mm). After 1 or 8 weeks of home cage recovery, animals were given a large bilateral craniotomy (ii). VSD imaging was completed for sensory stimulation (iii), regional photostimulation at functional ROIs (iv), and grid photostimulation in the peri-infarct (iv). Scale bar = 2 mm.

3.2.2 In vivo VSD imaging

At 1 week or 8 weeks after stroke or sham surgery (Figure 3.1, i), mice were anesthetized with isoflurane (1.0%) and given a large (8 x 8 mm window) bilateral craniotomy (Mohajerani et al., 2011). We chose a voltage sensitive dye (VSD) from the RH series (Shoham et al., 1999) - RH1692. The dye was prepared as previously described (Brown et al., 2009) and applied to the exposed cortex for 90 min, staining all cortical layers (Mohajerani et al., 2010). Following VSD application, the cortex was covered in agarose (1%) and a glass coverslip was applied. VSD imaging followed immediately. Images (12-bit images with 6.67 ms temporal resolution) were captured on a CCD camera (1M60 Pantera, Dalsa, Waterloo, ON, Canada), as described previously (Lim et al., 2012). For each stimulus, 2-5 trials were averaged together to reduce the effect of any spontaneous cortical activity (Mohajerani et al., 2010).

3.2.3 Cortical electroencephalogram recordings

Throughout the experiment, electroencephalogram (EEG) activity was monitored. Teflon coated chlorided silver wires (0.125 mm) were placed on the left and right edge of the craniotomy, with a reference electrode placed on the nasal bone. The signal was amplified and filtered (0.1-1000 Hz), using an AM-systems (Squim, WA, USA) Model 1700 AC amplifier. To ensure that cortical excitability did not vary after stroke, the amplitude of the first EEG

depolarization following photostimulation was measured at sites both near and distant to the lesion core and average peak amplitude was compared across groups using unpaired t-tests.

3.2.4 Sensory stimulation

In order to generate functional maps of the primary sensory cortical areas, a number of sensory stimuli were presented (Figure 3.1, iii). Probes were inserted subcutaneously to each of the paws and a 1ms 1mA pulse was delivered to map the forelimb and hindlimb areas of the primary somatosensory cortex in each hemisphere. A single whisker (C2) was given a 1 ms tap using a piezo device to map the somatosensory barrel cortex, and a 1ms combined green and blue light stimulus was presented to map the primary visual cortex. These functional maps were then used to determine coordinates for regional photostimulation.

3.2.5 Photostimulation

We used a 1ms, 5 mW pulse generated by a 473 nm diode pumped solid state laser (CNI Optoelectronics, Changchun, China) to stimulate ChR2-expressing neurons, as previously described (Lim et al., 2012). Regional photostimulation sites (Figure 3.1, iv) were targeted based on functional sensory areas defined through sensory stimulation or based on stereotaxic coordinates. These regions of interest (ROI) included: secondary motor cortex (M2); motor barrel cortex (MB); motor forelimb cortex (MF); forelimb area of the primary somatosensory cortex (FL); hindlimb area of the primary somatosensory cortex (HL); somatosensory barrel cortex (BC); parietal cortex (PT); retrosplenial cortex (RS); secondary/medial visual cortex (V2); primary visual cortex (V1). To determine grid photostimulation sites within the peri-infarct zone, a 5x5 photostimulation grid was centered over the lesion and over the homotopic region in the left hemisphere (Figure 3.1, v). Grid photostimulation sites were 500 μm apart, resulting in the grid extending 1 mm from the lesion core in the anterior, posterior, lateral, and medial directions.

Each site was photostimulated 2-4 times in an interleaved, semi-random order to reduce any time-dependent effects of anesthetic depth as well as any possibility of cortical damage due to repetitive stimulation. A 10 s inter-trial interval ensured full recovery of VSD fluorescence. VSD responses were taken from all other ROIs and replicate responses were averaged together.

3.2.6 Data analysis

VSD responses to stimulation were calculated as the normalized difference to the average baseline recorded before stimulation (% $\Delta F/F_0$) in MatLab (Mathworks, Natick, MA). For each

stimulation type (each of the 5 sensory modalities, each of the 20 regional photostimulation sites, and each of the 50 peri-infarct grid photostimulation sites), 2-5 trials were collected and % $\Delta F/F_0$ responses were averaged across trials. Custom-written MatLab programs were used to analyze and quantify the VSD responses (peak amplitude, time to peak amplitude, and area under the curve). Peak amplitude was calculated by finding the maximum response in the first 127 ms post-stimulus in the trial averaged % $\Delta F/F_0$. To ensure that the peak was not noise, the response had to be greater than 2.5 times the standard deviation of the baseline (initial 180 ms of the recording). Within the peri-infarct, we calculated loss, gain, and net difference per site according to the following formulas:

Loss = (sham VSD response - VSD response at 1 week post-stroke)

Gain = (VSD response at 8 weeks post-stroke - VSD response at 1 week post-stroke)

Difference = (Gain - Loss)

3.2.7 Network analysis

We used custom-written MatLab programs as well as scripts from the brain connectivity tool box [http://www.brain-connectivity-toolbox.net (Rubinov and Sporns, 2010)], to create a 20 x 20 connectivity matrix and network diagram based on the ChR2-evoked VSD responses from each ROI (Lim et al., 2012). Briefly, for each regional photostimulation site, we calculated the integrated VSD response at 20 ms after photostimulation (the sum of the VSD response in units of % $\Delta F/F_0$ from stimulus onset to 20 ms after photostimulation) at the remaining regional response sites. For each ROI, the connectivity matrix shows in-strength as the rows (the strength of the connections coming to the ROI when other areas were photostimulated) and out-strength as the columns (the strength of the connections to other areas when the ROI was photostimulated). We used the connectivity matrices to evaluate differences in connection strength between groups (for example, comparing average in- and out-strength per hemisphere). For illustrative purposes only, we used the data from the connectivity matrix and applied a consistent threshold across groups to create network diagrams with only the strongest VSD responses. We chose a threshold that did not affect the characteristic path length and clustering coefficient (common network metrics), as described previously (Lim et al., 2012). For the network diagrams, node size is proportional to the strength of the connections per node (sum of the weights per photostimulation site) and edge thickness between nodes is proportional to the

weight of the connections between nodes. For the post-stroke network diagrams, we calculated the change in strength from sham to 1 week post-stroke, and from 1 week to 8 weeks post-stroke. Network diagrams were color-coded to demonstrate changes in network connections over time with red indicating a loss of strength, green indicating a gain of strength, and gray representing a marginal change (less than 15%) in strength.

To predict which nodes would be most-at-risk and least-at-risk after the stroke, we calculated total node strength (sum of the weights per photostimulation site) as well as node strength related to the right FL (FLR; sum of in strength from FLR and out strength to FLR). We predicted that nodes with the highest strength within the regional network would also show the most impairment after stroke.

3.2.8 Histology

To investigate whether the stroke caused any changes in ChR2 expression after stroke, mice were deeply anesthetized and transcardially perfused, and brain sections were imaged and analyzed as described previously (Lim et al., 2012). In brief, coronal sections (100 μm) were cut on a vibratome and imaged using a Zeiss LSM 510 Meta confocal microscope with a multi-line argon laser and a Plan-Neofluar 5X (0.15 NA) objective. A 488-nm line argon laser excited the YFP-ChR2 fusion protein (Arenkiel et al., 2007). Tiled scans (12-bit; 512 x 512 pixels) were collected using Zen 2009 software. ChR2 expression was quantified in 5 sham and 5 1 week post-stroke animals at 3 different sections: anterior to lesion (Bregma + 1.1), near the lesion (Bregma -0.2), and posterior to the lesion (Bregma - 1.06). Each section was filtered (Gaussian filter of 6.0 pixel radius) and normalized relative to the fluorescence in the fornix (Bregma -1.06) using NIH Image J software (Version 1.42q). The fornix was chosen because it expresses YFP, but is distant from the lesion and not part of the cortex. A 100 pixel freehand line was drawn to plot the fluorescence profile from medial to lateral in each hemisphere.

3.2.9 Statistical analyses

A one-way analysis of variance (ANOVA) with Bonferroni post-tests was used for statistical analysis of peak amplitude, time to peak, and area under the curve. Two-way repeated measures ANOVA with Bonferroni post-tests were used to compare connectivity matrices between groups. Permutation tests (van den Heuvel and Sporns, 2011) were used to evaluate the mean difference in strength between groups. Kolmogorov-Smirnov (KS) tests were used to

compare cumulative distribution functions between groups before and after scaling to match the group means. Linear regression was calculated using GraphPad Prism (GraphPad Software, San Diego, CA, USA). All p values ≤ 0.05 were considered statistically significant. Data are expressed as the mean ± standard error of the mean (SEM).

3.3 Results

3.3.1 Sensory-evoked activity after stroke shows delayed and depressed VSD responses in the injured hemisphere

In the sham animals, sensory stimulation of the forelimb, hindlimb, whiskers, or visual system produced the expected stereotypical depolarizing signals within the somatosensory cortex (Lim et al., 2012; Mohajerani et al., 2013). In the stroke group, sensory stimulation of the whiskers and visual system produced VSD signals comparable to sham animals, however the VSD signal following stimulation to the affected forelimb was severely depressed and delayed (Figure 3.2 A). To quantify the VSD responses, we created intensity over time plots and analyzed three different aspects of the VSD signal: peak amplitude, time to peak, and area under the curve. After sensory stimulation to the left (affected) forelimb, the response in the right (injured) hemisphere was significantly greater in shams compared to the stroke animals at 1 week or 8 weeks post-stroke as revealed by one-way ANOVA and Bonferroni's post-hoc test: there was a significant effect of group on peak amplitude [$F(2,21) = 12.21$, $p = 0.0178$], time to peak amplitude [$F(2,18) = 8.610$, $p = 0.0024$], and area under the curve to 20 ms [$F(2,22) = 8.697$, $p = 0.0016$] (Figure 3.2 B). Similarly, the response in the left (non-injured) hemisphere was also significantly different between groups in peak amplitude [$F(2,22) = 5.770$, $p = 0.0097$], time to peak amplitude [$F(2,17) = 4.392$, $p = 0.0290$], and area under the curve [$F(2,22) = 5.524$, $p = 0.0114$] (Figure 3.2 C). This delayed and suppressed response within the ipsilesional hemisphere in the stroke animals was similar to previous reports using VSD imaging following somatosensory stroke (Brown et al., 2009).

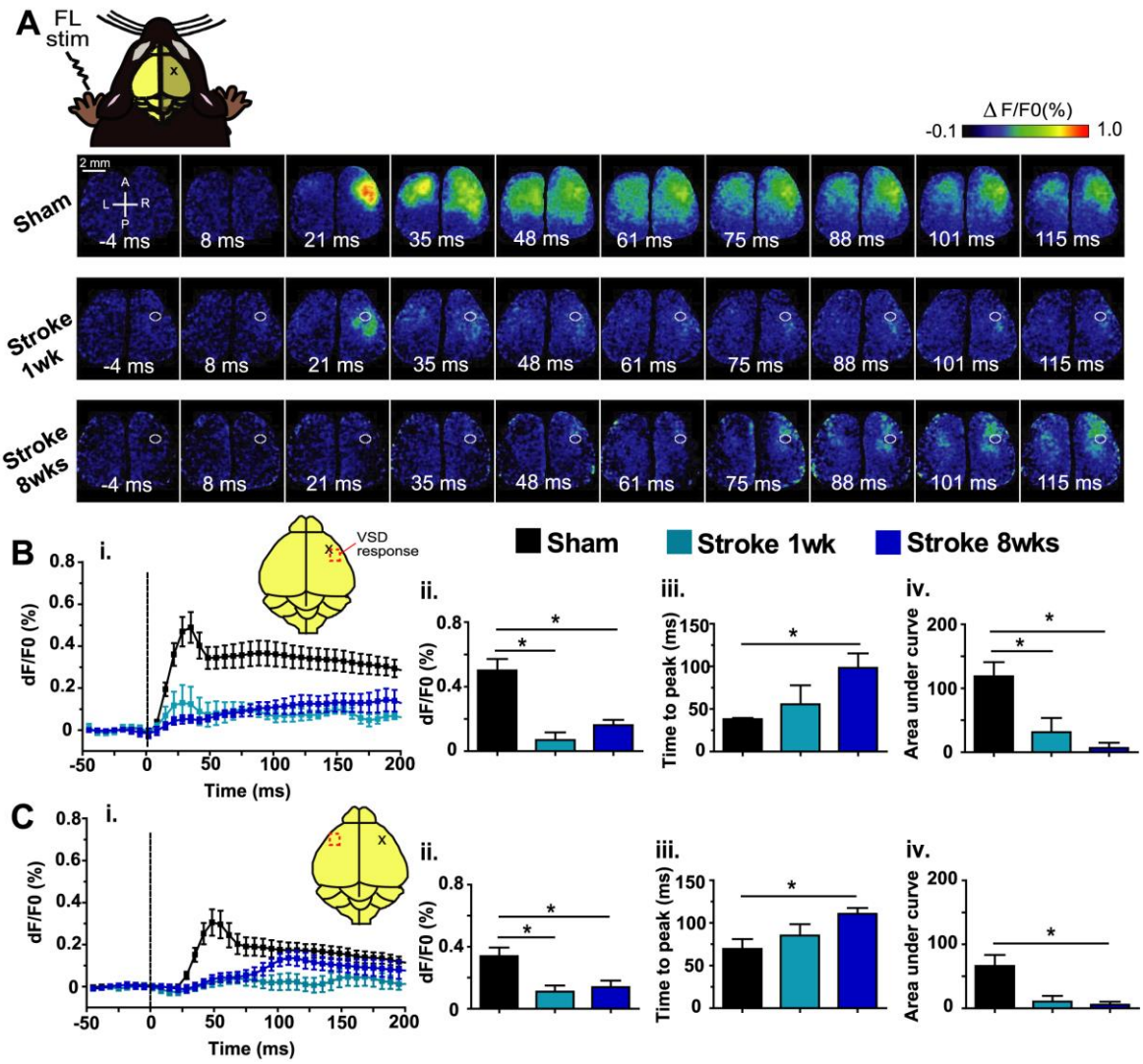

Figure 3.2 Voltage sensitive dye imaging maps of the injured limb shows delayed and decreased VSD responses in both hemispheres. (A) Example VSD responses in a bilateral craniotomy preparation after electrical stimulation of the left (injured) forelimb in a sham animal (top), 1 week post-stroke (middle) and 8 weeks post-stroke animal (bottom). The lesion in the stroke animals is indicated by the white circle. Quantitative comparisons of the VSD response from the right (injured) hemisphere (B) and left (non-injured) hemisphere (C). i. Intensity versus time plot of the VSD response; ii. Peak amplitude (dF/F0 %) VSD response; iii. Time (ms) to peak amplitude; iv. Area under the curve to 20 ms after stimulation. (* $p < 0.05$)

3.3.2 Channelrhodopsin-evoked activity shows depressed, but not delayed VSD responses after stroke in the injured hemisphere

Based on the location of cortical activations observed after sensory stimulation, a number of cortical regions were targeted for photostimulation (see Methods and Figure 3.1, iv). Twenty

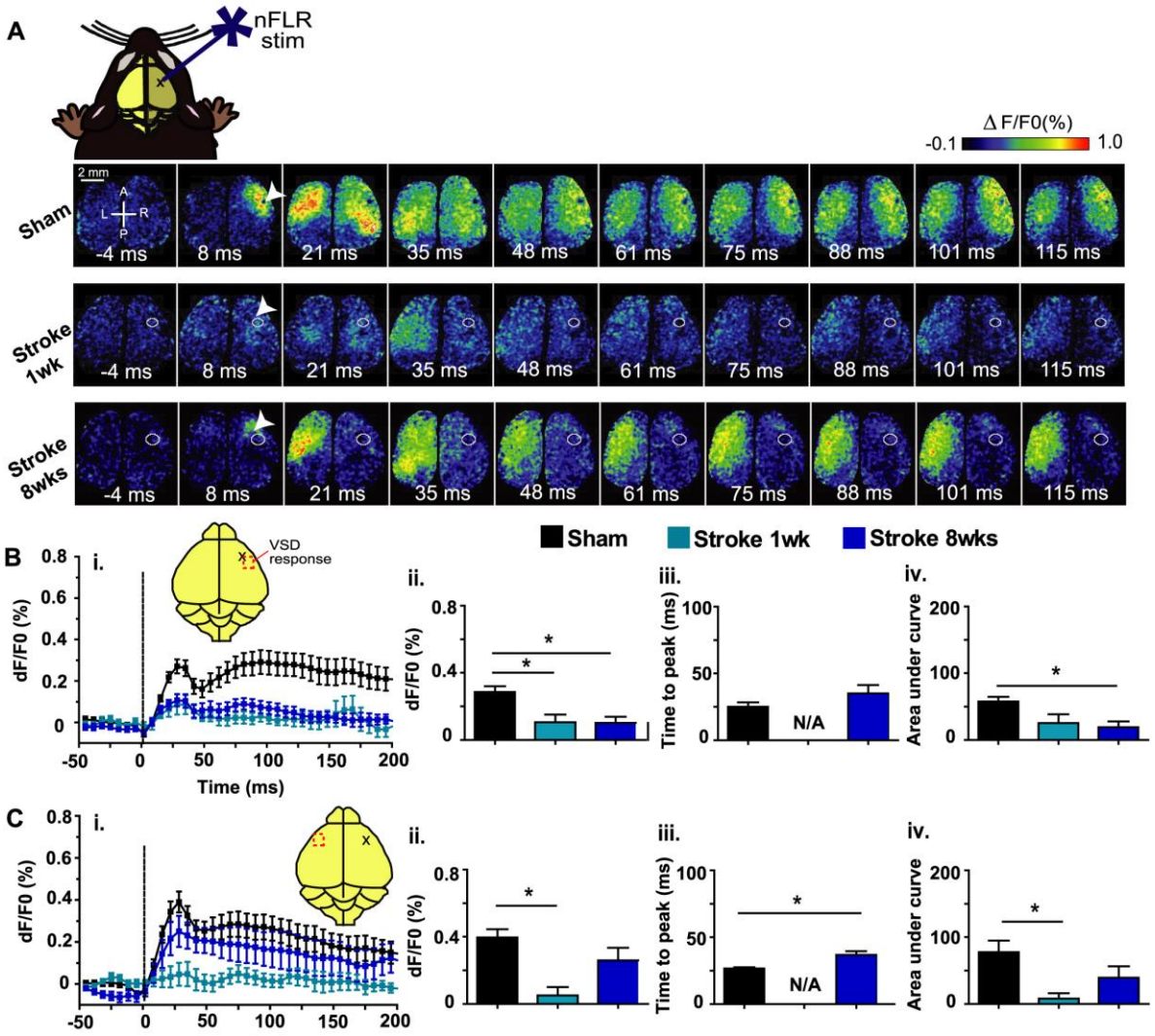

Figure 3.3 Voltage sensitive dye imaging maps of photostimulation of the injured forelimb cortex results in stronger and faster VSD responses than expected from sensory stimulation. (A) Example VSD responses in a bilateral craniotomy preparation after photostimulation of the right (injured) forelimb somatosensory cortex in a sham animal (top), 1 week post-stroke (middle) and 8 weeks post-stroke animal (bottom). The lesion in the stroke animals is indicated by the white circle. White arrows indicate laser photostimulation target. Quantitative comparisons of the VSD response from the right (injured) hemisphere (B) and left (non-injured) hemisphere (C). i. Intensity versus time plot of the VSD response; ii. Peak amplitude (dF/F0 %) VSD response; iii. Time (ms) to peak amplitude; iv. Area under the curve to 20 ms after stimulation. (* $p < 0.05$). Time to peak is not shown in the 1 week post-stroke condition due to only a few samples showing a well-defined peak in the response.

regions of interest (ROIs) were selected for photostimulation (10 per hemisphere) and recording of VSD responses. After photostimulation of each ROI, VSD responses were measured at the other ROIs, giving a total of 19 response sites per photostimulation site (VSD responses were not measured at the photostimulation site itself due to transient photobleaching). We were most interested in the VSD response following photostimulation of the FL in the right and left hemisphere, as these were the areas that showed the greatest changes following sensory

stimulation. Following photostimulation of the right forelimb area of the primary somatosensory cortex (FLR) in the sham group (Figure 3.3 A, top panel), the VSD response was similar to the response pattern seen with sensory stimulation of the left forepaw (compare to Figure 3.2a, top panel), as previously reported (Lim et al., 2012). In the stroke groups the FLR was the area targeted for stroke, thus the VSD response to sensory stimulation of the affected forepaw was termed the new FLR (nFLR), and was targeted for photostimulation. At 1 week post-stroke, the VSD signal in response to photostimulation of nFLR was depressed in both the left and right hemispheres (Figure 3.3 A, middle panel). By 8 weeks post-stroke, a small VSD response could be observed in the nFLR before activation of the left hemisphere. The contralateral (to stimulation) response (in the non-injured hemisphere) was much larger and lasted longer than the ipsilateral response (in the injured hemisphere) at 8 weeks post-stroke (Figure 3.3 A, bottom panel). Using a one-way ANOVA and Bonferroni's post-hoc test, we compared the response in the right (injured) hemisphere (Figure 3.3 B). There was a significant effect of group on the peak amplitude of the VSD response [$F(2,22) = 8.356$, $p = 0.0020$], and the area under the curve to 20 ms after photostimulation [$F(2,22) = 5.785$, $p = 0.0096$]. There was no significant effect of group for time to peak amplitude [$F(2,17) = 1.117$, $p = 0.3502$], unlike the sensory responses which were greatly delayed in the post-stroke groups. In the left (non-injured) hemisphere (Figure 3.3 C), a one-way ANOVA revealed a significant effect of groups for peak amplitude [$F(2,22) = 8.264$, $p = 0.0021$], time to peak amplitude [$F(2,17) = 17.21$, $p < 0.0001$], and area under the curve to 20 ms [$F(2,22) = 4.203$, $p = 0.0285$]. Results of Bonferroni post-tests are displayed in Figure 3.3.

3.3.3 Assessment of the inter- and intracortical network trends from connectivity matrices

In order to represent the data as a whole and to show relationships between and within the regional photostimulation sites, a 20 x 20 connectivity matrix was created for each group (sham, 1 week post-stroke, and 8 weeks post-stroke) to display the integrated VSD response at 20 ms after photostimulation (the sum of the VSD response in units of % $\Delta F/F_0$ from stimulus onset to 20 ms after photostimulation) of each ROI (Figure 2.4, left). In the sham connectivity matrix (Figure 3.4 A), well-known relationships can be identified in the connectivity matrix, such as between the somatosensory barrel cortex and motor cortex: when left somatosensory barrel cortex (BCL) is photostimulated, it evokes strong VSD responses from the motor areas, especially left motor representation of the barrel cortex (MBL).

In general, the strongest VSD responses in the sham matrix were in the regions functionally related to or neighboring the photostimulation site, and in the homotopic-to-stimulation site. For example, if the right FL (FLR) was photostimulated, the strongest response was seen in areas surrounding the FLR, such as the right motor area of the forelimb area (MFR), and right hindlimb area of the primary somatosensory cortex (HLR), and in the homotopic site (FLL). Photostimulation of the left FL (FLL) produced the mirror response. Permutation tests isolating the left hemisphere stimulation sites and the right hemisphere sites in the sham matrix showed no significant difference in out-going strength (left sites average out-strength = 2.91, right sites average out-strength = 2.71, $p = 0.1857$). Similarly, permutation tests comparing left vs. right hemisphere responses showed no significant difference in in-coming strength (left sites average in-strength = 2.84, right sites average in-strength = 2.78, $p = 0.3627$).

When network analysis was applied to this matrix using the brain connectivity tool box [http://www.brain-connectivity-toolbox.net (Rubinov and Sporns, 2010)], a distinct per-hemisphere module was identified. Within these modules, we divided the nodes into functional groups (somatomotor nodes including MB, MF, M2, FL, HL, BC as one group, "G1", and association and visual nodes including V2, V1, RS, PT as a second group, "G2"). The somatomotor group (G1) can be seen in the connectivity matrix as "hot-spots" - photostimulation of the nodes that make up the G1 group result in strong VSD responses in the G1 nodes in both the right and left hemispheres in the sham connectivity matrix (see black dashed boxes in Figure 3.4 A). Comparing the responses (the sum of the VSD response from stimulus onset to 20 ms after photostimulation) across the diagonal, responses appear relatively equal between left and right hemispheres (average left hemisphere response = 2.84, average right hemisphere response = 2.78; $p = 0.3627$), suggesting that the left and right hemisphere modules are relatively equal.

In contrast, the connectivity at 1 week post-stroke shows severely depressed VSD responses at all nodes (Figure 3.4 B). Because the stroke was targeted over the FLR, the connectivity matrix shows the nFLR. When the nFLR was photostimulated the response was depressed in both the right and left hemispheres. While the larger responses were still from regions neighboring the photostimulation site, these responses were low relative to sham animals. At 1 week post-stroke the responses are not equal between hemispheres (average left hemisphere response = 1.65, average right hemisphere response = 1.31; $p = 0.0064$) and the groups (“G1” and “G2”) are not as apparent as in the sham matrix - while there is a cluster of left

hemisphere responses to left somatomotor stimulation (upper left in the connectivity matrix in Figure 3.4 B), the other groups are not easily observed. By 8 weeks post-stroke the connectivity matrix is still somewhat depressed relative to the sham matrix, however, the node groupings are more distinct and in most cases these VSD responses were stronger compared to 1 week post-stroke (Figure 3.4 C). While the responses are not equal between hemispheres at 8 weeks post-stroke (average left hemisphere response = 2.04, average right hemisphere response = 1.73; p = 0.0222), the functional groups within the network appear to be returning to sham levels (see black dashed boxes outlining G1 clusters in the upper left and lower right of the matrix on Figure 3.4 C).

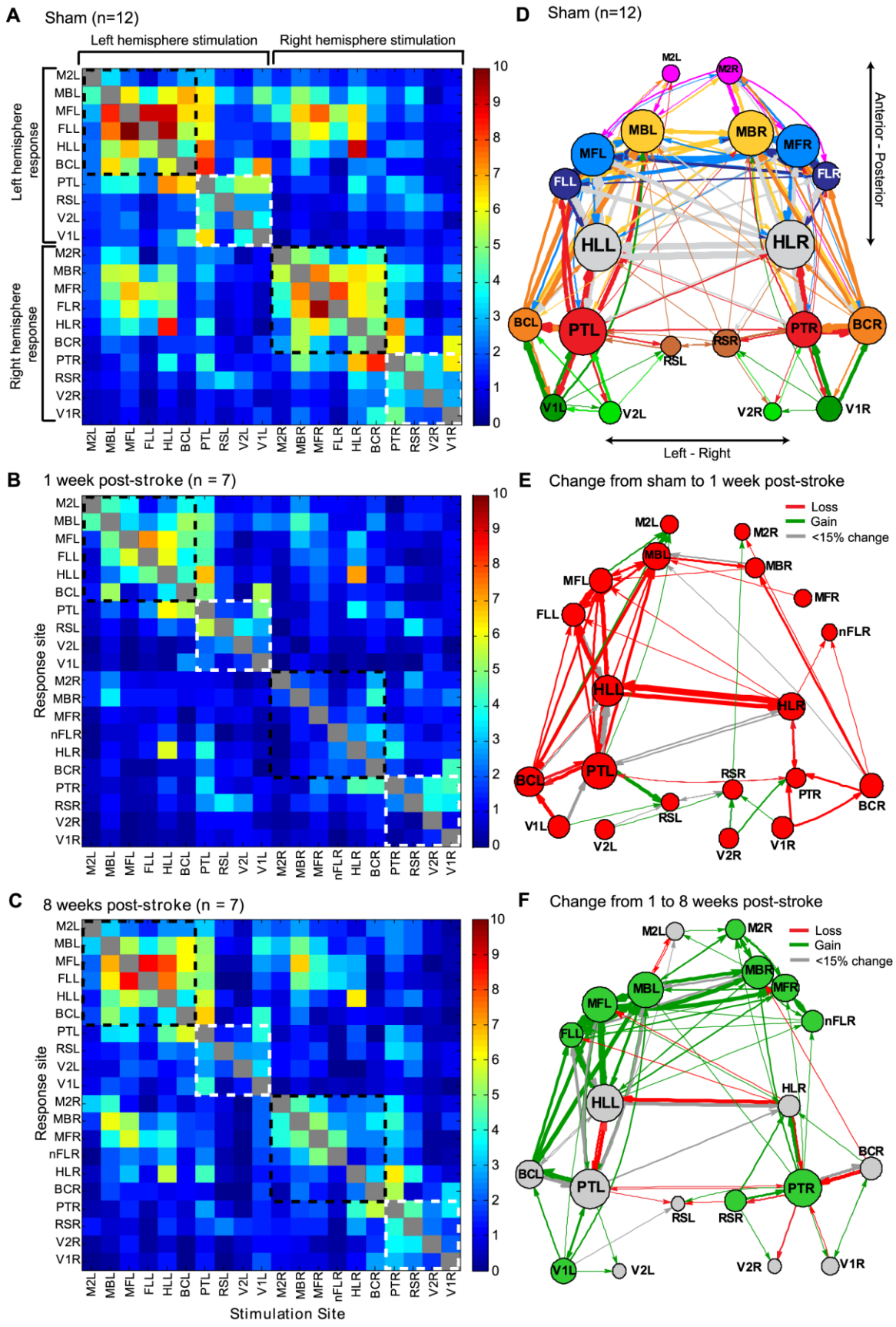
A
Sham (n=12)
Left hemisphere stimulation
Right hemisphere stimulation
Left hemisphere response
Right hemisphere response
M2L MBL MFL FLL HLL BCL PTL RSL V2L V1L M2R MBR MFR FLR HLR BCR PTR RSR V2R V1R
0 1 2 3 4 5 6 7 8 9 10
B
1 week post-stroke (n = 7)
Response site
M2L MBL MFL FLL HLL BCL PTL RSL V2L V1L M2R MBR MFR nFLR HLR BCR PTR RSR V2R V1R
C
8 weeks post-stroke (n = 7)
Response site
Stimulation Site
D
Sham (n=12)
Anterior - Posterior
Left - Right
E
Change from sham to 1 week post-stroke
Loss
Gain
<15% change
F
Change from 1 to 8 weeks post-stroke
Loss
Gain
<15% change

Figure 3.4 Connectivity changes over time reveal asymmetries after stroke (previous page)**.** Average connectivity matrices (left) and network diagrams (right) all derived from the VSD response at 20 ms after photostimulation in (A) the sham group (n=12), (B) 1 week post-stroke (n=7), and (C) 8 weeks post-stroke (n=7). Connectivity matrices are organized from left hemisphere to right hemisphere sites, and from anterior to posterior sites. Dashed lines indicate the somatomotor group, G1 (black), and the association group, G2 (white). A threshold (2.6) was used to create the network diagrams for the sham (D), 1 week post-stroke (E), and 8 weeks post-stroke (F) groups. Nodes were placed according to the site of photostimulation. Node size is proportional to the strength of the connections per node (sum of the weights). Edge thickness (arrows) between nodes is proportional to the weight of the connection between nodes. To demonstrate changes over time, network diagrams showing the change from sham to 1 week post stroke (E) and the change from 1 week to 8 weeks post stroke (F) were colour-coded to demonstrate changes in network strength. Red indicates a loss of strength, green indicates a gain of strength, and gray indicates a marginal change (less than 15% change in strength).

To facilitate the visualization of the relationships between cortical areas, we derived network diagrams from the connectivity matrices (Figure 3.4, right), as described previously (Lim et al., 2012). The diagrams represent only the strongest connections observed in each group (see Methods) and illustrate broad patterns within the network. In the sham diagram (Figure 3.4 D) the left and right hemisphere are relatively symmetrical. This symmetry is lost in the post-

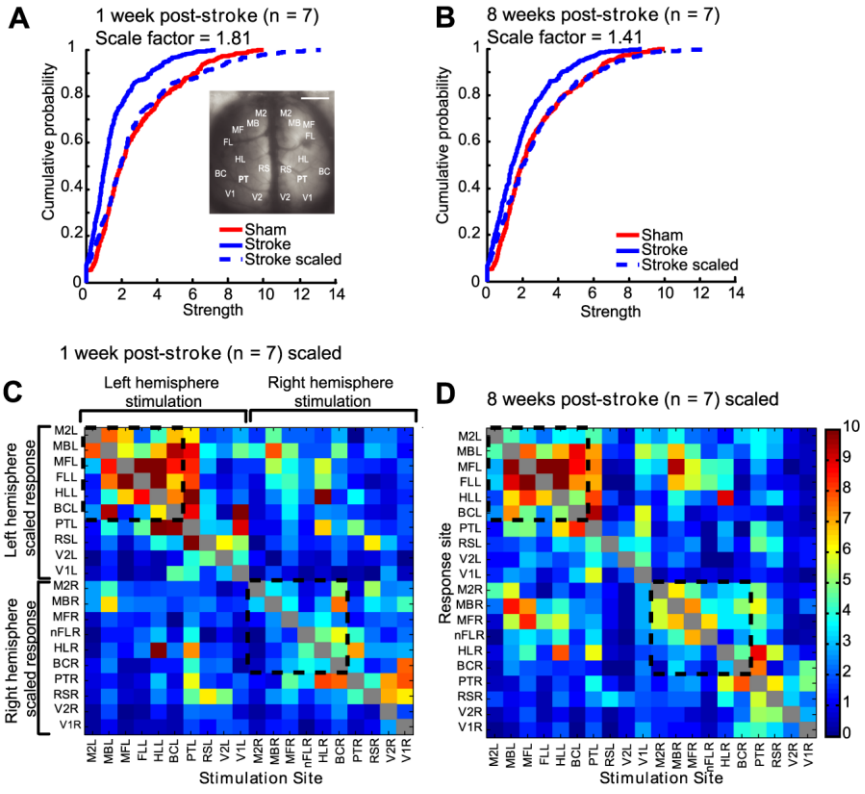

Figure 3.5 Regional network-wide scaling of the connectivity matrix leads to relative connectivity strengths similar to sham. Values from the connectivity matrices were scaled such that the mean of the stroke group matched the mean of the sham group. Cumulative distribution function for VSD responses at 1 week post-stroke (A) or 8 weeks post-stroke (B) compared to sham (red). Dashed lines indicate scaled values. Scaled values were used to create connectivity matrices for 1 week post-stroke (C) and 8 weeks post-stroke (D). Dashed black lines indicate the somatomotor group in the connectivity matrix. Compare these to the sham matrix in Figure 3.4 A.

stroke animals, and there are fewer strong connections in the post-stroke network diagrams (Figure 3.4, E-F). Interestingly, while the stroke is targeted to the right hemisphere FL, the left hemisphere in the post-stroke animals also has fewer connections and weaker node strength. By 8 weeks post-stroke (Figure 3.4 F) the network diagram appears to be returning towards sham levels: there are more connections relative to the 1 week post-stroke network diagram and some of the symmetry between the left and right hemisphere is re-established.

3.3.4 Assessment of the differences between groups using the connectivity matrices

In order to compare the changes between groups, we compared the mean connection strength between groups using t-tests between the matrices. The groups were significantly different as the responses from the stroke animals were greatly depressed (sham compared to 1 week post-stroke, sham compared to 8 weeks post-stroke, or 1 week post-stroke compared to 8 weeks post-stroke, $p < 0.0001$). To determine whether the depressed VSD responses we observed in the stroke animals could be normalized to the sham connectivity strength distribution by a constant scaling factor, we normalized the connectivity matrices so the group means were equal and checked for the equality of the resulting distributions using Kolmogorov-Smirnov (KS) tests before and after normalization by scaling the whole network. After normalization, the groups were statistically indistinguishable by KS tests (sham vs. 1 week post-stroke, $p = 0.3558$; sham vs. 8 weeks post-stroke, $p = 0.1055$), indicating widespread scaling down across the network in the stroke groups (Figure 3.5). It is possible that the stroke could affect the overall ChR2 expression, as it is known that stroke can affect gene and protein expression (Carmichael, 2003). However, examination of several anterior to posterior histological sections indicated that ChR2 expression was not significantly different between the injured and non-injured hemisphere ($p = 0.4102$), nor did it vary by more than 50% across the anterior-posterior axis when sections were normalized per animal to YFP expression in the fornix (see Methods). Furthermore, analysis of EEG recordings showed that ChR2-evoked depolarizations following photostimulation in 1 week post-stroke animals were not statistically different from sham animals at sites near to the lesion (HLR: sham = -0.403 ± 0.019 mV vs. stroke = -0.518 ± 0.072 mV, $p = 0.1310$) nor were they statistically different at sites distant from the lesion (V1L: sham = = -0.255 ± 0.051 mV vs. stroke = -0.273 ± 0.1 mV, $p = 0.8777$). This suggests the excitability of ChR2 or peri-infarct neurons did not differ significantly between groups. Conceivably, depression in regions

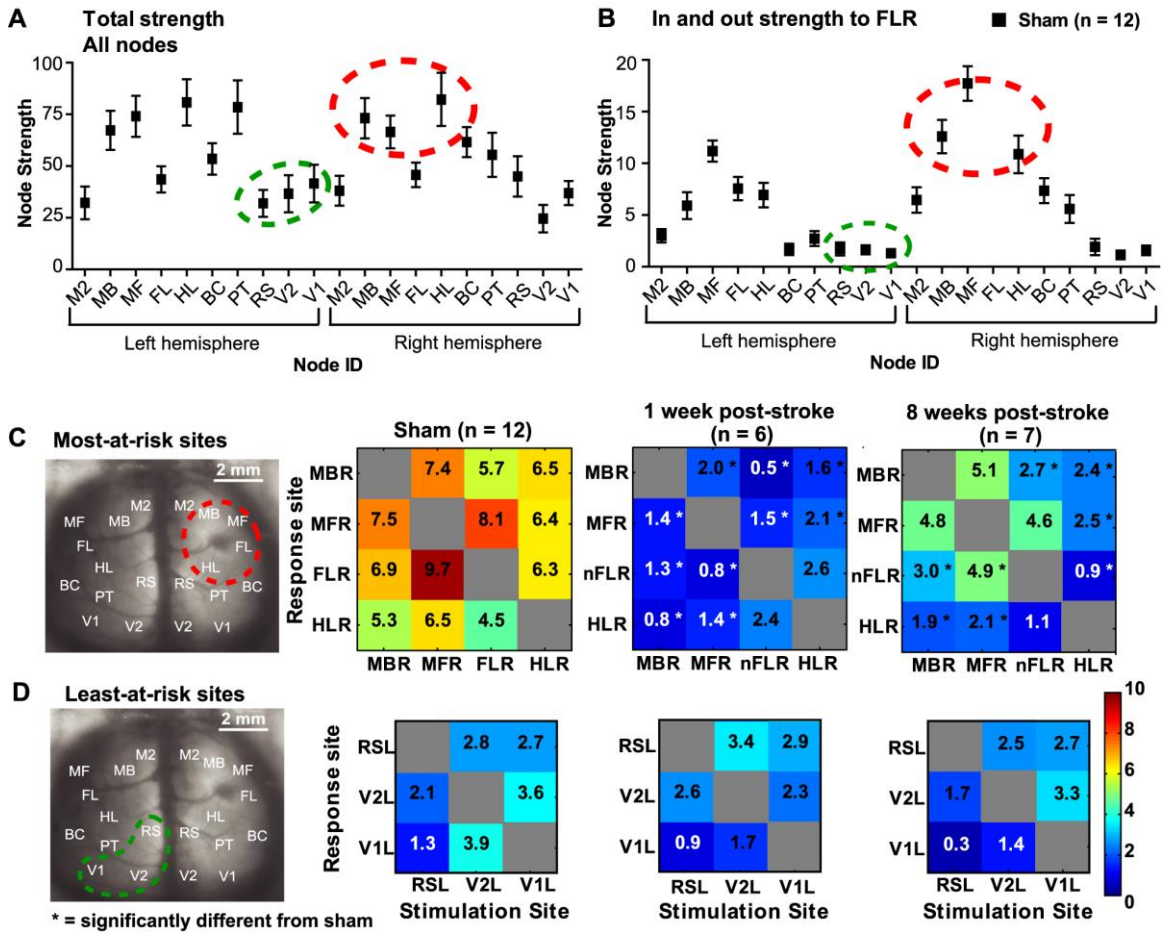

Figure 3.6 Node strength from the sham network predicts which sites will be most-affected and least-affected after stroke. Total node strength (A) and node strength relative to FLR (B) were calculated in the sham network to predict which regional sites would be most-at-risk and which would be least-at-risk after stroke. The predicted most-at-risk sites are high in strength within the regional network (circled in red in A & B) and close in proximity to the lesion. These sites are significantly depressed after stroke (C). The predicted least-at-risk sites are low in strength within the regional network (circled in green in A & B) and distant from the lesion. These sites are not significantly depressed after stroke (D). (* $p < 0.05$, significantly different than sham).

connected to a ChR2-photoactivation site was associated with defects in synaptic activity secondary to ChR2 activation.

We used network analysis on the sham network to predict which areas would be most-at-risk and least-at-risk to stroke based on expected connectivity and compared these predictions to experimental results from ChR2 stimulation and VSD imaging. Node strength (Figure 3.6 A) and node strength relative to FLR (Figure 3.6 B) revealed the strongest nodes in the network were also the most strongly connected to FLR. Generally the strongest sites relative to FLR also had the closest proximity to FLR (such as ipsilateral motor and sensory areas), and the weakest sites were more distant to FLR (such as contralateral visual areas). We selected three of the strongest sites (MBR, MFR, HLR) and FLR, as well as three of the weakest sites (RSL, V2L, V1L) and compared the VSD responses to photostimulation at these sites (Figure 3.6, C-D). A one-way ANOVA for the most-at-risk sites revealed a significant difference between sham and stroke groups [$F(2,33) = 57,72$, $p < 0.0001$], while the least-at-risk sites were not significantly different between groups [$F(2,15) = 0.8551$, $p = 0.4450$].

3.3.5 Assessment of the peri-infarct using grid photostimulation

In order to further examine the peri-infarct, we photostimulated 25 sites at fixed distances from the lesion and 25 homotopic sites in the non-injured hemisphere (see Methods and Figure 3.1,v). For analysis, we excluded the lesion area and considered only the furthest peri-infarct sites (16 border sites on the 5x5 grid). VSD responses were taken from both the left and right FL areas (FLL and nFLR) to investigate interhemispheric and intrahemispheric responses. We scaled the responses, as described above, in order to determine whether areas within the peri-infarct could also be normalized by network-wide scaling. Before and after normalizations, the groups were significantly different from one another using KS tests (sham vs. 1 week post-stroke $p = 0.0138$; sham vs. 8 weeks post-stroke $p = 0.0507$), indicating heterogeneity rather than homogeneity in these areas (Figure 3.7). To further investigate how the peri-infarct was responding after stroke, we calculated pre-stroke (sham) strength (Figure 3.8 A), "loss" (difference in VSD strength between sham and 1 week post-stroke; Figure 3.8 B), "gain" (difference in VSD strength between 8 weeks and 1 week post-stroke; (Figure 3.8 C), and overall difference (Figure 3.8 D) per photostimulation site. We also plotted the overall difference as a function of sham strength (Figure 3.8 E). We found that while posterior-medial sites were the

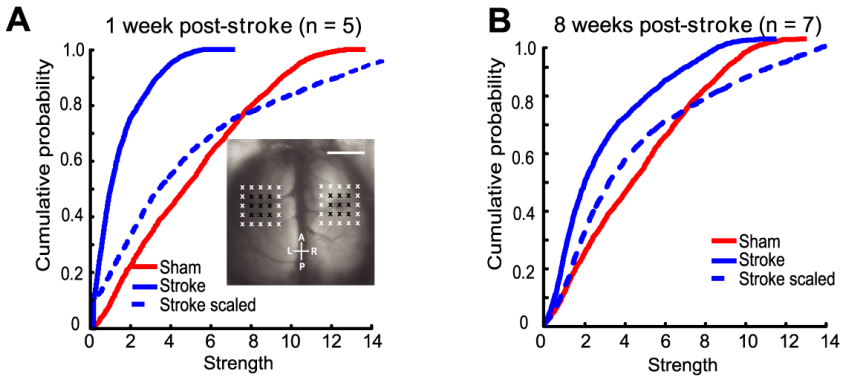

Figure 3.7 Scaling the responses in the peri-infarct zone does not lead to relative connectivity strength similar to shams. Within the peri-infarct zone, scaling to match the mean of the sham group did not result in the stroke groups having a similar distribution of strength compared to shams at 1 week post-stroke (A) nor 8 weeks post-stroke (B).

strongest in the sham animals, the gains in these areas by 8 weeks post-stroke did not equal the losses seen at 1 week post-stroke. In fact, it was the relatively weaker anteriolateral areas that showed the greatest relative gains (compared to loss per site) after stroke, sometimes exceeding sham strength. This trend was observed for both intrahemispheric connections (Figure 3.8 i and ii) and interhemispheric connections (Figure 3.8 iii and iv).

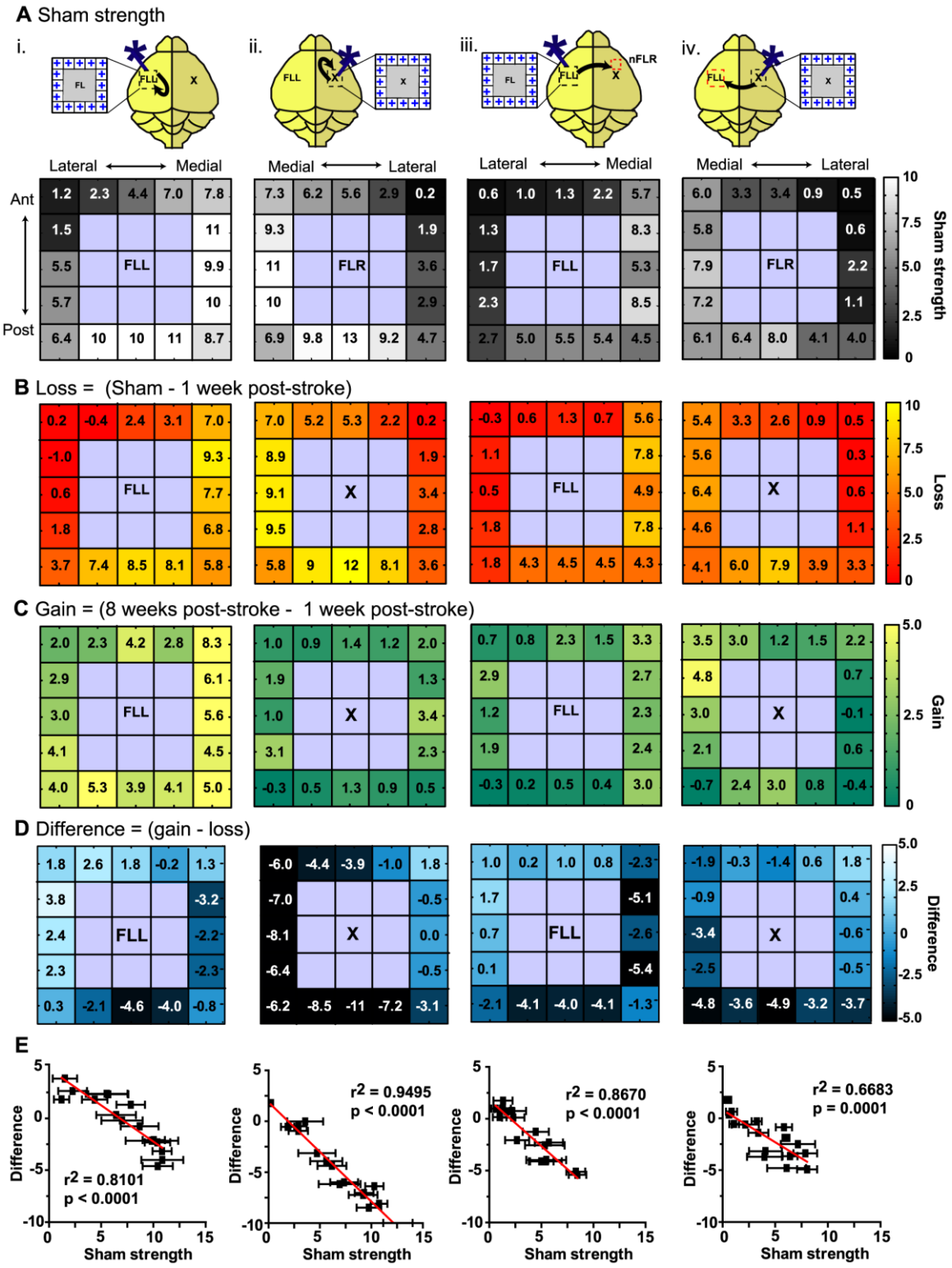

Figure 3.8 Response strength within the peri-infarct and homotopic FL reveals that the weakest pre-stroke sites have the greatest relative gains post-stroke, resulting in heterogeneous recovery. 16 regions in the non-injured (left) hemisphere and injured (right) hemisphere were photostimulated. Responses were taken from either the non-injured FLL or the new FLR. (i) Stimulation of the non-injured hemisphere, intrahemispheric FL response (from the non-injured hemisphere), (ii) stimulation of the peri-infarct, intrahemispheric nFLR response (from the injured hemisphere), (iii) Stimulation of the left hemisphere, interhemispheric response from the nFLR (injured hemisphere), and (iv) stimulation of the peri-infarct (injured hemisphere),

(Figure 3.8 continued) interhemispheric response from the FLL (non-injured hemisphere). (A) Sham strength after photostimulation at the 16 regions indicated. Note that medial and posterior sites are generally stronger compared to lateral and anterior sites. (B) Loss of strength at 1 week post-stroke (relative to sham). Note that all sites are depressed, but often sites that were strongest in (A) show the largest losses. (C) Gain of strength at 8 weeks post-stroke (relative to 1 week post-stroke). Note that gains appear higher when the response is taken from the non-injured FLL (Ci, Civ), and gains are minimal when the injured hemisphere is photostimulated and the response is taken from this hemisphere (Cii). (D) Difference in strength per site. Note that the sites that were the strongest in the pre-stroke (sham) condition (A) show a negative difference, indicating they are weaker than the pre-stroke condition, while sites that were the weakest in the pre-stroke condition show a difference near or above zero, indicating they have gained as much as they lost or more. (E) Negative correlations between sham strength and difference in strength over time (gain-loss) demonstrate a trend for weaker sites to recover more than stronger sites.

3.4 Discussion

3.4.1 VSD imaging and ChR2 stimulation reveals network-wide plasticity after stroke

The stroke core (infarct) suffers irreversible ischemic damage, and the penumbra (peri-infarct) suffers from reduced blood flow, but this tissue is potentially salvageable (Murphy and Corbett, 2009). Stroke may also cause diaschisis - impairment and dysfunction in areas remote from the lesion core. Remote changes may take place over minutes to weeks, and play an important role in post-stroke recovery (Carmichael et al., 2004; Cramer, 2008). For this reason, it is necessary to consider more than just the ischemic territory when investigating post-stroke recovery. We used ChR2 stimulation and VSD imaging to directly monitor wide-scale cortical activity changes over time after a localized stroke to the primary somatosensory cortex. Due to limitations of the craniotomy and VSD imaging (Lim et al., 2012), our model does not address prefrontal connections or subcortical contributions to recovery after stroke, although these have been shown to be of importance (Sharma et al., 2009; Grefkes and Fink, 2011). Our conclusions should be considered in the context of local cortical connectivity, and not as a comprehensive connectome for recovery after stroke.

Previous studies have used resting-state (rs) or functional connectivity (fc) functional magnetic resonance imaging (fMRI) to investigate wide-scale network changes over time after stroke (van Meer et al., 2010; van Meer et al., 2012). In the clinical setting, fc-fMRI is advantageous because it is possible to investigate multiple networks in a single scan, it is readily obtained, even in cases of severe stroke, and longitudinal imaging is possible (Carter et al., 2012a). Similar network properties to those used here (e.g. centrality, clustering), may be calculated to predict behavioral recovery after stroke (Ward et al., 2003b, a). However, the frequency of resting-state activity (<0.1 Hz) is low and its nature is not completely understood (van den Heuvel and Hulshoff Pol, 2010). rs-fMRI (van Meer et al., 2010; van Meer et al., 2012)

and similar spontaneous activity measures (Mohajerani et al., 2013; Bauer et al., 2014) have been used to describe networks in animal studies, however, these techniques are based on correlation, which can be less sensitive to amplitude changes and does not indicate directional connectivity. By using targeted ChR2 stimulation and VSD imaging, we more directly determine connection strength and direction (Lim et al., 2012).

Previous work has indicated strong parallels between cortical connectivity derived by photostimulation of ChR2 and sensory stimulation (Lim et al., 2012). However, we find differences between the methods: while sensory stimulation yielded weak VSD responses after stroke (Figure 3.2), optogenetic stimulation resulted in stronger-than-expected VSD responses (Figure 3.3). This may indicate deficits within cortical-thalamic circuits after stroke (that sensation may track), and optogenetic stimulation may help to reveal functional intracortical circuits after stroke that are not easily probed using sensation. Many genes and proteins undergo altered expression following stroke (Carmichael, 2003), so it could be argued that stroke alters the expression of ChR2 or intracortical excitability. However, we failed to observe significant changes in either ChR2 expression or intracortical excitability (EEG) in regions that were targeted for photostimulation and were outside of the infarct.

Based on the regional optogenetic stimulation, we found that the stroke groups demonstrated globally depressed VSD responses (Figure 3.4), however, the relative distribution of strengths between nodes at a regional level was largely maintained after stroke (Figure 3.5). Although we observed consistent scaling when we considered the regional network as a whole, closer analysis of individual sites revealed that some nodes were more vulnerable than others after stroke (Figure 3.6). These nodes were in close proximity to the stroke. While this may not be surprising since it is generally known that functionally-related cortical regions tend to be co-localized, the conclusion that sites closest to the lesion are most affected did not hold true in the peri-infarct. Instead, photostimulation of the peri-infarct revealed heterogeneous recovery, with some areas remaining depressed (the anterolateral areas) and some areas showing strength greater than baseline (the posterior-medial areas) by 8 weeks post-stroke (Figure 3.8).

3.4.2 Non-uniform recovery of peri-infarct connections

Clinical studies have shown that the global network is affected by stroke (Grefkes and Fink, 2011; Carter et al., 2012b), and the peri-infarct zone is especially sensitive and may be an important predictor for recovery (Furlan et al., 1996). Previous studies have shown that the peri-

infarct undergoes a number of changes over time, including cell death (Dirnagl et al., 1999), initial loss of spines (Brown et al., 2008), retraction of axons (Brown et al., 2007), and axonal sprouting (Carmichael, 2006, 2008), as well as a recovery of spine density (Mostany et al., 2010).

Here, we found that the network at 1 and at 8 weeks post-stroke had similar relative connectivity strength to the sham network when we considered the network as a whole, but not if we isolated responses from the peri-infarct. Homogeneous scaling of the responses could not account for the changes within the peri-infarct (Figure 3.7). Breakdown of the recovery process into "Loss" (the difference in strength between sham strength and 1 week post-stroke) and "Gain" (the difference in strength between 1 week and 8 weeks post-stroke) revealed that both hemispheres were affected by stroke. It was the areas that were the weakest in the pre-stroke (sham) condition that showed the greatest relative gains (Figure 3.8). The grid photostimulation sites that were the strongest in the sham condition were the posterior-medial areas. While these areas were not functionally defined, the posterior-medial areas are close to HL somatosensory cortex, which is known to overlap with FL (Oh et al., 2014). In contrast, the weakest sites in the grid photostimulation were the anteriolateral areas. These are close to oral-facial areas such as the jaw, however, our craniotomy window was not lateral enough to encompass these areas. While it could be argued that the weakest sites experience the least amount of absolute change, analysis of the losses and gains in these areas show that these sites undergo significant relative changes, sometimes demonstrating complete loss at 1 week post-stroke before re-gaining strength at 8 weeks post-stroke.

Overall, this suggests that the local connections in the peri-infarct are too severely damaged to maintain the optimal pre-stroke distribution of connection strengths, and instead undergo heterogeneous recovery: partial recovery in some areas, and better-than-expected recovery in others. It is possible that this reflects a form of synaptic scaling where less active sites more effectively engage homeostatic mechanisms, resulting in increased excitability and synaptic transmission of less active networks (Turrigiano and Nelson, 2004). However, because stroke triggers a cascade of events, the changes observed here may also result from other factors such as alterations in neuronal excitability (Carmichael, 2003), axonal sprouting (Carmichael, 2006), changes in collateral inhibition (Butefisch et al., 2003), or astrocytic changes (Barreto et al., 2011).

3.4.3 Implications for future work

We observe global depression of the network at 1 week post-stroke. By 8 weeks post-stroke, and without any explicit treatment or rehabilitation, the global network showed some recovery towards a sham-like pattern of relative connectivity strengths, despite having lower overall strength. This suggests that the sham network pattern of relative connectivity strengths represents the desired 'set-point' (Turrigiano and Nelson, 2000) and the stroke networks recover in such a way that this relative strength distribution is maintained - relative connectivity strength between nodes is parallel to shams despite having depressed strength.

Our results are consistent with the concept that stroke affects the entire network, but the injured hemisphere (specifically the peri-infarct), can be severely depressed after stroke (Brown et al., 2009; Mohajerani et al., 2011). This may suggest that the early post-stroke period is a sensitive time for the network and brings about the question of when treatment and rehabilitation strategies should begin. While we did not explicitly test treatment after stroke in this study, future work could incorporate skilled training (Kerr et al., 2013) or enriched environments (Biernaskie et al., 2004) to determine the effects of such experience on the recovery of the post-stroke network.

3.4.4 Conclusion

We suggest the following scenario after stroke: in the early stages after stroke (up to 1 week post-stroke), cortical activity is globally depressed. The global depression gradually resolves over time, such that by 8 weeks post-stroke the qualitative features of the original network have returned, even though the overall strength of the network remains depressed. At a local level, there is evidence of recovery in the peri-infarct zone by 8 weeks post-stroke, but it is not uniform. Between 1 and 8 weeks post-stroke, novel connections form to potentially compensate for stroke damage (Dancause et al., 2005; Carmichael, 2006, 2008; Brown et al., 2009), leading to circuit reorganization and functional re-mapping. This suggests that treatment and rehabilitation strategies that target the entire network will be most effective in returning the network to a pre-stroke state. Although we have focused on cortex, it will be interesting to determine how agents that induce the sprouting of new connections within either the spinal cord (Wahl et al., 2014) or cortex (Overman et al., 2012) affect the relative balance of connection strength after stroke.

4. General discussion

4.1 Strengths and limitations of the imaging method

4.1.1 Strengths of simultaneous VSD imaging and ChR2 stimulation

The studies presented here are the first studies to use simultaneous wide-scale VSD imaging and ChR2 stimulation in an *in vivo* preparation. Taken together, there are a number of strengths that lend to the power of this method and make it an attractive option for *in vivo* cortical mapping. One of the main benefits of VSD imaging is that it is based on direct measures of membrane depolarization and has high spatial and temporal resolution (Grinvald and Hildesheim, 2004). This allows for the collection of real-time neuronal activity. In our case, we were able to image an area that spanned almost the entire dorsal cortex by creating an 8 x 8 mm bilateral window or a large 7 x 6 mm unilateral window. In this way, we were able to image activity over a number of cortical systems. We chose a number of well-studied regions (such as the primary somatosensory cortices) as well as in a number of lesser-studied regions (such as secondary sensory areas and associational areas) to investigate large-scale cortical connectivity. By using some well-studied regions, we were able to compare our conclusions with already-established results. For example, the relationship between primary somatosensory barrel cortex and motor cortex in rodents is well-established and has been demonstrated both structurally and functionally (Ferezou et al., 2006; Ferezou et al., 2007). This relationship was one of the first relationships that we investigated during our pilot studies. Indeed, we were able to see a functional correlation between the somatosensory barrel cortex and the motor cortex both with sensory stimulation of the whiskers and with optogenetic stimulation of the somatosensory barrel cortex (Lim et al., 2012). This gave us confidence that this method was revealing functional cortical connections, and not simply resulting in coincidental activations between cortical sites.

The use of optogenetics has taken off over the past decade. Perhaps the greatest advantage with the advent of *in vivo* optogenetics is that a specific population of cells can be targeted and controlled through photostimulation (Boyden et al., 2005). Here, we use a transgenic mouse that has ChR2 incorporated primarily into the layer 5B neurons (Arenkiel et al., 2007). The advantage of using such mice is that there is no invasive procedure necessary to introduce the ChR2 (as there would be if you were doing a viral transfection into a specific

region of cortex), and the mice are readily attainable from Jackson Laboratories. Furthermore, because layer 5B is distributed throughout the cortex, we are able to photostimulate ChR2 at any cortical area (Lim et al., 2012). This is especially useful given our wide-scale approach with VSD imaging. Through combining VSD imaging and ChR2 stimulation in these transgenic mice, we have created both a wide-scale recording and a wide-scale stimulation method so that we can actively stimulate and record resulting activity across a very large window of the mouse dorsal cortex (Lim et al., 2012). Another great benefit to using ChR2 stimulation is that it has high temporal resolution – ChR2-expressing neurons respond almost immediately to photostimulation (within a matter of several ms), and will stop firing once the photostimulation is removed (Boyden et al., 2005). This allows for high temporal control of the system through optogenetic stimulation, while VSD imaging allows for high temporal resolution recording of the response.

In the past, direct cortical stimulation has been slow and invasive. Techniques such as intracortical microstimulation (ICMS) make use of microelectrodes that need to be lowered into the cortex to deliver an electric current and stimulate the surrounding cells (Ayling et al., 2009). In order to minimize damage to the cortex, the microelectrode must be raised and lowered slowly, and brief pulses of electrical stimulation are used in an attempt to find the minimum current that surpasses the threshold. Because of this, ICMS is a relatively slow mapping technique. This, combined with the invasive nature of inserting a microelectrode, makes ICMS less optimal for *in vivo* experiments compared to optogenetic mapping which is less invasive, is much faster, and can be automated (Ayling et al., 2009). Furthermore, because ChR2 can be specifically expressed in a population of cells (Nagel et al., 2003; Boyden et al., 2005), optogenetic stimulation offers more precise control over the cortical area that is being stimulated and subsequently mapped, compared to direct electrical stimulation which will stimulate all cells in the vicinity of the electrode without discrimination (Lim et al., 2013).

There are a number of other *in vivo* imaging methods that are useful for macroscale imaging and mapping. Methods such as functional magnetic resonance imaging (fMRI), (van Meer et al., 2010; van Meer et al., 2012), or functional connectivity optical intrinsic signal imaging (fcOIS), (Bauer et al., 2014), have been used to investigate large-scale changes to cortical connectivity after stroke. These methods draw conclusions about functional connectivity based on correlative activity and are attractive due to their non-invasive nature and the possibility of doing longitudinal imaging within animals. However, these methods are based on changes in

blood flow, and therefore can only infer neuronal activity. They also have a slower temporal resolution compared to VSD imaging. There are some compelling alternative imaging methods in development that demonstrate high spatial and temporal resolution and also directly measure neuronal activity – such as genetically encoded calcium imaging (GECI), (Hires et al., 2008; Tian et al., 2009). This method has an advantage over VSD imaging in that it measures spiking activity, while the VSD signal represents both supra and subthreshold activity. These methods are still being optimized, but will likely be important for future studies of cortical mapping.

4.1.2 Weaknesses of simultaneous VSD imaging and ChR2 stimulation

Perhaps the biggest disadvantage of using VSD imaging is that it is very challenging to use for longitudinal imaging. VSD imaging experiments require an invasive surgical procedure, as the dura mater must be removed for the VSD to bind to the cell membranes (Chemla and Chavane, 2010). This means that the brain is exposed and vulnerable. In most cases, VSD imaging experiments are designed to last several hours before termination, although there has been some limited success in long-term VSD imaging over a small area of cortex in a primate model through the use of an artificial (silicone) dura substitute (Arieli et al., 2002; Slovin et al., 2002). Despite this success, there have been no follow-up studies on long-term VSD imaging, and most VSD imaging experiments remain acute with no possibility of repeated imaging sessions in the same animal. This disadvantage is particularly unfortunate when studying cortical connectivity changes after stroke, as the progression of recovery cannot be tracked within the same animal. Instead, cohorts of animals must be compared at separate time points, which introduces additional variables. Perhaps the best way to overcome this limitation is to implement voltage-sensitive fluorescent proteins (VSFPs) (Perron et al., 2009; Akemann et al., 2010), which would have similar spatial and temporal resolution to VSDs, but which would not require invasive dye-loading before imaging (see below).

A criticism of VSD imaging is that the VSD signal spread is large – the VSD signal crosses functional and anatomical boundaries (for example, spreading over an entire hemisphere), and so the significance of this signal has been questioned. It is known that the VSD response reflects both supra and sub-threshold activity, thus the spread of the response is not necessarily spiking activity (Grinvald and Hildesheim, 2004). However, this does not mean that the signal is unnecessary or simply an artefact. While we did not correlate our VSD signal with classical electrophysiology measures (such as whole-cell recordings or local field potentials), a

number of previous studies have (Petersen et al., 2003a; Petersen et al., 2003b; Ferezou et al., 2006; Ferezou et al., 2007). These studies demonstrate that VSD fluorescence changes correlate with the subthreshold membrane potential changes of local layer 2/3 pyramidal neurons *in vivo* in both small (Ferezou et al., 2006) and large craniotomies (Ferezou et al., 2007), suggesting the signal represents excitation and is not an artefact. An elegant study combining VSD imaging, calcium-sensitive dye (CaSD) imaging, and whole cell recording showed that the VSD and CaSD signals represented different aspects of cortical function (Berger et al., 2007). The VSD fluorescence represented mainly subthreshold activation and the VSD signal spread further compared to the CaSD signal, which was composed mostly of action potential firings and remained more localized. The authors suggest that the subthreshold excitation that is seen with VSD imaging could modulate other inputs, and may represent a type of priming for multimodal integration (for example, across multiple barrel columns) (Berger et al., 2007).

One of the potential problems with combining VSD imaging and ChR2 stimulation is the possible risk of phototoxicity. Phototoxicity is a concern for both VSD imaging (Chemla and Chavane, 2010) and for optogenetic stimulation (Ayling et al., 2009). It has been suggested that prolonged or intense optogenetic photostimulation may cause heating and damage within the brain, however, it has also been shown that photostimulation causes negligible changes in brain temperature if done in an intermittent and spatially distributed manner (Christie et al., 2012), as we do here. Nonetheless, we were considerate of this possibility during our experiments and introduced a 10-20 sec inter-trial time between stimulation trials to minimize light exposure and minimize the possibility of phototoxicity. We also ensured that we were using the shortest duration and smallest laser power necessary to stimulate a ChR2 response (1 ms, 5 mW), although previous studies in our lab have used much longer trains of stimulation (up to 500 ms trains), (Harrison et al., 2012) and variable light intensity (40-600 mW/mm^2), (Ayling et al., 2009) and have not reported negative side effects.

4.1.3 Channelrhodopsin-2 transgenic mice

The transgenic thy1-ChR2-eYFP mice that are used in this thesis express ChR2 primarily in the layer VB neurons of the neocortex (Wang 2007; Arenkiel 2007). In order to understand what it means to photostimulate these neurons, a discussion on these mice and the connectivity of layer VB neurons is warranted.

The distribution of the cortical layers is not consistent across the entire cortex. For example, layer 4 is entirely absent in the some areas of the frontal cortex (which is also known as the agranular layer due to the absence of the granular layer 4 cells) (Shepherd, 2009), and layer 5 has been shown to be distributed as a double blade in motor-frontal cortex in a line of YFP-expressing mice (strain B5.Cg-tg(thy-1-YFPH)2Jrs/J; Jackson Laboratory), making the layer 5B distribution much thicker in the motor-frontal cortex compared to other cortical areas, such as the sensory cortex (Yu et al., 2008). In our experiments, variation in layer 5B distribution in the neocortex would have an effect on the number of ChR2-expressing neurons activated by our photostimulation. While we (Ayling et al., 2009; Lim et al., 2012), and others (Arenkiel et al., 2007; Wang et al., 2007a), have not noted significant changes in ChR2 expression distribution throughout the neocortex, we did not conduct careful histological experiments to quantify the distribution of ChR2 expression across the neocortex, and the possibility for variation in expression between animals always exists. Nonetheless, the transgenic line currently still offers the best and most consistent model of large-scale ChR2 expression, which is necessary for the wide-field imaging we completed here. Alternative methods of expression, such as multiple injections of viral vectors, may result in even more variable expression within and between animals due to incomplete sampling or tissue damage due to the injection procedure (Cardin et al., 2010).

Layer 5 neurons are generally divided into two sublayers: layer 5A and 5B (Manns et al., 2004). These layers have been studied extensively within the rodent barrel cortex, and are thought to function in parallel, but with discrete morphology and physiology (Hattox and Nelson, 2007), and with unique sets of afferent and efferent fibers (Manns et al., 2004). The layer 5A pyramidal neurons have smaller somata and are thin tufted, regular-spiking cells (firing trains of action potentials) (Hattox and Nelson, 2007). These cells receive thalamic input from the medial posterior nucleus and project ipsilaterally to the caudate nucleus, primary motor cortex, and somatosensory cortex (Harris and Shepherd, 2015), and they project contralaterally through the corpus callosum (Hattox and Nelson, 2007). The layer 5B neurons are made of large pyramidal neurons that are thick tufted, with extensive projections in layer 2/3, and are intrinsically-bursting (firing bursts of action potentials in response to depolarizing current injections) (Hattox and Nelson, 2007). These deeper layer 5B cells receive thalamic input from the ventral posteromedial nucleus and project to subcerebral targets such as the superior colliculus, pontine

nucleus, and spinothalamic tract (Manns et al., 2004; Harris and Shepherd, 2015). Both layer 5A and layer 5B have extensive intralaminar collaterals (Harris and Shepherd, 2015). When we photostimulate the transgenic ChR2 mice, we selectively stimulate the layer 5B neurons which have extensive intralaminar projections, as well as long-range projections to both subcortical and subcerebral areas. Therefore, the response that we observe will likely contain contribution from subcortical structures. We have restricted our network analysis to the first 20 ms of the VSD response in order to minimize the degree of subcortical contribution, however, we acknowledge that these connections exist and could contribute to the VSD response.

While the mice that we use express ChR2 in layer 5B neurons, our protocol could easily be applied to animals expressing ChR2 in a different population of cells. We have shown a robust similarity in sensory-evoked and ChR2-evoked VSD responses (Lim et al., 2012; Lim et al., 2014), and further studies in our lab have shown similarity in ChR2-evoked VSD responses, spontaneous VSD responses and the underlying structural connectivity (Mohajerani et al., 2013). Interestingly, the structural connectivity patterns were preserved across the cortical laminae (Mohajerani et al., 2013). Taken together, the consistency of the VSD responses we have observed in sensory-evoked, ChR2-evoked, and spontaneous activity correlations suggest that there is a robust pattern of structural and functional connectivity that can be observed using ChR2-stimulation and VSD imaging. Because of this, and because it is well-known that there is dense recurrent laminar connectivity within the intratelencephalic cells (layers 2-6) and intralaminar connectivity within each cortical layer (Harris and Shepherd, 2015), if ChR2 were expressed in a different population of excitatory neurons (for example, layer 2/3) we would expect to see a similar VSD response as we report here. However, if ChR2 were expressed in inhibitory neurons (Katzel et al., 2010), the VSD response would likely be very different. Expression of ChR2 in different populations of cells could therefore be used to reveal further properties of the functional network.

4.2 Future improvements and directions

The aim of this thesis was to develop a method for large-scale *in vivo* cortical mapping in the mouse, and then apply this method to a stroke model. While these aims were achieved, there

are a number of ways that the method could be improved to bolster and strengthen the conclusions drawn about cortical reorganization after stroke.

4.2.1 Voltage-sensitive fluorescent proteins and genetically-encoded calcium indicators

Even greater specificity for regional functional mapping could be achieved with the development of new *in vivo* probes such as voltage-sensitive fluorescent proteins (VSFPs), which can be targeted to specific cell populations and provide signals with no contribution from glia cells, blood vessels, or nearby silent neurons (Sakai et al., 2001; Akemann et al., 2010; Mancuso et al., 2010). Several variants of VSFPs have been developed (Perron et al., 2009; Perron et al., 2012). In particular, second generation VSFPs (VSFP2) have been developed through a molecular fusion of a voltage-sensing domain with a fluorescent reporter protein and report membrane potential change based on the Fluorescence Resonance Energy Transfer (FRET) principle (Perron et al., 2009). Similar to VSDs, VSFPs are capable of reading out supra- and subthreshold activity from a large cortical area (Akemann et al., 2010). The greatest advantage of these probes over VSDs is that they can be targeted to a specific cell population, eliminating background contribution to the fluorescent signal, thus providing a more specific readout of neuronal activity (Akemann et al., 2010). This feature will be crucial in distinguishing whether different neuronal sub-types within a circuit serve different functions (Peterka et al., 2012). However, VSFPs are limited by slow kinetics, with on-rates on the order of 10 s of milliseconds (Scanziani and Hausser, 2009), and genetic voltage sensors have only had limited application in *in vivo* studies where high levels of expression were needed (however, see (Akemann et al., 2010). There will also be considerable spectral overlap between VSFP and ChR2 necessitating the use of red-shifted opsins for neuronal stimulation and VSFP mapping.

Another set of tools for precise, cell-specific targeting are genetically encoded calcium indicators (GECIs). Calcium imaging has been applied over a range of spatial scales, from single cell calcium dynamics (Helmchen et al., 1999; Winship and Murphy, 2008; Golshani et al., 2009), to wide-field calcium imaging of population activity (Homma et al., 2009; Minderer et al., 2012). This wide scope of applications makes calcium imaging an attractive method for addressing functional mapping questions (Mancuso et al., 2010). GECIs are developed through a fusion of a calcium- sensitive molecule to one or two fluorescent protein molecules (Looger and Griesbeck, 2012), and report changes in calcium dynamics. Compared to VSDs and VSFPs, calcium probes are less-sensitive to subthreshold activity and, at the cellular level, are more

related to spiking activity (Tian et al., 2009). However, because GECI signals are based on the timescale of calcium dynamics, they have a relatively slow decay time course, which may make it challenging to detect single action potentials *in vivo* (Scanziani and Hausser, 2009). GECIs also have the advantage of being stable over long periods of time *in vivo* (Looger and Griesbeck, 2012), making them attractive for longitudinal studies (Minderer et al., 2012). In mouse models, expression of GECIs has generally been achieved through adeno-associated virus (AAV) viral vector injection producing a spread of only 1–2 mm, however, new transgenic lines provide a widespread expression of GECI throughout the cortex (Zariwala et al., 2011; Chen et al., 2012b), allowing for large-scale functional connectivity studies. Moreover, there have been efforts to improve the sensitivity, temporal dynamics, and stability within the GCaMP family, a class of GECIs that fuses calmodulin to a single fluorescent protein (Tian et al., 2009; Zhao et al., 2011; Akerboom et al., 2012; Chen et al., 2012a), and to create blue and red-shifted GECIs for multi-color calcium imaging in single cells (Zhao et al., 2011). Until now, the use of GECIs with optogenetic stimulation has been limited due to spectral overlap between ChR2 and green GECIs (Hires et al., 2008), because both absorb blue light. However, the recent development of a new red-shifted rhodopsin (i.e. C1V1), (Yizhar et al., 2011), allowed for high-resolution two-photon imaging of green fluorescent proteins with simultaneous two-photon photostimulation (Rickgauer and Tank, 2012). This demonstrates the ability to combine optogenetic stimulation with calcium imaging, and the possibility for cell-specific probing of evoked calcium dynamics.

4.2.2 Optogenetic expression

New opsins are being continuously engineered, as described in the introduction (Chapter 1, section 3.2). Red-shifted opsins would be particularly beneficial for more precise cortical mapping, as they would decrease the amount of light scattering in the tissue, especially when targeting deeper cortical layers. Red-shifted opsins would open doors to many more elegant experiments, such as using multiple opsins to control multiple cell populations in a single animal, perhaps even having dual control (excitatory and inhibitory) over the same population of cells. This offers exciting possibilities for the creation of "virtual lesions" which could be accomplished with transient optogenetic inhibition. The creation of virtual lesions would allow the investigation of immediate cortical reorganization or, more likely, the unmasking of latent circuits that may be important for functional compensation and recovery after stroke (Mohajerani et al., 2011). Because such lesions are transient, one could hypothetically create multiple virtual

lesions in the same animal in a single imaging session, allowing comparisons between cortical areas. Hypothetically, creating a virtual lesion over a hub node (such as the parietal cortex, as described in Chapter 2) would create much greater disturbances to the functional network compared to a virtual lesion over a node that has fewer strong functional connections (such as the auditory cortex).

Perhaps the greatest advance in this technique would be the application of this technique in a more sophisticated and complex animal model, such as rats or primates. The larger cortices in these animals would greatly improve the spatial resolution and would enable us to ask more intricate questions about functional networks. In addition, more sophisticated behavioral testing could be done with these models. While VSD imaging has been successfully used in both rats (Aronoff et al., 2010) and primates (Slovin et al., 2002), ChR2 expression in these models has been challenging because of the complexity of the genetics of rats or primates. Optogenetic experiments in these animal models have relied on viral expression of ChR2 (Aravanis et al., 2007; Diester et al., 2011), which results in limited expression and potential variability between animals. Nonetheless, there is great interest in creating transgenic optogenetic models and progress is being made in the creation of a rat transgenic model (Tomita et al., 2009).

4.2.3 Additional testing of the stroke model

To strengthen the conclusions from the stroke study (Chapter 3), it would be ideal to incorporate behavioural testing to determine if the network changes that we observed correlate with behavioural changes after stroke. We chose not to include sophisticated behavioural testing in this study because it is known that behavioural training and testing may induce cortical plasticity (Kleim et al., 1998; Kleim and Jones, 2008), however, it would be interesting to have a separate cohort of animals that undergo behavioural testing to see if there is a noticeable change within the network. This would likely depend on the behavioural paradigm used. It may be that simple behavioural tasks, such as the cylinder task (Brown et al., 2009), have negligible or only slight effects on the global networks while more rigorous tasks, such as the skilled reaching task (Lim et al., 2009), would have noticeable effects on the network.

Future studies could easily incorporate behavioural testing and relatively simple treatments, such as enriched environments, which are known to induce plasticity (Zeiler and Krakauer, 2013; Lay and Frostig, 2014). It has been suggested that there is a critical window after stroke where treatments are most optimal (Murphy and Corbett, 2009; Lay et al., 2010),

however, there is no consensus on when this window may be. Future studies could use our imaging method combined with behavioural testing to determine optimal parameters for treatment after stroke at both a behavioural and cortical level.

4.2.4 Modification of the experimental design for translational relevance

The photothrombotic stroke method was chosen for Chapter 3 because this method allows for strict control of the location and size of the stroke. It was our intent to create a stroke over a small cortical area and measure the effects of that stroke on the global and local network. Future studies could replicate the experimental design and place the stroke over different cortical areas to test for network changes. Presumably, placing a stroke in a hub node (such as hindlimb somatosensory cortex or parietal cortex) would cause greater changes to the global network compared to placing a stroke in a less-well-connected node (such as secondary visual cortex).

The photothrombotic stroke is advantageous for precise control over the stroke location and size. The diameter of the stroke can be regulated based on the size of the illumination light, however, photothrombosis does not typically damage the white matter (Carmichael 2005). Indeed, in our experiments the stroke penetrated all of the cortical layers but did not damage the underlying white matter (see section 3.2.1). This is problematic because in the clinical setting it is rare to have a single cortical focal stroke that does not damage the white matter. In human patients, strokes can be located anywhere within the brain and are often found in subcortical structures. Clinical cases may also present with multiple small strokes rather than single focal stroke. Thus, for the conclusions in our experiments to be more applicable to the clinical setting, it may be more appropriate to use a stroke model with multiple small strokes, and/or choose a different model of stroke that includes white matter damage.

A further consideration for future studies is increasing the sample sizes of the study to increase the statistical power. We had relatively low standard deviation between groups in our first imaging experiments, which had between 6 and 10 animals per group (Chapter 2, section 2.3.2), and in our stroke experiment, which had between 6 and 12 animals per group (Chapter 3, section 3.3), however, it has been suggested that experimental stroke studies tend to be underpowered (Dirnagl, 2010). We did not calculate an *a priori* power test to determine the group sizes in our experiments, however, future experiments should consider this to ensure adequate sample sizes to determine significant effects.

4.2.5 Further applications of the method: beyond stroke models

While we applied this method in a stroke model, this mapping method could be applied to any type of brain disease model. It may be especially informative to look at global cortical network changes for diseases that have unclear etiology, such as autism spectrum disorder, as it is possible that the effects of such psychiatric diseases may be reflected in subtle network changes and imbalances (Qiu et al., 2011).

More generally, it would be important to consider various brain states (including anesthetized, quiet-awake, or awake and freely-moving), as well as various developmental states or ages (juvenile, adult, and aged adult) to draw more comprehensive conclusions about regional functional connectivity. VSD imaging has been completed on anesthetized and quiet-awake mice (Mohajerani et al., 2013), and optogenetics have also been completed on quiet awake mice (Desai et al., 2011), making the concept of comparing across brain states using this method quite plausible.

To support the conclusions drawn here about regional brain organization, it would be useful to have additional supporting data, so future studies could broaden the scope of these experiments through histological experiments (for example, completing structural tracing studies within the peri-infarct to determine if structural connectivity relates to the functional connectivity we see with the VSD responses in Chapter 3), or additional electrophysiology experiments (for example, recording local field potentials in the cortex to determine whether electrical activity would correlate with the VSD responses we saw here).

4.3 Translation: relevance to clinical studies

4.3.1 Comparison to clinical techniques of non-invasive stimulation

Non-invasive brain stimulation (NIBS) uses electrical or magnetically-induced currents to stimulate the brain. Depending on the stimulation frequency and duration, these currents can be used to excite or inhibit activity over a cortical region of interest. It is thought that NIBS modulates neural activity and may stimulate brain plasticity through the induction of LTP-like protocols (Huerta and Volpe, 2009; Liew et al., 2014).

The two most commonly used NIBS techniques in the clinical setting are transcranial direct current stimulation (tDCS) or transcranial magnetic stimulation (TMS). tDCS uses

electrically-induced currents to stimulate the brain. A battery-powered direct current (DC) generator connected to an anodal and catholdal electrode is positioned over the scalp while low amplitude currents are generated. tDCS does not induce action potentials, but instead seems to modify neuronal thresholds (Liew et al., 2014). Depending on the stimulation type (anodal or cathodal) the stimulation can increase or decrease cortical excitability, although the specific mechanisms underlying these effects remain unclear (Liew et al., 2014). TMS uses a coil placed on the scalp to magnetically-induce a current in the underlying cortical tissue. Various cortical depths can be targeted by varying the protocol and magnetic coil design (Liew et al., 2014). Generally, low-frequency (< 1 Hz) TMS can be used to inhibit – and can even create a virtual lesion by creating a transient perturbation in the underlying cortical tissue (Pascual-Leone et al., 2000) - while high-frequency stimulation (> 5 Hz) TMS can be used to excite cortical tissue. There are a number of different TMS forms which result in different effects - repetitive TMS can be inhibitory or excitatory depending on stimulation frequency, paired-pulse TMS can be used to determine physiology, continuous TMS which is inhibitory, and intermittent TMS which is excitatory. TMS can also be used for motor mapping in humans (Huerta and Volpe, 2009) although the low spatial resolution (~ 1 cm) prevents this from being a useful mapping technique in a smaller brain.

One of the greatest benefits of NIBS techniques is that they are relatively easy to implement – they neither take a lot of space nor cost a lot of resources to establish. Because of this, these techniques have been used in rehabilitative settings for various types of brain diseases, especially in the induction of motor plasticity after stroke (Hallett, 2000; Wassermann and Lisanby, 2001; Shimizu et al., 2002; Butefisch et al., 2003; Butefisch et al., 2006; Huerta and Volpe, 2009), however, there have been mixed results regarding NIBS after stroke (for a review, see Liew et al., 2014). Interestingly, stimulation effects seem to last longer and have a larger effect when paired with behavioural tasks, such as motor training (Raffin and Siebner, 2014). Stimulation parameters have yet to be optimized, and there is a wealth of questions yet to be answered in this field: what is the optimal stimulation frequency? Should repetitive NIBS treatments be used? If so, what is the optimal time to wait between stimulation treatments? Should stimulation vary for the acute vs. chronic stage in stroke patients? Should stimulation be focused on a single site, or would dual-site or multi-site stimulation paradigms be more

beneficial? NIBS offers exciting possibilities, but well-controlled large-scale clinical trials will be required to answer these questions.

Because so many questions remain about optimal stimulation parameters for therapeutic use of NIBS after stroke, it will be useful to investigate some of these parameters in animal models. Unfortunately, the coils used for both TMS and tDCS are both too large to create focal stimulation points in the much smaller rodent brain. Fortunately, optogenetic stimulation can be delivered in a similar, minimally-invasive fashion (through a closed skull), and has been shown to elicit similar responses in mice as TMS induces in humans (Ayling et al., 2009). Optogenetics may therefore offer a parallel means to studying NIBS in an animal of stroke. There are some clear differences between optogenetics and NIBS in human patients that will need to be taken into consideration – first, optogenetics targets a cell-specific population whereas NIBS affects all underlying cortical tissue in a nonspecific manner. Second, the spatial resolution between optogenetics (on the order of 100s of microns) and TMS (on the order of 1 cm), is vastly different. Optogenetics therefore can be used for more precise point-stimulation of cortical tissue. Although it currently remains hypothetical, using optogenetics in the human brain for cell-specific point stimulation and treatment after stroke may be a possibility in the future, especially if animal models of neurological disease show marked improvement resulting from such cortical stimulation (Cheng et al., 2014).

4.3.2 Translation from basic preclinical to clinical studies

The track record for translation from animal studies to clinical studies is very poor within the field of stroke recovery. Over the past couple decades, there have been numerous preclinical studies using animal models that have reported success in developing treatments or beneficial rehabilitation strategies after stroke, however, these results have not translated well in clinical trials. Some of the treatments that have been demonstrated to be neuroprotective in animal studies but have failed in preliminary clinical trials include free radical scavengers, glutamate receptor antagonists, and ion channel modulators (for a review, see Cheng et al., 2004). The reasons for the failures for many of the other treatments have been discussed in detail (Cheng et al., 2004; Ginsberg, 2008), however, several points are worth highlighting here.

One of the biggest advantages of using animal models to study stroke is that the location, size, and timing of the stroke can be tightly controlled. This is not so in clinical studies. Preliminary clinical studies are often composed of patients that have strokes in various locations

and present with various behavioural deficits. This added variability makes it challenging to determine the effects of treatment in an objective way. Furthermore, many human patients present with comorbidities such as diabetes, hypertension, or previous incidence of stroke (Cheng et al., 2004). While several labs have recently begun to incorporate comorbidities such as diabetes (Sweetnam et al., 2012), or high-fat diets leading to hypertension (Langdon et al., 2011), in animal models of stroke, most animal models thus far have used healthy, young animals. The implications of this are not inconsequential: younger, healthier brains such as those used in many animal models of stroke may be naturally more receptive to treatment strategies compared to an older brain, with possible comorbidities, which is more typically found in human stroke patients.

In the past, many experimental studies measured the size of the infarct to determine treatment efficacy (Cheng 2004; Dirnagl, 2010). This may not be the most accurate measure of treatment effect because cortical damage changes and evolves over time. For example, it is possible that infarct size may be overestimated in the early post-stroke period due to brain edema. Later changes to infarct size could be a matter of decreased edema rather than a result of treatment (Dirnagl, 2010). Rather than measuring lesion size, clinical studies often base the measure of treatment success on a comprehensive behavioural score (for example, the National Institute of Health stroke scale, or the modified Rankin scale). Even a small lesion can cause widespread functional deficits depending on its location (and function), in the brain. This discrepancy between measures of treatment efficacy keeps the translation between preclinical studies (which focus almost exclusively on lesion size as the measure of success) to preliminary clinical studies (which focus almost exclusively on behavioural recovery) vague and difficult to compare in an objective way. To move beyond this limited perspective, it may be helpful for preclinical studies using animal models to focus more on behavioural changes after stroke. Perhaps instead of investigating agents for neuroprotection (to decrease the lesion size), it would be more fruitful to explore strategies that enhance plasticity and remapping after stroke, allowing healthy tissue to compensate for the infarcted tissue and re-gain of function. This is an important perspective because the result that is the most important from the patient's perspective is the return of function and/or the decrease in behavioural deficits – lesion size is regardless. To create better translation then, it may be necessary for sophisticated behavioural testing to be included in all animal studies of stroke. It may also be insightful for animal studies to be designed to be more strategic about the placement of the stroke (i.e. creating a large focal stroke over a known hub

area so that there are more obvious functional and behavioural deficits to be measured rather than using the MCAO method to create a stroke that covers most of one hemisphere). This could create the conditions for a model of reorganization and recovery that is more typical of human patients after stroke.

While many treatments and strategies have failed to translate well, there are a few treatments that remain promising, including induction of mild hypothermia (34^{o} C) after stroke (van der Worp et al., 2010). Examples of successfully-translated strategies include tissue plasminogen activator (tPA), (Hacke et al., 1995), which must be administered within a short time-window after an ischemic stroke, and constraint-induced movement therapy (CIMT), which has been shown to produce significant and lasting improvements in arm and motor function after stroke (Wolf et al., 2006).

4.4 Concluding remarks

While creating a connectome of the brain is a substantial undertaking, technological advances, such as optogenetic mapping, are making this goal more manageable. Because of the complexity of the human brain, animal models of neuronal connectivity will be essential in discovering and describing basic principles of connectivity before creating a comprehensive connectome of the human brain. There has already been progress in mapping large-scale connectivity in a number of simple organisms. Already, a comprehensive connectome is available for *C. elegans* (White et al., 1986), and great progress is being made into generating neuronal connectivity maps in the mouse (Oh et al., 2014) and the rat brain (Zakiewicz et al., 2011).

New lines of research regarding the disruption of large-scale connectivity that is caused by brain injury, such as a stroke, is now revealing new information about how the disruptions to connectivity may affect entire networks of connections, having broad effects on the connectome (Carrera and Tononi, 2014). This information will be invaluable towards the creation of the much-sought-after human connectome, and ultimately, the goal of using that connectome in health research and health care.

References

Abe Y, Sekino M, Terazono Y, Ohsaki H, Fukazawa Y, Sakai S, Yawo H, Hisatsune T (2012) Opto-fMRI analysis for exploring the neuronal connectivity of the hippocampal formation in rats. Neuroscience research 74:248-255.

Akemann W, Mutoh H, Perron A, Rossier J, Knopfel T (2010) Imaging brain electric signals with genetically targeted voltage-sensitive fluorescent proteins. Nat Methods 7:643-649.

Akerboom J et al. (2012) Optimization of a GCaMP calcium indicator for neural activity imaging. J Neurosci 32:13819-13840.

Alloway KD, Olson ML, Smith JB (2008) Contralateral corticothalamic projections from MI whisker cortex: potential route for modulating hemispheric interactions. J Comp Neurol 510:100-116.

Altura BM, Weinberg J (1979) Urethane and contraction of vascular smooth muscle. Br J Pharmacol 67:255-263.

Andersen RA (1997) Multimodal integration for the representation of space in the posterior parietal cortex. Philos Trans R Soc Lond B Biol Sci 352:1421-1428.

Anderson CT, Sheets PL, Kiritani T, Shepherd GM (2010) Sublayer-specific microcircuits of corticospinal and corticostriatal neurons in motor cortex. Nat Neurosci 13:739-744.

Anenberg E, Arstikaitis P, Niitsu Y, Harrison TC, Boyd JD, Hilton BJ, Tetzlaff W, Murphy TH (2014) Ministrokes in channelrhodopsin-2 transgenic mice reveal widespread deficits in motor output despite maintenance of cortical neuronal excitability. J Neurosci 34:1094-1104.

Antognini JF, Wang XW, Carstens E (1999) Quantitative and qualitative effects of isoflurane on movement occurring after noxious stimulation. Anesthesiology 91:1064-1071.

Aravanis AM, Wang LP, Zhang F, Meltzer LA, Mogri MZ, Schneider MB, Deisseroth K (2007) An optical neural interface: in vivo control of rodent motor cortex with integrated fiberoptic and optogenetic technology. J Neural Eng 4:S143-156.

Arenkiel BR, Peca J, Davison IG, Feliciano C, Deisseroth K, Augustine GJ, Ehlers MD, Feng G (2007) In vivo light-induced activation of neural circuitry in transgenic mice expressing channelrhodopsin-2. Neuron 54:205-218.

Arieli A, Grinvald A, Slovin H (2002) Dural substitute for long-term imaging of cortical activity in behaving monkeys and its clinical implications. Journal of neuroscience methods 114:119-133.

Arieli A, Sterkin A, Grinvald A, Aertsen A (1996) Dynamics of ongoing activity: explanation of the large variability in evoked cortical responses. Science 273:1868-1871.

Aronoff R, Matyas F, Mateo C, Ciron C, Schneider B, Petersen CC (2010) Long-range connectivity of mouse primary somatosensory barrel cortex. Eur J Neurosci 31:2221-2233.

Asanuma H, Arnold A, Zarzecki P (1976) Further study on the excitation of pyramidal tract cells by intracortical microstimulation. Exp Brain Res 26:443-461.

Assaf Y, Pasternak O (2008) Diffusion tensor imaging (DTI)-based white matter mapping in brain research: a review. J Mol Neurosci 34:51-61.

Atasoy D, Aponte Y, Su HH, Sternson SM (2008) A FLEX switch targets Channelrhodopsin-2 to multiple cell types for imaging and long-range circuit mapping. J Neurosci 28:7025-7030.

Avermann M, Tomm C, Mateo C, Gerstner W, Petersen CC (2012) Microcircuits of excitatory and inhibitory neurons in layer 2/3 of mouse barrel cortex. J Neurophysiol 107:3116-3134.

Ayling OG, Harrison TC, Boyd JD, Goroshkov A, Murphy TH (2009) Automated light-based mapping of motor cortex by photoactivation of channelrhodopsin-2 transgenic mice. Nat Methods 6:219-224.

Barreto G, White RE, Ouyang Y, Xu L, Giffard RG (2011) Astrocytes: targets for neuroprotection in stroke. Cent Nerv Syst Agents Med Chem 11:164-173.

Bauer AQ, Kraft AW, Wright PW, Snyder AZ, Lee JM, Culver JP (2014) Optical imaging of disrupted functional connectivity following ischemic stroke in mice. Neuroimage.

Berger T, Borgdorff A, Crochet S, Neubauer FB, Lefort S, Fauvet B, Ferezou I, Carleton A, Luscher HR, Petersen CC (2007) Combined voltage and calcium epifluorescence imaging in vitro and in vivo reveals subthreshold and suprathreshold dynamics of mouse barrel cortex. J Neurophysiol 97:3751-3762.

Bi A, Cui J, Ma YP, Olshevskaya E, Pu M, Dizhoor AM, Pan ZH (2006) Ectopic expression of a microbial-type rhodopsin restores visual responses in mice with photoreceptor degeneration. Neuron 50:23-33.

Biernaskie J, Chernenko G, Corbett D (2004) Efficacy of rehabilitative experience declines with time after focal ischemic brain injury. J Neurosci 24:1245-1254.

Biswal BB et al. (2010) Toward discovery science of human brain function. Proceedings of the National Academy of Sciences of the United States of America 107:4734-4739.

Bivard A, Spratt N, Levi CR, Parsons MW (2011) Acute stroke thrombolysis: time to dispense with the clock and move to tissue-based decision making? Expert Rev Cardiovasc Ther 9:451-461.

Bohland JW et al. (2009) A proposal for a coordinated effort for the determination of brainwide neuroanatomical connectivity in model organisms at a mesoscopic scale. PLoS Comput Biol 5:e1000334.

Borghuis BG, Tian L, Xu Y, Nikonov SS, Vardi N, Zemelman BV, Looger LL (2011) Imaging light responses of targeted neuron populations in the rodent retina. J Neurosci 31:2855-2867.

Boyden ES, Zhang F, Bamberg E, Nagel G, Deisseroth K (2005) Millisecond-timescale, genetically targeted optical control of neural activity. Nat Neurosci 8:1263-1268.

Brown CE, Dyck RH (2005) Retrograde tracing of the subset of afferent connections in mouse barrel cortex provided by zincergic neurons. J Comp Neurol 486:48-60.

Brown CE, Wong C, Murphy TH (2008) Rapid morphologic plasticity of peri-infarct dendritic spines after focal ischemic stroke. Stroke 39:1286-1291.

Brown CE, Li P, Boyd JD, Delaney KR, Murphy TH (2007) Extensive turnover of dendritic spines and vascular remodeling in cortical tissues recovering from stroke. J Neurosci 27:4101-4109.

Brown CE, Aminoltejari K, Erb H, Winship IR, Murphy TH (2009) In vivo voltage-sensitive dye imaging in adult mice reveals that somatosensory maps lost to stroke are replaced over weeks by new structural and functional circuits with prolonged modes of activation within both the peri-infarct zone and distant sites. J Neurosci 29:1719-1734.

Buchkremer-Ratzmann I, August M, Hagemann G, Witte OW (1996) Electrophysiological transcortical diaschisis after cortical photothrombosis in rat brain. Stroke 27:1105-1109; discussion 1109-1111.

Bullmore E, Sporns O (2009) Complex brain networks: graph theoretical analysis of structural and functional systems. Nature reviews Neuroscience 10:186-198.

Butefisch CM, Kleiser R, Seitz RJ (2006) Post-lesional cerebral reorganisation: evidence from functional neuroimaging and transcranial magnetic stimulation. J Physiol Paris 99:437-454.

Butefisch CM, Netz J, Wessling M, Seitz RJ, Homberg V (2003) Remote changes in cortical excitability after stroke. Brain 126:470-481.

Callaway EM, Katz LC (1993) Photostimulation using caged glutamate reveals functional circuitry in living brain slices. Proc Natl Acad Sci U S A 90:7661-7665.

Campo P, Garrido MI, Moran RJ, Maestu F, Garcia-Morales I, Gil-Nagel A, del Pozo F, Dolan RJ, Friston KJ (2012) Remote effects of hippocampal sclerosis on effective connectivity during working memory encoding: a case of connectional diaschisis? Cerebral cortex 22:1225-1236.

Canada PHAo (2011) Tracking Heart Disease and Stroke in Canada. In: Government of Canada.

Cardin JA, Carlen M, Meletis K, Knoblich U, Zhang F, Deisseroth K, Tsai LH, Moore CI (2010) Targeted optogenetic stimulation and recording of neurons in vivo using cell-type-specific expression of Channelrhodopsin-2. Nat Protoc 5:247-254.

Carmichael ST (2003) Plasticity of cortical projections after stroke. Neuroscientist 9:64-75.

Carmichael ST (2005) Rodent models of focal stroke: size, mechanism, and purpose. NeuroRx 2:396-409.

Carmichael ST (2006) Cellular and molecular mechanisms of neural repair after stroke: making waves. Ann Neurol 59:735-742.

Carmichael ST (2008) Themes and strategies for studying the biology of stroke recovery in the poststroke epoch. Stroke 39:1380-1388.

Carmichael ST, Tatsukawa K, Katsman D, Tsuyuguchi N, Kornblum HI (2004) Evolution of diaschisis in a focal stroke model. Stroke 35:758-763.

Carrera E, Tononi G (2014) Diaschisis: past, present, future. Brain.

Carter AR, Shulman GL, Corbetta M (2012a) Why use a connectivity-based approach to study stroke and recovery of function? Neuroimage 62:2271-2280.

Carter AR, Astafiev SV, Lang CE, Connor LT, Rengachary J, Strube MJ, Pope DL, Shulman GL, Corbetta M (2010) Resting interhemispheric functional magnetic resonance imaging connectivity predicts performance after stroke. Ann Neurol 67:365-375.

Carter AR, Patel KR, Astafiev SV, Snyder AZ, Rengachary J, Strube MJ, Pope A, Shimony JS, Lang CE, Shulman GL, Corbetta M (2012b) Upstream dysfunction of somatomotor functional connectivity after corticospinal damage in stroke. Neurorehabil Neural Repair 26:7-19.

Chapman B, Stryker MP, Bonhoeffer T (1996) Development of orientation preference maps in ferret primary visual cortex. J Neurosci 16:6443-6453.

Chemla S, Chavane F (2010) Voltage-sensitive dye imaging: Technique review and models. J Physiol Paris 104:40-50.

Chen-Bee CH, Frostig RD (1996) Variability and interhemispheric asymmetry of single-whisker functional representations in rat barrel cortex. J Neurophysiol 76:884-894.

Chen Q, Cichon J, Wang W, Qiu L, Lee SJ, Campbell NR, Destefino N, Goard MJ, Fu Z, Yasuda R, Looger LL, Arenkiel BR, Gan WB, Feng G (2012a) Imaging neural activity using Thy1-GCaMP transgenic mice. Neuron 76:297-308.

Chen TW, Wardill TJ, Hasseman JP, Tsegaye G, Fosque BF, Schreiter ER, Kimmel BE, Kerr RA, Jayaraman V, Svoboda K, Looger LL, Kim DS (2012b) Engineering the next generation GCaMP calcium indicators using neuron-based screening. In: 2012 Neuroscience meeting planner. New Orleans, LA: Society for Neuroscience.

Cheng L, Wu Z, Fu Y, Miao F, Sun J, Tong S (2012) Reorganization of functional brain networks during the recovery of stroke: a functional MRI study. Conf Proc IEEE Eng Med Biol Soc 2012:4132-4135.

Cheng MY, Wang EH, Woodson WJ, Wang S, Sun G, Lee AG, Arac A, Fenno LE, Deisseroth K, Steinberg GK (2014) Optogenetic neuronal stimulation promotes functional recovery after stroke. Proceedings of the National Academy of Sciences of the United States of America 111:12913-12918.

Cheng YD, Al-Khoury L, Zivin JA (2004) Neuroprotection for ischemic stroke: two decades of success and failure. NeuroRx 1:36-45.

Chow BY, Han X, Bernstein J, Monahan PE, Boyden E (2012) Light-activated ion pumps and channels for temporally precise optical control of activity in genetically targeted neurons. Neuromethods 67:305-338.

Christie IN, Wells JA, Southern P, Marina N, Kasparov S, Gourine AV, Lythgoe MF (2012) fMRI response to blue light delivery in the naive brain: Implications for combined optogenetic fMRI studies. Neuroimage 66C:634-641.

Cramer SC (2008) Repairing the human brain after stroke: I. Mechanisms of spontaneous recovery. Ann Neurol 63:272-287.

Culham JC, Kanwisher NG (2001) Neuroimaging of cognitive functions in human parietal cortex. Curr Opin Neurobiol 11:157-163.

Damoiseaux JS, Greicius MD (2009) Greater than the sum of its parts: a review of studies combining structural connectivity and resting-state functional connectivity. Brain Struct Funct 213:525-533.

Dancause N (2006) Vicarious function of remote cortex following stroke: recent evidence from human and animal studies. Neuroscientist 12:489-499.

Dancause N, Nudo RJ (2011) Shaping plasticity to enhance recovery after injury. Prog Brain Res 192:273-295.

Dancause N, Barbay S, Frost SB, Plautz EJ, Chen D, Zoubina EV, Stowe AM, Nudo RJ (2005) Extensive cortical rewiring after brain injury. J Neurosci 25:10167-10179.

Deisseroth K, Feng G, Majewska AK, Miesenbock G, Ting A, Schnitzer MJ (2006) Next-generation optical technologies for illuminating genetically targeted brain circuits. The Journal of neuroscience : the official journal of the Society for Neuroscience 26:10380-10386.

Denk W, Horstmann H (2004) Serial block-face scanning electron microscopy to reconstruct three-dimensional tissue nanostructure. PLoS Biol 2:e329.

Desai M, Kahn I, Knoblich U, Bernstein J, Atallah H, Yang A, Kopell N, Buckner RL, Graybiel AM, Moore CI, Boyden ES (2011) Mapping brain networks in awake mice using combined optical neural control and fMRI. J Neurophysiol 105:1393-1405.

Diester I, Kaufman MT, Mogri M, Pashaie R, Goo W, Yizhar O, Ramakrishnan C, Deisseroth K, Shenoy KV (2011) An optogenetic toolbox designed for primates. Nat Neurosci 14:387-397.

Dijkhuizen RM, Ren J, Mandeville JB, Wu O, Ozdag FM, Moskowitz MA, Rosen BR, Finklestein SP (2001) Functional magnetic resonance imaging of reorganization in rat brain after stroke. Proc Natl Acad Sci U S A 98:12766-12771.

Dijkhuizen RM, Singhal AB, Mandeville JB, Wu O, Halpern EF, Finklestein SP, Rosen BR, Lo EH (2003) Correlation between brain reorganization, ischemic damage, and neurologic status after transient focal cerebral ischemia in rats: a functional magnetic resonance imaging study. J Neurosci 23:510-517.

Dirnagl U (2010) Complexities, confounders, and challenges in experimental stroke research: A checklist for researchers and reviewers. In: Rodent models of stroke (Dirnagl U, ed), pp 263-277: Springer Science+Business Media.

Dirnagl U, Iadecola C, Moskowitz MA (1999) Pathobiology of ischaemic stroke: an integrated view. Trends Neurosci 22:391-397.

Douglas RJ, Martin KA (1991) A functional microcircuit for cat visual cortex. J Physiol 440:735-769.

Douglas RJ, Martin KA (2004) Neuronal circuits of the neocortex. Annu Rev Neurosci 27:419-451.

Douglas RJ, Martin KA (2007) Mapping the matrix: the ways of neocortex. Neuron 56:226-238.

Durukan A, Tatlisumak T (2007) Acute ischemic stroke: overview of major experimental rodent models, pathophysiology, and therapy of focal cerebral ischemia. Pharmacol Biochem Behav 87:179-197.

Erchova IA, Lebedev MA, Diamond ME (2002) Somatosensory cortical neuronal population activity across states of anaesthesia. Eur J Neurosci 15:744-752.

Fabri M, Burton H (1991) Ipsilateral cortical connections of primary somatic sensory cortex in rats. J Comp Neurol 311:405-424.

Feeney DM, Baron JC (1986) Diaschisis. Stroke 17:817-830.

Feldt S, Bonifazi P, Cossart R (2011) Dissecting functional connectivity of neuronal microcircuits: experimental and theoretical insights. Trends Neurosci 34:225-236.

Feng G, Mellor RH, Bernstein M, Keller-Peck C, Nguyen QT, Wallace M, Nerbonne JM, Lichtman JW, Sanes JR (2000) Imaging neuronal subsets in transgenic mice expressing multiple spectral variants of GFP. Neuron 28:41-51.

Ferezou I, Bolea S, Petersen CC (2006) Visualizing the cortical representation of whisker touch: voltage-sensitive dye imaging in freely moving mice. Neuron 50:617-629.

Ferezou I, Haiss F, Gentet LJ, Aronoff R, Weber B, Petersen CC (2007) Spatiotemporal dynamics of cortical sensorimotor integration in behaving mice. Neuron 56:907-923.

Fino E, Yuste R (2011) Dense inhibitory connectivity in neocortex. Neuron 69:1188-1203.

Foundation HaS (2014) Stroke Report 2014. In: Heart and Stroke Foundation.

Fox K (1992) A critical period for experience-dependent synaptic plasticity in rat barrel cortex. J Neurosci 12:1826-1838.

Fox MD, Raichle ME (2007) Spontaneous fluctuations in brain activity observed with functional magnetic resonance imaging. Nat Rev Neurosci 8:700-711.

Fox MD, Snyder AZ, Vincent JL, Raichle ME (2007) Intrinsic fluctuations within cortical systems account for intertrial variability in human behavior. Neuron 56:171-184.

Frost SB, Barbay S, Friel KM, Plautz EJ, Nudo RJ (2003) Reorganization of remote cortical regions after ischemic brain injury: a potential substrate for stroke recovery. J Neurophysiol 89:3205-3214.

Frostig RD, Xiong Y, Chen-Bee CH, Kvasnak E, Stehberg J (2008) Large-scale organization of rat sensorimotor cortex based on a motif of large activation spreads. J Neurosci 28:13274-13284.

Furlan M, Marchal G, Viader F, Derlon JM, Baron JC (1996) Spontaneous neurological recovery after stroke and the fate of the ischemic penumbra. Ann Neurol 40:216-226.

Garey LJ, ed (2006) Brodmann's: Localisation in the cerebral cortex 1909. New York, NY: Springer.

Gerloff C, Bushara K, Sailer A, Wassermann EM, Chen R, Matsuoka T, Waldvogel D, Wittenberg GF, Ishii K, Cohen LG, Hallett M (2006) Multimodal imaging of brain reorganization in motor areas of the contralesional hemisphere of well recovered patients after capsular stroke. Brain : a journal of neurology 129:791-808.

Gerriets T, Li F, Silva MD, Meng X, Brevard M, Sotak CH, Fisher M (2003) The macrosphere model: evaluation of a new stroke model for permanent middle cerebral artery occlusion in rats. Journal of neuroscience methods 122:201-211.

Gharbawie OA, Gonzalez CL, Williams PT, Kleim JA, Whishaw IQ (2005) Middle cerebral artery (MCA) stroke produces dysfunction in adjacent motor cortex as detected by intracortical microstimulation in rats. Neuroscience 130:601-610.

Ginsberg MD (2008) Neuroprotection for ischemic stroke: past, present and future. Neuropharmacology 55:363-389.

Go AS et al. (2014) Executive summary: heart disease and stroke statistics--2014 update: a report from the American Heart Association. Circulation 129:399-410.

Golshani P, Goncalves JT, Khoshkhoo S, Mostany R, Smirnakis S, Portera-Cailliau C (2009) Internally mediated developmental desynchronization of neocortical network activity. J Neurosci 29:10890-10899.

Gong H, Zeng S, Yan C, Lv X, Yang Z, Xu T, Feng Z, Ding W, Qi X, Li A, Wu J, Luo Q (2013) Continuously tracing brain-wide long-distance axonal projections in mice at a one-micron voxel resolution. Neuroimage 74:87-98.

Gradinaru V, Mogri M, Thompson KR, Henderson JM, Deisseroth K (2009) Optical deconstruction of parkinsonian neural circuitry. Science 324:354-359.

Grefkes C, Fink GR (2011) Reorganization of cerebral networks after stroke: new insights from neuroimaging with connectivity approaches. Brain 134:1264-1276.

Griffin DM, Hudson HM, Belhaj-Saif A, Cheney PD (2011) Hijacking cortical motor output with repetitive microstimulation. J Neurosci 31:13088-13096.

Grinvald A, Hildesheim R (2004) VSDI: a new era in functional imaging of cortical dynamics. Nat Rev Neurosci 5:874-885.

Grinvald A, Manker A, Segal M (1982) Visualization of the spread of electrical activity in rat hippocampal slices by voltage-sensitive optical probes. The Journal of physiology 333:269-291.

Gunaydin LA, Yizhar O, Berndt A, Sohal VS, Deisseroth K, Hegemann P (2010) Ultrafast optogenetic control. Nat Neurosci 13:387-392.

Hacke W, Kaste M, Fieschi C, Toni D, Lesaffre E, von Kummer R, Boysen G, Bluhmki E, Hoxter G, Mahagne MH, et al. (1995) Intravenous thrombolysis with recombinant tissue plasminogen activator for acute hemispheric stroke. The European Cooperative Acute Stroke Study (ECASS). JAMA 274:1017-1025.

Hallett M (2000) Transcranial magnetic stimulation and the human brain. Nature 406:147-150.

Han X, Boyden ES (2007) Multiple-color optical activation, silencing, and desynchronization of neural activity, with single-spike temporal resolution. PLoS One 2:e299.

Harris KD, Shepherd GM (2015) The neocortical circuit: themes and variations. Nat Neurosci 18:170-181.

Harrison TC, Ayling OG, Murphy TH (2012) Distinct cortical circuit mechanisms for complex forelimb movement and motor map topography. Neuron 74:397-409.

Hattox AM, Nelson SB (2007) Layer V neurons in mouse cortex projecting to different targets have distinct physiological properties. J Neurophysiol 98:3330-3340.

Haubensak W, Kunwar PS, Cai H, Ciocchi S, Wall NR, Ponnusamy R, Biag J, Dong HW, Deisseroth K, Callaway EM, Fanselow MS, Luthi A, Anderson DJ (2010) Genetic dissection of an amygdala microcircuit that gates conditioned fear. Nature 468:270-276.

Heiss WD (2012) The ischemic penumbra: how does tissue injury evolve? Ann N Y Acad Sci 1268:26-34.

Helmchen F, Svoboda K, Denk W, Tank DW (1999) In vivo dendritic calcium dynamics in deep-layer cortical pyramidal neurons. Nat Neurosci 2:989-996.

Hira R, Honkura N, Noguchi J, Maruyama Y, Augustine GJ, Kasai H, Matsuzaki M (2009) Transcranial optogenetic stimulation for functional mapping of the motor cortex. J Neurosci Methods 179:258-263.

Hira R, Ohkubo F, Ozawa K, Isomura Y, Kitamura K, Kano M, Kasai H, Matsuzaki M (2013) Spatiotemporal dynamics of functional clusters of neurons in the mouse motor cortex during a voluntary movement. The Journal of neuroscience : the official journal of the Society for Neuroscience 33:1377-1390.

Hires SA, Tian L, Looger LL (2008) Reporting neural activity with genetically encoded calcium indicators. Brain Cell Biol 36:69-86.

Histed MH, Bonin V, Reid RC (2009) Direct activation of sparse, distributed populations of cortical neurons by electrical microstimulation. Neuron 63:508-522.

Hjornevik T, Leergaard TB, Darine D, Moldestad O, Dale AM, Willoch F, Bjaalie JG (2007) Three-dimensional atlas system for mouse and rat brain imaging data. Frontiers in neuroinformatics 1:4.

Homma R, Baker BJ, Jin L, Garaschuk O, Konnerth A, Cohen LB, Zecevic D (2009) Wide-field and two-photon imaging of brain activity with voltage- and calcium-sensitive dyes. Philos Trans R Soc Lond B Biol Sci 364:2453-2467.

Honey CJ, Thivierge JP, Sporns O (2010) Can structure predict function in the human brain? Neuroimage 52:766-776.

Hooks BM, Mao T, Gutnisky DA, Yamawaki N, Svoboda K, Shepherd GM (2013) Organization of cortical and thalamic input to pyramidal neurons in mouse motor cortex. J Neurosci 33:748-760.

Hooks BM, Hires SA, Zhang YX, Huber D, Petreanu L, Svoboda K, Shepherd GM (2011) Laminar analysis of excitatory local circuits in vibrissal motor and sensory cortical areas. PLoS Biol 9:e1000572.

Horie N, Maag AL, Hamilton SA, Shichinohe H, Bliss TM, Steinberg GK (2008) Mouse model of focal cerebral ischemia using endothelin-1. Journal of neuroscience methods 173:286-290.

Huber D, Petreanu L, Ghitani N, Ranade S, Hromadka T, Mainen Z, Svoboda K (2008) Sparse optical microstimulation in barrel cortex drives learned behaviour in freely moving mice. Nature 451:61-64.

Hudetz AG, Imas OA (2007) Burst activation of the cerebral cortex by flash stimuli during isoflurane anesthesia in rats. Anesthesiology 107:983-991.

Huerta PT, Volpe BT (2009) Transcranial magnetic stimulation, synaptic plasticity and network oscillations. J Neuroeng Rehabil 6:7.

Iizuka H, Sakatani K, Young W (1990) Neural damage in the rat thalamus after cortical infarcts. Stroke; a journal of cerebral circulation 21:790-794.

Jablonka JA, Burnat K, Witte OW, Kossut M (2010) Remapping of the somatosensory cortex after a photothrombotic stroke: dynamics of the compensatory reorganization. Neuroscience 165:90-100.

Jazayeri M, Lindbloom-Brown Z, Horwitz GD (2012) Saccadic eye movements evoked by optogenetic activation of primate V1. Nat Neurosci 15:1368-1370.

Jiwa NS, Garrard P, Hainsworth AH (2010) Experimental models of vascular dementia and vascular cognitive impairment: a systematic review. J Neurochem 115:814-828.

Kaas JH (1999) Is most of neural plasticity in the thalamus cortical? Proc Natl Acad Sci U S A 96:7622-7623.

Kaas JH, Merzenich MM, Killackey HP (1983) The reorganization of somatosensory cortex following peripheral nerve damage in adult and developing mammals. Annual review of neuroscience 6:325-356.

Kahn I, Desai M, Knoblich U, Bernstein J, Henninger M, Graybiel AM, Boyden ES, Buckner RL, Moore CI (2011) Characterization of the functional MRI response temporal linearity via optical control of neocortical pyramidal neurons. J Neurosci 31:15086-15091.

Katz LC, Dalva MB (1994) Scanning laser photostimulation: a new approach for analyzing brain circuits. J Neurosci Methods 54:205-218.

Katzel D, Zemelman BV, Buetfering C, Wolfel M, Miesenbock G (2010) The columnar and laminar organization of inhibitory connections to neocortical excitatory cells. Nat Neurosci 14:100-107.

Kenet T, Bibitchkov D, Tsodyks M, Grinvald A, Arieli A (2003) Spontaneously emerging cortical representations of visual attributes. Nature 425:954-956.

Kerr AL, Wolke ML, Bell JA, Jones TA (2013) Post-stroke protection from maladaptive effects of learning with the non-paretic forelimb by bimanual home cage experience in C57BL/6 mice. Behav Brain Res 252:180-187.

Kertzman C, Schwarz U, Zeffiro TA, Hallett M (1997) The role of posterior parietal cortex in visually guided reaching movements in humans. Exp Brain Res 114:170-183.

Kitagawa K, Matsumoto M, Yang G, Mabuchi T, Yagita Y, Hori M, Yanagihara T (1998) Cerebral ischemia after bilateral carotid artery occlusion and intraluminal suture occlusion in mice: evaluation of the patency of the posterior communicating artery. J Cereb Blood Flow Metab 18:570-579.

Kleim JA, Jones TA (2008) Principles of experience-dependent neural plasticity: implications for rehabilitation after brain damage. J Speech Lang Hear Res 51:S225-239.

Kleim JA, Barbay S, Nudo RJ (1998) Functional reorganization of the rat motor cortex following motor skill learning. J Neurophysiol 80:3321-3325.

Kleinfeld D, Delaney KR (1996) Distributed representation of vibrissa movement in the upper layers of somatosensory cortex revealed with voltage-sensitive dyes. J Comp Neurol 375:89-108.

Kleinfeld D, Ahissar E, Diamond ME (2006) Active sensation: insights from the rodent vibrissa sensorimotor system. Curr Opin Neurobiol 16:435-444.

Kleinfeld D, Bharioke A, Blinder P, Bock DD, Briggman KL, Chklovskii DB, Denk W, Helmstaedter M, Kaufhold JP, Lee WC, Meyer HS, Micheva KD, Oberlaender M, Prohaska S, Reid RC, Smith SJ, Takemura S, Tsai PS, Sakmann B (2011) Large-scale automated histology in the pursuit of connectomes. The Journal of neuroscience : the official journal of the Society for Neuroscience 31:16125-16138.

Knopfel T (2012) Genetically encoded optical indicators for the analysis of neuronal circuits. Nat Rev Neurosci 13:687-700.

Kohl MM, Shipton OA, Deacon RM, Rawlins JN, Deisseroth K, Paulsen O (2011) Hemisphere-specific optogenetic stimulation reveals left-right asymmetry of hippocampal plasticity. Nat Neurosci 14:1413-1415.

Kolb B, Walkey J (1987) Behavioural and anatomical studies of the posterior parietal cortex in the rat. Behav Brain Res 23:127-145.

Kolb B, Whishaw IQ (1998) Brain plasticity and behavior. Annu Rev Psychol 49:43-64.

Kolb B, Sutherland RJ, Nonneman AJ, Whishaw IQ (1982) Asymmetry in the cerebral hemispheres of the rat, mouse, rabbit, and cat: the right hemisphere is larger. Exp Neurol 78:348-359.

Komiyama T, Sato TR, O'Connor DH, Zhang YX, Huber D, Hooks BM, Gabitto M, Svoboda K (2010) Learning-related fine-scale specificity imaged in motor cortex circuits of behaving mice. Nature 464:1182-1186.

Konnerth A, Orkand RK (1986) Voltage-sensitive dyes measure potential changes in axons and glia of the frog optic nerve. Neurosci Lett 66:49-54.

Koralek KA, Olavarria J, Killackey HP (1990) Areal and laminar organization of corticocortical projections in the rat somatosensory cortex. J Comp Neurol 299:133-150.

Krakauer JW, Carmichael ST, Corbett D, Wittenberg GF (2012) Getting neurorehabilitation right: what can be learned from animal models? Neurorehabilitation and neural repair 26:923-931.

Lakhan SE, Kirchgessner A, Hofer M (2009) Inflammatory mechanisms in ischemic stroke: therapeutic approaches. J Transl Med 7:97.

Lanciego JL, Wouterlood FG (2011) A half century of experimental neuroanatomical tracing. J Chem Neuroanat 42:157-183.

Langdon KD, Clarke J, Corbett D (2011) Long-term exposure to high fat diet is bad for your brain: exacerbation of focal ischemic brain injury. Neuroscience 182:82-87.

Lay CC, Frostig RD (2014) Complete protection from impending stroke following permanent middle cerebral artery occlusion in awake, behaving rats. The European journal of neuroscience.

Lay CC, Davis MF, Chen-Bee CH, Frostig RD (2010) Mild sensory stimulation completely protects the adult rodent cortex from ischemic stroke. PLoS One 5:e11270.

Lee JH, Durand R, Gradinaru V, Zhang F, Goshen I, Kim DS, Fenno LE, Ramakrishnan C, Deisseroth K (2010) Global and local fMRI signals driven by neurons defined optogenetically by type and wiring. Nature 465:788-792.

Lein ES et al. (2007) Genome-wide atlas of gene expression in the adult mouse brain. Nature 445:168-176.

Li P, Murphy TH (2008) Two-photon imaging during prolonged middle cerebral artery occlusion in mice reveals recovery of dendritic structure after reperfusion. The Journal of neuroscience : the official journal of the Society for Neuroscience 28:11970-11979.

Lichtman JW, Denk W (2011) The big and the small: challenges of imaging the brain's circuits. Science 334:618-623.

Liew SL, Santarnecchi E, Buch ER, Cohen LG (2014) Non-invasive brain stimulation in neurorehabilitation: local and distant effects for motor recovery. Front Hum Neurosci 8:378.

Lim DH, Alaverdashvili M, Whishaw IQ (2009) Nicotine does not improve recovery from learned nonuse nor enhance constraint-induced therapy after motor cortex stroke in the rat. Behav Brain Res 198:411-419.

Lim DH, LeDue JM, Mohajerani MH, Murphy TH (2014) Optogenetic mapping after stroke reveals network-wide scaling of functional connections and heterogeneous recovery of the peri-infarct. J Neurosci 34:16455-16466.

Lim DH, Ledue J, Mohajerani MH, Vanni MP, Murphy TH (2013) Optogenetic approaches for functional mouse brain mapping. Front Neurosci 7:54.

Lim DH, Mohajerani MH, Ledue J, Boyd J, Chen S, Murphy TH (2012) In vivo Large-Scale Cortical Mapping Using Channelrhodopsin-2 Stimulation in Transgenic Mice Reveals Asymmetric and Reciprocal Relationships between Cortical Areas. Front Neural Circuits 6:11.

Lin JY (2011) A user's guide to channelrhodopsin variants: features, limitations and future developments. Exp Physiol 96:19-25.

Lin JY (2012) Optogenetic excitation of neurons with channelrhodopsins: light instrumentation, expression systems, and channelrhodopsin variants. Prog Brain Res 196:29-47.

Lin JY, Lin MZ, Steinbach P, Tsien RY (2009) Characterization of engineered channelrhodopsin variants with improved properties and kinetics. Biophys J 96:1803-1814.

Lipp HP, Collins RL, Nauta WJ (1984) Structural asymmetries in brains of mice selected for strong lateralization. Brain Res 310:393-396.

Logothetis NK (2007) The ins and outs of fMRI signals. Nat Neurosci 10:1230-1232.

Logothetis NK (2010) Bold claims for optogenetics. Nature 468:E3-4; discussion E4-5.

Logothetis NK, Pfeuffer J (2004) On the nature of the BOLD fMRI contrast mechanism. Magn Reson Imaging 22:1517-1531.

London JA, Cohen LB, Wu JY (1989) Optical recordings of the cortical response to whisker stimulation before and after the addition of an epileptogenic agent. J Neurosci 9:2182-2190.

Longa EZ, Weinstein PR, Carlson S, Cummins R (1989) Reversible middle cerebral artery occlusion without craniectomy in rats. Stroke; a journal of cerebral circulation 20:84-91.

Looger LL, Griesbeck O (2012) Genetically encoded neural activity indicators. Curr Opin Neurobiol 22:18-23.

Lu J, Fiala JC, Lichtman JW (2009) Semi-automated reconstruction of neural processes from large numbers of fluorescence images. PLoS One 4:e5655.

Lutcke H, Murayama M, Hahn T, Margolis DJ, Astori S, Zum Alten Borgloh SM, Gobel W, Yang Y, Tang W, Kugler S, Sprengel R, Nagai T, Miyawaki A, Larkum ME, Helmchen F, Hasan MT (2010) Optical recording of neuronal activity with a genetically-encoded calcium indicator in anesthetized and freely moving mice. Front Neural Circuits 4:9.

Lynch JC (1980) The functional organization of posterior parietal association cortex. Behavioral and Brain Sciences 3:485-199.

Madisen L et al. (2012) A toolbox of Cre-dependent optogenetic transgenic mice for light-induced activation and silencing. Nat Neurosci 15:793-802.

Majewska AK, Sur M (2006) Plasticity and specificity of cortical processing networks. Trends Neurosci 29:323-329.

Mancuso JJ, Kim J, Lee S, Tsuda S, Chow NB, Augustine GJ (2010) Optogenetic probing of functional brain circuitry. Exp Physiol 96:26-33.

Mank M, Santos AF, Direnberger S, Mrsic-Flogel TD, Hofer SB, Stein V, Hendel T, Reiff DF, Levelt C, Borst A, Bonhoeffer T, Hubener M, Griesbeck O (2008) A genetically encoded calcium indicator for chronic in vivo two-photon imaging. Nat Methods 5:805-811.

Manns ID, Sakmann B, Brecht M (2004) Sub- and suprathreshold receptive field properties of pyramidal neurones in layers 5A and 5B of rat somatosensory barrel cortex. J Physiol 556:601-622.

Mao T, Kusefoglu D, Hooks BM, Huber D, Petreanu L, Svoboda K (2011) Long-range neuronal circuits underlying the interaction between sensory and motor cortex. Neuron 72:111-123.

Markram H (2006) The blue brain project. Nat Rev Neurosci 7:153-160.

Matyas F, Sreenivasan V, Marbach F, Wacongne C, Barsy B, Mateo C, Aronoff R, Petersen CC (2010) Motor control by sensory cortex. Science 330:1240-1243.

McVea DA, Mohajerani MH, Murphy TH (2012) Voltage-sensitive dye imaging reveals dynamic spatiotemporal properties of cortical activity after spontaneous muscle twitches in the newborn rat. J Neurosci 32:10982-10994.

Merzenich MM, Kaas JH, Wall J, Nelson RJ, Sur M, Felleman D (1983) Topographic reorganization of somatosensory cortical areas 3b and 1 in adult monkeys following restricted deafferentation. Neuroscience 8:33-55.

Meyer HS, Wimmer VC, Hemberger M, Bruno RM, de Kock CP, Frick A, Sakmann B, Helmstaedter M (2010) Cell type-specific thalamic innervation in a column of rat vibrissal cortex. Cereb Cortex 20:2287-2303.

Minderer M, Liu W, Sumanovski LT, Kugler S, Helmchen F, Margolis DJ (2012) Chronic imaging of cortical sensory map dynamics using a genetically encoded calcium indicator. J Physiol 590:99-107.

Mitz AR, Wise SP (1987) The somatotopic organization of the supplementary motor area: intracortical microstimulation mapping. J Neurosci 7:1010-1021.

Miyake K, Takeo S, Kaijihara H (1993) Sustained decrease in brain regional blood flow after microsphere embolism in rats. Stroke; a journal of cerebral circulation 24:415-420.

Mohajerani MH, Aminoltejari K, Murphy TH (2011) Targeted mini-strokes produce changes in interhemispheric sensory signal processing that are indicative of disinhibition within minutes. Proc Natl Acad Sci U S A 108:E183-191.

Mohajerani MH, McVea DA, Fingas M, Murphy TH (2010) Mirrored bilateral slow-wave cortical activity within local circuits revealed by fast bihemispheric voltage-sensitive dye imaging in anesthetized and awake mice. J Neurosci 30:3745-3751.

Mohajerani MH, Chan AW, Mohsenvand M, LeDue J, Liu R, McVea DA, Boyd JD, Wang YT, Reimers M, Murphy TH (2013) Spontaneous cortical activity alternates between motifs defined by regional axonal projections. Nat Neurosci 16:1426-1435.

Mostany R, Chowdhury TG, Johnston DG, Portonovo SA, Carmichael ST, Portera-Cailliau C (2010) Local hemodynamics dictate long-term dendritic plasticity in peri-infarct cortex. J Neurosci 30:14116-14126.

Murphy TH, Corbett D (2009) Plasticity during stroke recovery: from synapse to behaviour. Nat Rev Neurosci 10:861-872.

Nagel G, Brauner M, Liewald JF, Adeishvili N, Bamberg E, Gottschalk A (2005) Light activation of channelrhodopsin-2 in excitable cells of Caenorhabditis elegans triggers rapid behavioral responses. Curr Biol 15:2279-2284.

Nagel G, Szellas T, Huhn W, Kateriya S, Adeishvili N, Berthold P, Ollig D, Hegemann P, Bamberg E (2003) Channelrhodopsin-2, a directly light-gated cation-selective membrane channel. Proc Natl Acad Sci U S A 100:13940-13945.

Neafsey EJ, Bold EL, Haas G, Hurley-Gius KM, Quirk G, Sievert CF, Terreberry RR (1986) The organization of the rat motor cortex: a microstimulation mapping study. Brain Res 396:77-96.

Nguyen QT, Kleinfeld D (2005) Positive feedback in a brainstem tactile sensorimotor loop. Neuron 45:447-457.

Nicolelis MA, Lebedev MA (2009) Principles of neural ensemble physiology underlying the operation of brain-machine interfaces. Nat Rev Neurosci 10:530-540.

Nudo RJ, Milliken GW (1996) Reorganization of movement representations in primary motor cortex following focal ischemic infarcts in adult squirrel monkeys. J Neurophysiol 75:2144-2149.

Nudo RJ, Plautz EJ, Frost SB (2001) Role of adaptive plasticity in recovery of function after damage to motor cortex. Muscle Nerve 24:1000-1019.

O'Leary DD, Chou SJ, Sahara S (2007) Area patterning of the mammalian cortex. Neuron 56:252-269.

Oh SW et al. (2014) A mesoscale connectome of the mouse brain. Nature 508:207-214.

Orbach HS, Cohen LB (1983) Optical monitoring of activity from many areas of the in vitro and in vivo salamander olfactory bulb: a new method for studying functional organization in the vertebrate central nervous system. The Journal of neuroscience : the official journal of the Society for Neuroscience 3:2251-2262.

Overgaard K, Sereghy T, Boysen G, Pedersen H, Diemer NH (1992) Reduction of infarct volume and mortality by thrombolysis in a rat embolic stroke model. Stroke; a journal of cerebral circulation 23:1167-1173; discussion 1174.

Overman JJ, Clarkson AN, Wanner IB, Overman WT, Eckstein I, Maguire JL, Dinov ID, Toga AW, Carmichael ST (2012) A role for ephrin-A5 in axonal sprouting, recovery, and activity-dependent plasticity after stroke. Proc Natl Acad Sci U S A 109:E2230-2239.

Packer AM, Peterka DS, Hirtz JJ, Prakash R, Deisseroth K, Yuste R (2012) Two-photon optogenetics of dendritic spines and neural circuits. Nat Methods 9:1202-1205.

Papagiakoumou E, Anselmi F, Begue A, de Sars V, Gluckstad J, Isacoff EY, Emiliani V (2010) Scanless two-photon excitation of channelrhodopsin-2. Nat Methods 7:848-854.

Pascual-Leone A, Walsh V, Rothwell J (2000) Transcranial magnetic stimulation in cognitive neuroscience--virtual lesion, chronometry, and functional connectivity. Current opinion in neurobiology 10:232-237.

Paxinos G, Franklin KBJ (2001) The mouse brain in stereotaxic coordinates, 2nd Edition. San Diego: Academic Press.

Penfield W (1950) The supplementary motor area in the cerebral cortex of man. Arch Psychiatr Nervenkr Z Gesamte Neurol Psychiatr 185:670-674.

Penfield W, Boldrey E (1937) Somatic motor and sensory representation in the cerebral cortex of man as studied by electrical stimulation. Brain 60:389-443.

Perlmutter JS, Mink JW (2006) Deep brain stimulation. Annu Rev Neurosci 29:229-257.

Perron A, Akemann W, Mutoh H, Knopfel T (2012) Genetically encoded probes for optical imaging of brain electrical activity. Prog Brain Res 196:63-77.

Perron A, Mutoh H, Akemann W, Gautam SG, Dimitrov D, Iwamoto Y, Knopfel T (2009) Second and third generation voltage-sensitive fluorescent proteins for monitoring membrane potential. Front Mol Neurosci 2:5.

Peterka DS, Takahashi H, Yuste R (2012) Imaging voltage in neurons. Neuron 69:9-21.

Petersen CC, Grinvald A, Sakmann B (2003a) Spatiotemporal dynamics of sensory responses in layer 2/3 of rat barrel cortex measured in vivo by voltage-sensitive dye imaging combined with whole-cell voltage recordings and neuron reconstructions. J Neurosci 23:1298-1309.

Petersen CC, Hahn TT, Mehta M, Grinvald A, Sakmann B (2003b) Interaction of sensory responses with spontaneous depolarization in layer 2/3 barrel cortex. Proc Natl Acad Sci U S A 100:13638-13643.

Petreanu L, Huber D, Sobczyk A, Svoboda K (2007) Channelrhodopsin-2-assisted circuit mapping of long-range callosal projections. Nat Neurosci 10:663-668.

Petreanu L, Mao T, Sternson SM, Svoboda K (2009) The subcellular organization of neocortical excitatory connections. Nature 457:1142-1145.

Qiu S, Anderson CT, Levitt P, Shepherd GM (2011) Circuit-specific intracortical hyperconnectivity in mice with deletion of the autism-associated Met receptor tyrosine kinase. J Neurosci 31:5855-5864.

Raffin E, Siebner HR (2014) Transcranial brain stimulation to promote functional recovery after stroke. Curr Opin Neurol 27:54-60.

Reiner A, Veenman CL, Medina L, Jiao Y, Del Mar N, Honig MG (2000) Pathway tracing using biotinylated dextran amines. J Neurosci Methods 103:23-37.

Rickgauer JP, Tank DW (2012) Optical instrumentation for simultaneous imaging and patterned photostimulation at cellular resolution in awake mice. In: 2012 Neuroscience meeting planner. New Orleans, LA: Society for Neuroscience.

Ringach DL (2009) Spontaneous and driven cortical activity: implications for computation. Curr Opin Neurobiol 19:439-444.

Roome RB, Bartlett RF, Jeffers M, Xiong J, Corbett D, Vanderluit JL (2014) A reproducible Endothelin-1 model of forelimb motor cortex stroke in the mouse. J Neurosci Methods 233C:34-44.

Rubinov M, Sporns O (2010) Complex network measures of brain connectivity: uses and interpretations. Neuroimage 52:1059-1069.

Sakai R, Repunte-Canonigo V, Raj CD, Knopfel T (2001) Design and characterization of a DNA-encoded, voltage-sensitive fluorescent protein. Eur J Neurosci 13:2314-2318.

Scanziani M, Hausser M (2009) Electrophysiology in the age of light. Nature 461:930-939.

Scott NA, Murphy TH (2012) Hemodynamic responses evoked by neuronal stimulation via channelrhodopsin-2 can be independent of intracortical glutamatergic synaptic transmission. PLoS One 7:e29859.

Seitz RJ, Azari NP, Knorr U, Binkofski F, Herzog H, Freund HJ (1999) The role of diaschisis in stroke recovery. Stroke 30:1844-1850.

Sharkey J, Butcher SP (1995) Characterisation of an experimental model of stroke produced by intracerebral microinjection of endothelin-1 adjacent to the rat middle cerebral artery. Journal of neuroscience methods 60:125-131.

Sharma N, Baron JC, Rowe JB (2009) Motor imagery after stroke: relating outcome to motor network connectivity. Ann Neurol 66:604-616.

Sharon D, Grinvald A (2002) Dynamics and constancy in cortical spatiotemporal patterns of orientation processing. Science 295:512-515.

Shepherd GM (2009) Intracortical cartography in an agranular area. Front Neurosci 3:337-343.

Shepherd GM, Pologruto TA, Svoboda K (2003) Circuit analysis of experience-dependent plasticity in the developing rat barrel cortex. Neuron 38:277-289.

Shepherd GM, Stepanyants A, Bureau I, Chklovskii D, Svoboda K (2005) Geometric and functional organization of cortical circuits. Nat Neurosci 8:782-790.

Shih AY, Blinder P, Tsai PS, Friedman B, Stanley G, Lyden PD, Kleinfeld D (2013) The smallest stroke: occlusion of one penetrating vessel leads to infarction and a cognitive deficit. Nat Neurosci 16:55-63.

Shimizu T, Hosaki A, Hino T, Sato M, Komori T, Hirai S, Rossini PM (2002) Motor cortical disinhibition in the unaffected hemisphere after unilateral cortical stroke. Brain 125:1896-1907.

Shoham D, Glaser DE, Arieli A, Kenet T, Wijnbergen C, Toledo Y, Hildesheim R, Grinvald A (1999) Imaging cortical dynamics at high spatial and temporal resolution with novel blue voltage-sensitive dyes. Neuron 24:791-802.

Sigler A, Mohajerani MH, Murphy TH (2009) Imaging rapid redistribution of sensory-evoked depolarization through existing cortical pathways after targeted stroke in mice. Proc Natl Acad Sci U S A 106:11759-11764.

Slovin H, Arieli A, Hildesheim R, Grinvald A (2002) Long-term voltage-sensitive dye imaging reveals cortical dynamics in behaving monkeys. Journal of neurophysiology 88:3421-3438.

Sotelo C (2003) Viewing the brain through the master hand of Ramon y Cajal. Nat Rev Neurosci 4:71-77.

Sporns O, Tononi G, Kotter R (2005) The human connectome: A structural description of the human brain. PLoS computational biology 1:e42.

Stern EA, Kincaid AE, Wilson CJ (1997) Spontaneous subthreshold membrane potential fluctuations and action potential variability of rat corticostriatal and striatal neurons in vivo. J Neurophysiol 77:1697-1715.

Strogatz SH (2001) Exploring complex networks. Nature 410:268-276.

Sur M, Rubenstein JL (2005) Patterning and plasticity of the cerebral cortex. Science 310:805-810.

Sweetnam D, Holmes A, Tennant KA, Zamani A, Walle M, Jones P, Wong C, Brown CE (2012) Diabetes impairs cortical plasticity and functional recovery following ischemic stroke. J Neurosci 32:5132-5143.

Tasaki I, Takenaka T, Yamagishi S (1968a) Abrupt depolarization and bi-ionic action potentials in internally perfused squid giant axons. Am J Physiol 215:152-159.

Tasaki I, Watanabe A, Sandlin R, Carnay L (1968b) Changes in fluorescence, turbidity, and birefringence associated with nerve excitation. Proc Natl Acad Sci U S A 61:883-888.

Tehovnik EJ (1996) Electrical stimulation of neural tissue to evoke behavioral responses. J Neurosci Methods 65:1-17.

Theyel BB, Llano DA, Sherman SM (2010) The corticothalamocortical circuit drives higher-order cortex in the mouse. Nat Neurosci 13:84-88.

Thinus-Blanc C, Save E, Rossi-Arnaud C, Tozzi A, Ammassari-Teule M (1996) The differences shown by C57BL/6 and DBA/2 inbred mice in detecting spatial novelty are subserved by a different hippocampal and parietal cortex interplay. Behav Brain Res 80:33-40.

Thomson AM, Bannister AP (2003) Interlaminar connections in the neocortex. Cereb Cortex 13:5-14.

Thomson AM, Lamy C (2007) Functional maps of neocortical local circuitry. Front Neurosci 1:19-42.

Tian L, Hires SA, Mao T, Huber D, Chiappe ME, Chalasani SH, Petreanu L, Akerboom J, McKinney SA, Schreiter ER, Bargmann CI, Jayaraman V, Svoboda K, Looger LL (2009) Imaging neural activity in worms, flies and mice with improved GCaMP calcium indicators. Nat Methods 6:875-881.

Tomita H, Sugano E, Fukazawa Y, Isago H, Sugiyama Y, Hiroi T, Ishizuka T, Mushiake H, Kato M, Hirabayashi M, Shigemoto R, Yawo H, Tamai M (2009) Visual properties of transgenic rats harboring the channelrhodopsin-2 gene regulated by the thy-1.2 promoter. PLoS One 4:e7679.

Triarhou LC, ed (2007) von Economo and Koskinas: Atlas of cytoarchitectonics of the adult human cerebral cortex: S Karger Pub.

Tsai PS, Kaufhold JP, Blinder P, Friedman B, Drew PJ, Karten HJ, Lyden PD, Kleinfeld D (2009) Correlations of neuronal and microvascular densities in murine cortex revealed by direct counting and colocalization of nuclei and vessels. The Journal of neuroscience : the official journal of the Society for Neuroscience 29:14553-14570.

Turrigiano GG, Nelson SB (2000) Hebb and homeostasis in neuronal plasticity. Curr Opin Neurobiol 10:358-364.

Turrigiano GG, Nelson SB (2004) Homeostatic plasticity in the developing nervous system. Nat Rev Neurosci 5:97-107.

van den Heuvel MP, Hulshoff Pol HE (2010) Exploring the brain network: a review on resting-state fMRI functional connectivity. Eur Neuropsychopharmacol 20:519-534.

van den Heuvel MP, Sporns O (2011) Rich-club organization of the human connectome. J Neurosci 31:15775-15786.

van der Worp HB, Macleod MR, Kollmar R (2010) Therapeutic hypothermia for acute ischemic stroke: ready to start large randomized trials? J Cereb Blood Flow Metab 30:1079-1093.

van Meer MP, Otte WM, van der Marel K, Nijboer CH, Kavelaars A, van der Sprenkel JW, Viergever MA, Dijkhuizen RM (2012) Extent of bilateral neuronal network reorganization and functional recovery in relation to stroke severity. J Neurosci 32:4495-4507.

van Meer MP, van der Marel K, Wang K, Otte WM, El Bouazati S, Roeling TA, Viergever MA, Berkelbach van der Sprenkel JW, Dijkhuizen RM (2010) Recovery of sensorimotor function after experimental stroke correlates with restoration of resting-state interhemispheric functional connectivity. J Neurosci 30:3964-3972.

Veenman CL, Reiner A, Honig MG (1992) Biotinylated dextran amine as an anterograde tracer for single- and double-labeling studies. J Neurosci Methods 41:239-254.

Veenman CL, Wild JM, Reiner A (1995) Organization of the avian "corticostriatal" projection system: a retrograde and anterograde pathway tracing study in pigeons. J Comp Neurol 354:87-126.

Vincent JL, Patel GH, Fox MD, Snyder AZ, Baker JT, Van Essen DC, Zempel JM, Snyder LH, Corbetta M, Raichle ME (2007) Intrinsic functional architecture in the anaesthetized monkey brain. Nature 447:83-86.

Wahl AS, Omlor W, Rubio JC, Chen JL, Zheng H, Schroter A, Gullo M, Weinmann O, Kobayashi K, Helmchen F, Ommer B, Schwab ME (2014) Neuronal repair. Asynchronous therapy restores motor control by rewiring of the rat corticospinal tract after stroke. Science 344:1250-1255.

Wang H, Peca J, Matsuzaki M, Matsuzaki K, Noguchi J, Qiu L, Wang D, Zhang F, Boyden E, Deisseroth K, Kasai H, Hall WC, Feng G, Augustine GJ (2007a) High-speed mapping of synaptic connectivity using photostimulation in Channelrhodopsin-2 transgenic mice. Proc Natl Acad Sci U S A 104:8143-8148.

Wang Y, Jin K, Greenberg DA (2007b) Neurogenesis associated with endothelin-induced cortical infarction in the mouse. Brain research 1167:118-122.

Ward NS, Brown MM, Thompson AJ, Frackowiak RS (2003a) Neural correlates of outcome after stroke: a cross-sectional fMRI study. Brain 126:1430-1448.

Ward NS, Brown MM, Thompson AJ, Frackowiak RS (2003b) Neural correlates of motor recovery after stroke: a longitudinal fMRI study. Brain 126:2476-2496.

Wassermann EM, Lisanby SH (2001) Therapeutic application of repetitive transcranial magnetic stimulation: a review. Clin Neurophysiol 112:1367-1377.

Watson BD, Dietrich WD, Busto R, Wachtel MS, Ginsberg MD (1985) Induction of reproducible brain infarction by photochemically initiated thrombosis. Annals of neurology 17:497-504.

Watts DJ, Strogatz SH (1998) Collective dynamics of 'small-world' networks. Nature 393:440-442.

Weiler N, Wood L, Yu J, Solla SA, Shepherd GM (2008) Top-down laminar organization of the excitatory network in motor cortex. Nat Neurosci 11:360-366.

White JG, Southgate E, Thomson JN, Brenner S (1986) The structure of the nervous system of the nematode Caenorhabditis elegans. Philos Trans R Soc Lond B Biol Sci 314:1-340.

Wiemer JC (2003) The time-organized map algorithm: extending the self-organizing map to spatiotemporal signals. Neural Comput 15:1143-1171.

Winship IR, Murphy TH (2008) In vivo calcium imaging reveals functional rewiring of single somatosensory neurons after stroke. J Neurosci 28:6592-6606.

Witte OW, Bidmon HJ, Schiene K, Redecker C, Hagemann G (2000) Functional differentiation of multiple perilesional zones after focal cerebral ischemia. J Cereb Blood Flow Metab 20:1149-1165.

Wolf SL, Winstein CJ, Miller JP, Taub E, Uswatte G, Morris D, Giuliani C, Light KE, Nichols-Larsen D (2006) Effect of constraint-induced movement therapy on upper extremity function 3 to 9 months after stroke: the EXCITE randomized clinical trial. JAMA 296:2095-2104.

Wu JY, Xiaoying H, Chuan Z (2008) Propagating waves of activity in the neocortex: what they are, what they do. Neuroscientist 14:487-502.

Xerri C (2012) Plasticity of cortical maps: multiple triggers for adaptive reorganization following brain damage and spinal cord injury. Neuroscientist 18:133-148.

Yang G, Kitagawa K, Matsushita K, Mabuchi T, Yagita Y, Yanagihara T, Matsumoto M (1997) C57BL/6 strain is most susceptible to cerebral ischemia following bilateral common

carotid occlusion among seven mouse strains: selective neuronal death in the murine transient forebrain ischemia. Brain Res 752:209-218.

Yizhar O, Fenno LE, Prigge M, Schneider F, Davidson TJ, O'Shea DJ, Sohal VS, Goshen I, Finkelstein J, Paz JT, Stehfest K, Fudim R, Ramakrishnan C, Huguenard JR, Hegemann P, Deisseroth K (2011) Neocortical excitation/inhibition balance in information processing and social dysfunction. Nature 477:171-178.

Yu J, Anderson CT, Kiritani T, Sheets PL, Wokosin DL, Wood L, Shepherd GM (2008) Local-Circuit Phenotypes of Layer 5 Neurons in Motor-Frontal Cortex of YFP-H Mice. Front Neural Circuits 2:6.

Zakiewicz IM, van Dongen YC, Leergaard TB, Bjaalie JG (2011) Workflow and atlas system for brain-wide mapping of axonal connectivity in rat. PLoS One 6:e22669.

Zariwala HA, Madisen L, Ahrens KF, Bernard A, Lein ES, Jones AR, Zeng H (2011) Visual tuning properties of genetically identified layer 2/3 neuronal types in the primary visual cortex of cre-transgenic mice. Front Syst Neurosci 4:162.

Zeiler SR, Krakauer JW (2013) The interaction between training and plasticity in the poststroke brain. Curr Opin Neurol 26:609-616.

Zemelman BV, Lee GA, Ng M, Miesenbock G (2002) Selective photostimulation of genetically chARGed neurons. Neuron 33:15-22.

Zhang F, Prigge M, Beyriere F, Tsunoda SP, Mattis J, Yizhar O, Hegemann P, Deisseroth K (2008) Red-shifted optogenetic excitation: a tool for fast neural control derived from Volvox carteri. Nat Neurosci 11:631-633.

Zhao Y, Araki S, Wu J, Teramoto T, Chang YF, Nakano M, Abdelfattah AS, Fujiwara M, Ishihara T, Nagai T, Campbell RE (2011) An expanded palette of genetically encoded Ca(2)(+) indicators. Science 333:1888-1891.